Mathematical Problems in Engineering

Wind Energy

Guest Editors: Ming-Hung Hsu, Wei-Jen Lee, Jao-Hwa Kuang, and Hua-Shan Tai

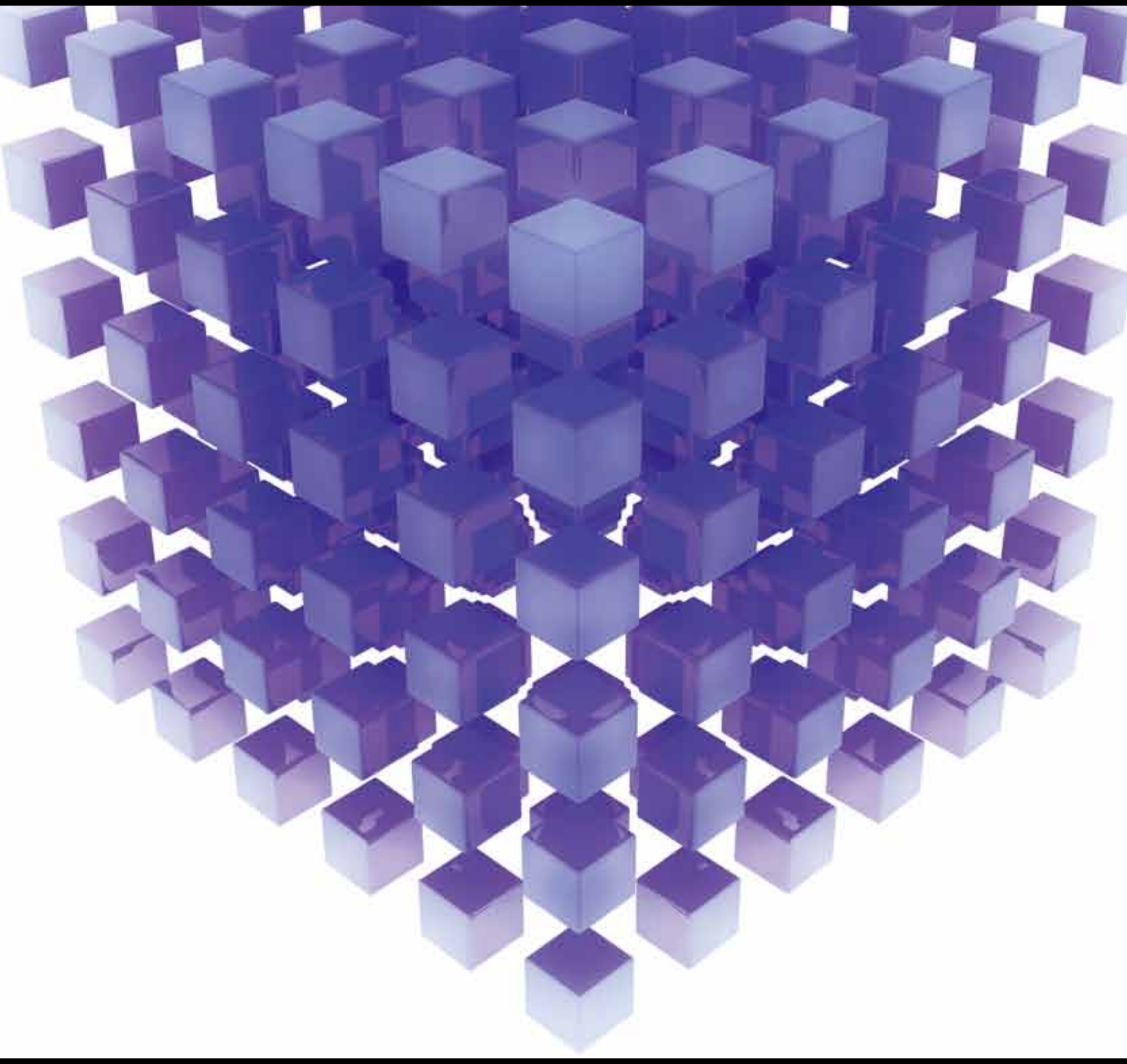

Wind Energy

Mathematical Problems in Engineering

Wind Energy

Guest Editors: Ming-Hung Hsu, Wei-Jen Lee, Jao-Hwa Kuang, and Hua-Shan Tai

Editorial Board

Contents

Hindawi Publishing Corporation
Mathematical Problems in Engineering
Volume 2013, Article ID 759686, 1 page
http://dx.doi.org/10.1155/2013/759686

Editorial
Wind Energy

Ming-Hung Hsu,[1] Wei-Jen Lee,[2] Jao-Hwa Kuang,[3] and Hua-Shan Tai[4]

[1] *Department of Electrical Engineering, National Penghu University of Science and Technology, Taiwan*
[2] *Energy Systems Research Center, The University of Texas at Arlington, USA*
[3] *Department of Mechanical and Electro-Mechanical Engineering, National Sun Yat-Sen University, Taiwan*
[4] *Department of Safety, Health and Environmental Engineering, National Kaohsiung First University of Science and Technology, Taiwan*

Correspondence should be addressed to Ming-Hung Hsu; hsu@npu.edu.tw

Received 1 December 2013; Accepted 1 December 2013

Clean energies are becoming the major energy resources of the future. Wind power does not generate pollution and is a clean source. Recent engineering advances in wind energy production have contributed to the successful solution of real problems thus improving the quality of life. This special issue aims at gathering research works focusing on the development of mathematical model for the recent developments of wind energy. X. Zhang, in the paper "*Transient simulation of wind turbine towers under lightning stroke*," proposed a simulation algorithm for lightning transient analysis of the wind turbine (WT) towers. N. Haouas and P. R. Bertrand, in their paper "*Wind farm power forecasting*," studied the relationship between the power productions to avoid interaction between each turbine of the farm. H. Coral-Enriquez et al., in their paper "*Robust active disturbance rejection control approach to maximize energy capture in variable-speed wind turbines*," proposed an alternative robust observer-based linear control technique to maximize energy capture in a 4.8 MW horizontal-axis variable-speed wind turbine. N. Chen et al., in their paper "*Multistep wind speed forecasting based on wavelet and Gaussian processes*," proposed a novel W-GP model (wavelet decomposition based Gaussian process learning paradigm) for short-term wind speed forecasting. Z. W. Geem and J. Hong, in their paper "*Improved formulation for the optimization of wind turbine placement in a wind farm*," proposed an efficient optimization formulation for the optimal layout of wind turbine placements under the resources (e.g., number of turbines) or budget limit by introducing corresponding constraints. L. A. Soriano et al., in their paper "*Modeling and control of wind turbine*," studied the characteristics of the wind turbine in the market and lab; it is focused on the recent advances of the wind turbine modeling with the aerodynamic power, and the wind turbine control with the nonlinear, fuzzy, and predictive techniques.

Ming-Hung Hsu
Wei-Jen Lee
Jao-Hwa Kuang
Hua-Shan Tai

Hindawi Publishing Corporation
Mathematical Problems in Engineering
Volume 2013, Article ID 142765, 9 pages
http://dx.doi.org/10.1155/2013/142765

Research Article

Transient Simulation of Wind Turbine Towers under Lightning Stroke

Xiaoqing Zhang

National Active Distribution Network Technology Research Center, Beijing Jiaotong University, Beijing 100044, China

Correspondence should be addressed to Xiaoqing Zhang; xqzhang2@bjtu.edu.cn

Received 23 March 2013; Revised 16 July 2013; Accepted 17 July 2013

Academic Editor: Ming-Hung Hsu

A simulation algorithm is proposed in this paper for lightning transient analysis of the wind turbine (WT) towers. In the proposed algorithm, the tower body is first subdivided into a discrete multiconductor system. A set of formulas are given to calculate the electrical parameters of the branches in the multiconductor system. By means of the electrical parameters, each branch unit in the multiconductor system is replaced as a coupled π-type circuit and the multiconductor system is converted into a circuit model. Then, the lightning transient responses can be obtained in different parts on the tower body by solving the circuit equations of the equivalent discretization network. The laboratory measurement is also made by a reduced-scale tower for checking the validity of the proposed algorithm.

1. Introduction

Global warming effect accelerates the utilization of wind energy. As a clean energy source, wind energy can be used to generate electric power without emission of carbon dioxide into the atmospheric environment. In consequence of the rapid growth in the utilization of wind energy for electric power supply, wind turbines (WTs) have increased constantly in size and rated power during recent decades. WTs are particularly vulnerable to lightning strokes due to their great height, distinctive shape, and rather exposed position. The lightning stroke effect on WTs has become a major concern as the number of the installed WTs continues to increase. Therefore, lightning protection of WTs is crucially important for the operational reliability of large wind power generation systems. The lightning protection design needs to obtain the lightning transient responses on WT towers since the tower body is the main conducting path of lightning current. The simulation algorithms were presented in the literature [1–3], in which the tower body was simply represented by a transmission line or a chain capacitance circuit. However, these existing algorithms are difficult to use for calculating the transient responses in different parts on the tower body due to the fact that they ignore the structural feature of the tower body. To overcome the shortcoming in these existing algorithms, a novel simulation algorithm is proposed in this paper. The proposed algorithm subdivides the continuous conducting shell of the tower body into a discrete multiconductor system and can give due consideration for the structural feature of the tower body. In the multiconductor system, the electrical parameters of the branches are calculated by an efficient procedure, and the branch units are represented by the coupled π-type circuits. A circuit model, constituted by a series of the coupled π-type circuits, is built for the multiconductor system. On the basis of the circuit model, the equivalent discretization network is further formed. The transient calculation is performed for the equivalent discretization network, and then the lightning transient responses can be obtained in different parts on the tower body. The measurement of the transient response is also taken on a reduced-scale WT tower, and the validity of the proposed algorithm is examined by comparing simulated and measured results.

2. Calculation of Electrical Parameters

2.1. Discretization Description of the WT Tower. After a WT is struck by lightning, lightning current usually passes from the blade root to the tower and then dissipates in the

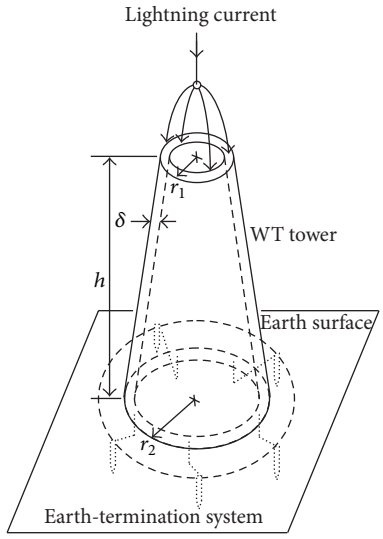

Figure 1: WT tower.

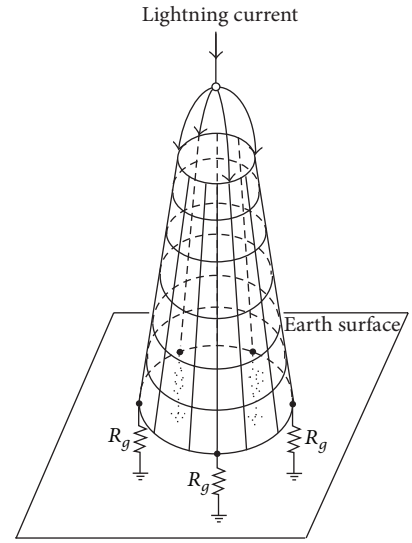

Figure 2: Multiconductor system.

ground through the earth-termination system. Since most manufactures have used many kinds of brushes and sliding contact systems to divert the lightning current from the main shaft, only a much smaller part of lightning current flows through the gearbox and the generator. For the WT structure, the tower is the longest conducting path of lightning current. When the tower conducts lightning current, serious transient potential rise appears on the tower body and may result in flashback to the electrical and electronic components installed inside the tower. Much attention to the potential rise has been paid in the lightning protection design of WTs. For the sake of the transient analysis of the potential distribution on the tower, the blade and the conducting path in the nacelle are left out of consideration. Instead, lightning current is injected into the tower body from its top, as shown in Figure 1 [4]. In order to build the circuit model of the tower, the continuous conducting shell of the tower body needs to be subdivided into a discrete multiconductor system formed by longitudinal and transverse branches, as illustrated in Figure 2 [5]. The WT earth-termination system is modeled as the grounding resistances (R_g). The electrical parameters of the branches in the multiconductor system are represented by resistances, inductances, and capacitances. For simplifying the parameter calculation, the segmental arc of each transverse branch is replaced by its chord and all the branches are taken as the cylindrical conductors. The conductor radii are estimated from the average cross-sections of the respective branches.

2.2. Inductance and Resistance. The inductance parameters can be determined by Neumann's integral method [6, 7]. The typical branches in the multiconductor system are illustrated in Figure 3, where the presence of the ground is considered by symmetrically installing the image branches (depicted in dotted lines) below the earth surface [7]. According to Neumann's integral method, the mutual inductance between the branches j and k is calculated by

$$L_{jk} = \frac{\mu_0}{4\pi}\left[\int_{s_j}\int_{s_k}\frac{d\mathbf{s}_j \cdot d\mathbf{s}_k}{\mathbf{D}_{jk}} + \int_{s'_j}\int_{s_k}\frac{d\mathbf{s}'_j \cdot d\mathbf{s}_k}{\mathbf{D}'_{jk}}\right]. \quad (1)$$

The dot products of the vector differential segments become

$$\begin{aligned} d\mathbf{s}_j \cdot d\mathbf{s}_k &= \cos\varphi d\mathbf{s}_j d\mathbf{s}_k, \\ d\mathbf{s}'_j \cdot d\mathbf{s}_k &= \cos\varphi' ds'_j ds, \end{aligned} \quad (2)$$

where φ is the direction angle between the branches j and k, and φ' is that between the branches j' and k. Substituting (2) into (1) gives

$$L_{jk} = \frac{\mu_0}{4\pi}\left[\cos\varphi N(j,k) + \cos\varphi' N\left(j',k\right)\right], \quad (3)$$

where $N(j,k)$ and $N(j',k)$ are two double line integrals:

$$\begin{aligned} N(j,k) &= \int_{s_j}\int_{s_k}\frac{ds_j ds_k}{D_{jk}}, \\ N\left(j',k\right) &= \int_{s'_j}\int_{s_k}\frac{ds'_j ds_k}{D'_{jk}}. \end{aligned} \quad (4)$$

Equations (3) and (4) indicate that the calculation of the mutual inductance depends on the double line integrals $N(j,k)$ and $N(j',k)$. From the viewpoint of integral operation, the way to evaluate $N(j,k)$ is the same as that to evaluate $N(j',k)$. For this reason, the solution of $N(j,k)$ is only presented for the typical space positions in the multiconductor system, which holds for the evaluation of $N(j',k)$.

The integral $N(j,k)$ is first evaluated in the case of the coplanar branch pairs. For the two coplanar longitudinal

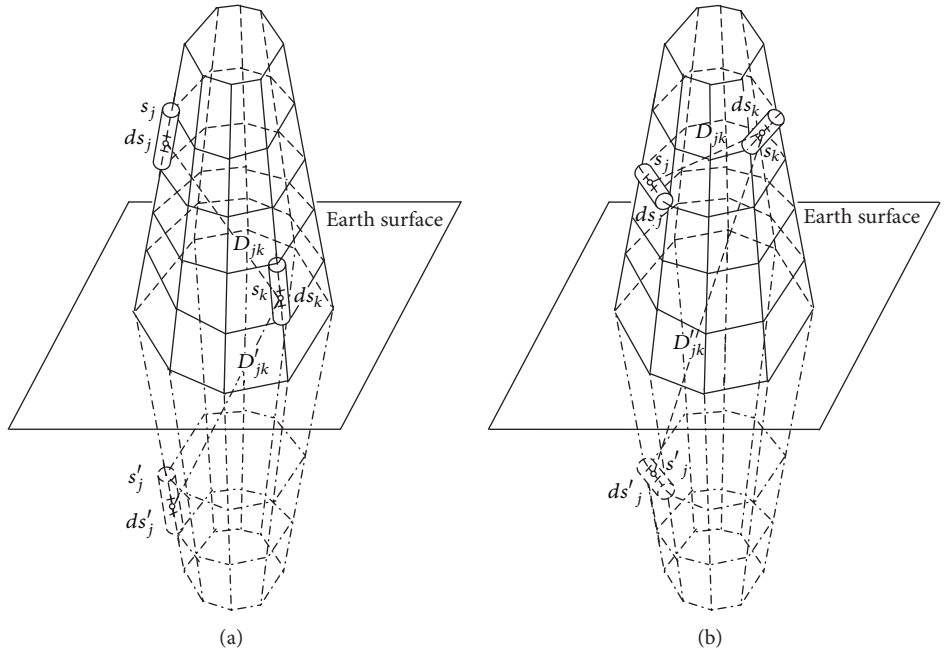

Figure 3: Branches in the multiconductor system.

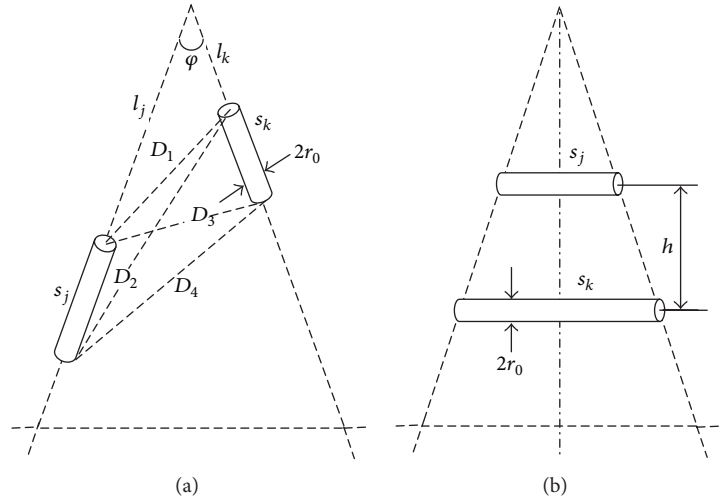

Figure 4: Coplanar branch pairs, (a) longitudinal pair, and (b) transverse pair.

branches, as shown in Figure 4(a), the integral $N(j,k)$ is given by

$$N(j,k) = \left(l_j + s_j\right)\ln\frac{D_2 + D_4 + s_k}{D_2 + D_4 - s_k} - l_j \ln\frac{D_1 + D_3 + s_k}{D_1 + D_3 - s_k} + \left(l_k + s_k\right)\ln\frac{D_3 + D_4 + s_j}{D_3 + D_4 - s_j} - l_k \ln\frac{D_1 + D_2 + s_j}{D_1 + D_2 - s_j}. \tag{5}$$

If the two longitudinal branches are flush with each other, the integral $N(j,k)$ is evaluated by putting $s_j = s_k$ and $D_2 = D_3$ into (5). Under the flush condition, the integral $N(j,j)$ is evaluated by again putting $D_1 = D_4 = r_0$ into (5). This can result in determining the self-inductance L_{jj} of the longitudinal branch j by (3).

For the two coplanar transverse branches ($\varphi = 0$), as shown in Figure 4(b), the integral $N(j,k)$ is given by

$$N(j,k) = -\left(s_k - s_j\right)\sinh^{-1}\frac{s_k - s_j}{2h} + \left(s_j + s_k\right)\sinh^{-1}\frac{s_j + s_k}{2h} + 2\sqrt{\left(\frac{s_k - s_j}{2}\right)^2 + h^2} - 2\sqrt{\left(\frac{s_j + s_k}{2}\right)^2 + h^2}. \tag{6}$$

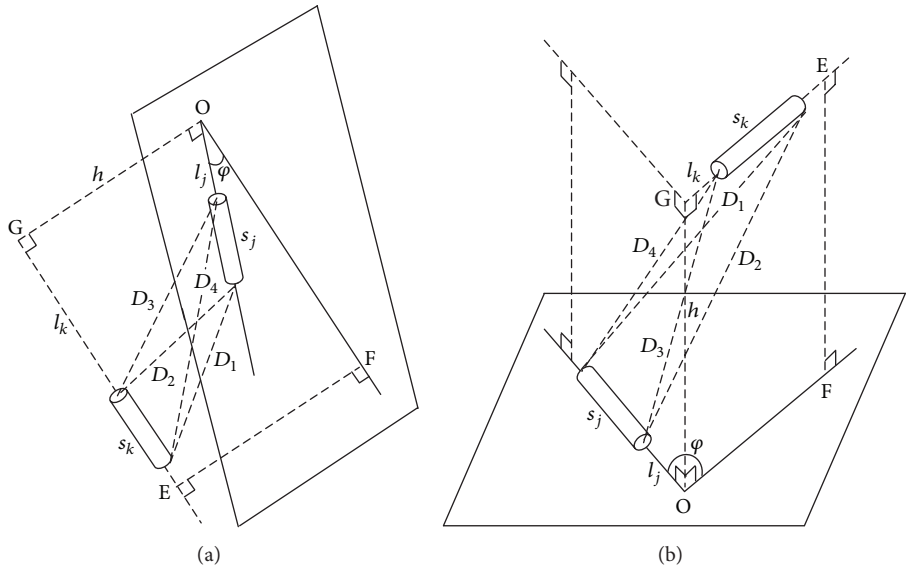

Figure 5: Noncoplanar branch pairs, (a) longitudinal pair, and (b) transverse pair.

In (6), letting $s_j = s_k$ and $h = r_0$ gives the integral $N(j, j)$. Then, $N(j, j)$ can be used to further determine the self-inductance L_{jj} of the transverse branch j by (3).

The noncoplanar branch pairs are shown in Figure 5, where line OG is the common perpendicular to the two branches and line OF lying on the plane containing the branch j is parallel to the branch k. The integral $N(j,k)$ for both the longitudinal branch pair (Figure 5(a)) and the transverse branch pair (Figure 5(b)) is given in the following complicated expression

$$\begin{aligned} N(j,k) &= 2\left[\left(l_j + s_j\right)\tanh^{-1}\frac{s_k}{D_1 + D_2} - l_j\tanh^{-1}\frac{s_k}{D_3 + D_4}\right. \\ &\quad \left. + \left(l_k + s_k\right)\tanh^{-1}\frac{s_j}{D_1 + D_4} - l_k\tanh^{-1}\frac{s_j}{D_2 + D_3}\right] \\ &\quad - \frac{\Phi h}{\sin\varphi}, \end{aligned} \tag{7}$$

where Φ is the solid angle

$$\begin{aligned} \Phi &= \tanh^{-1}\left[\frac{h^2\cos\varphi + \left(l_j + s_j\right)\left(l_k + s_k\right)\sin^2\varphi}{hD_1\sin\varphi}\right] \\ &\quad - \tanh^{-1}\left[\frac{h^2\cos\varphi + l_k\left(l_j + s_j\right)\sin^2\varphi}{hD_2\sin\varphi}\right] \\ &\quad + \tanh^{-1}\left[\frac{h^2\cos\varphi + l_j l_k\sin^2\varphi}{hD_3\sin\varphi}\right] \\ &\quad - \tanh^{-1}\left[\frac{h^2\cos\varphi + l_j\left(l_k + s_k\right)\sin^2\varphi}{hD_4\sin\varphi}\right]. \end{aligned} \tag{8}$$

On the basis of the formulas given previously, the self and mutual inductances can be calculated for a branch unit with M coupled branches in the multiconductor system, thus forming the inductance matrix

$$\mathbf{L} = \left\{L_{jk}\right\}_{M\times M}. \tag{9}$$

The branch resistance per unit length is approximately calculated by [8]

$$R = \frac{\rho}{\pi\sigma\left[\left(1 - \exp\left(-r_0/\sigma\right)\right)\right]\left[2r_0 - \sigma\left(1 - \exp\left(-r_0/\sigma\right)\right)\right]}, \tag{10}$$

where r_0 is the radius of the branch, ρ the material resistivity, and σ the skin depth:

$$\sigma = \frac{1}{\sqrt{\pi f\mu\gamma}}, \tag{11}$$

where f is the maximum frequency likely to affect the system transient, μ the material permeability, and $\gamma = 1/\rho$. f may be roughly evaluated by the waveform parameter of the injected lightning current [9].

2.3. Capacitance. The mutual potential coefficient between the branches j and k, as shown in Figure 3, can be calculated by the average potential method [10]:

$$\begin{aligned} p_{jk} &= \frac{1}{4\pi\varepsilon_0 s_j s_k}\left[\int_{s_j}\int_{s_k}\frac{ds_j ds_k}{D_{jk}} - \int_{s_j'}\int_{s_k}\frac{ds_j' ds_k}{D_{jk}'}\right] \\ &= \frac{1}{4\pi\varepsilon_0 s_j s_k}\left[N(j,k) - N\left(j',k\right)\right]. \end{aligned} \tag{12}$$

From (12), the self-potential coefficient p_{jj} of the branch j can also be obtained in a similar way to the self-inductance

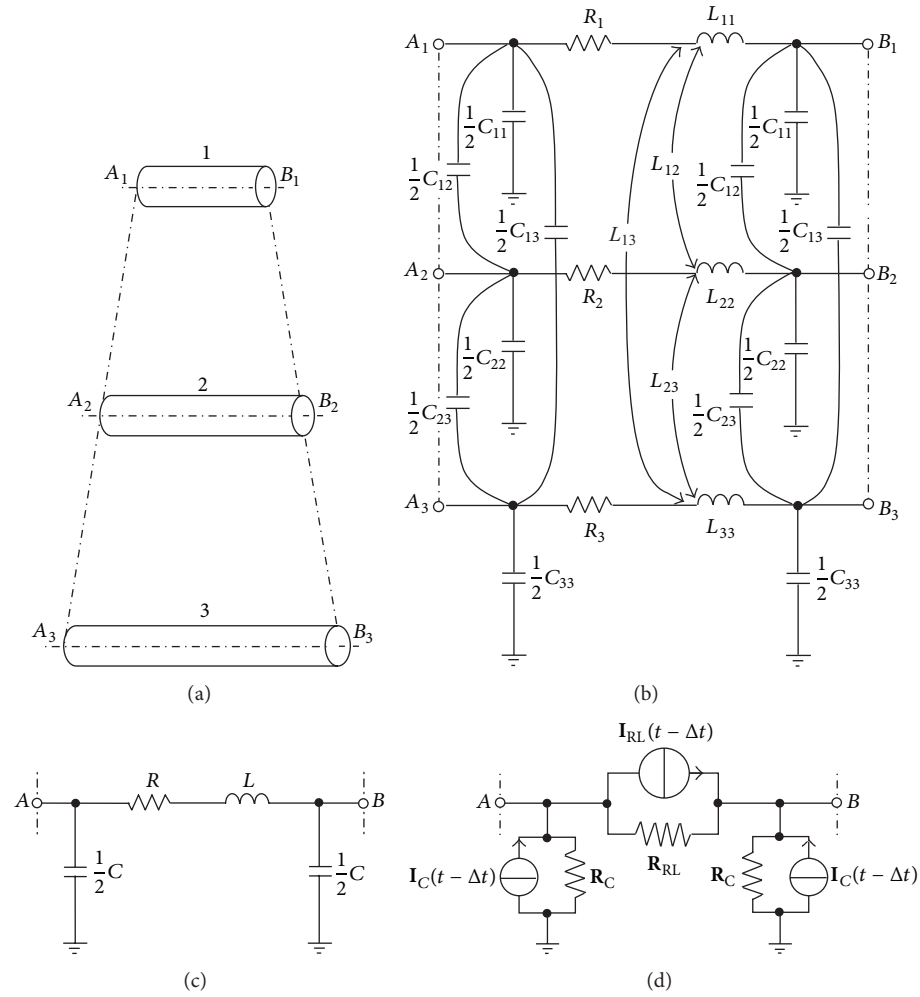

Figure 6: Coupled π-type circuit of three coupled branches: (a) three coupled branches, (b) coupled π-type circuit, (c) simplified π-type circuit expressed in matrix, and (d) discretization π-type circuit.

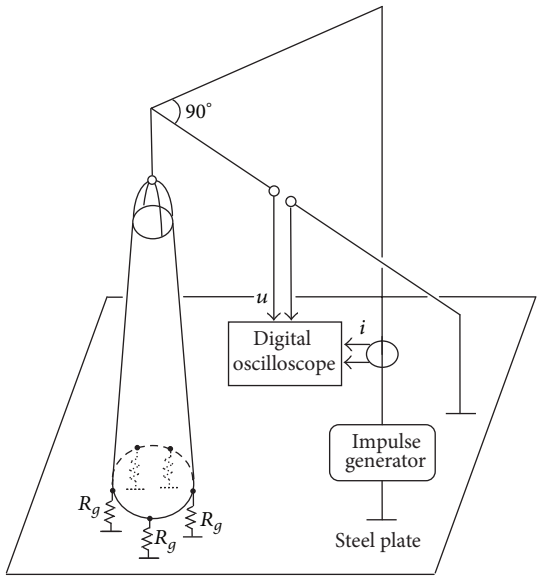

Figure 7: Experimental setup.

L_{jj}. Consequently, the potential coefficient matrix of a branch unit with M coupled branches in the multiconductor system is formed by

$$\mathbf{P} = \left\{p_{jk}\right\}_{M\times M}. \tag{13}$$

Calculating the inverse of $\mathbf{P}$ gives

$$\mathbf{P}^{-1} = \left\{q_{jk}\right\}_{M\times M}. \tag{14}$$

From the inverse matrix $\mathbf{P}^{-1}$, the capacitance matrix can be obtained as [10, 11]

$$\mathbf{C} = \left\{C_{jk}\right\}_{M\times M}, \tag{15}$$

where the diagonal and off-diagonal elements are determined as

$$\begin{aligned} C_{jj} &= \sum_{\zeta=1}^{M} q_{j\zeta} \quad (j = 1, 2, \ldots, M), \\ C_{jk} &= -q_{jk} \quad (j, k = 1, 2, \ldots, M,\ j \neq k). \end{aligned} \tag{16}$$

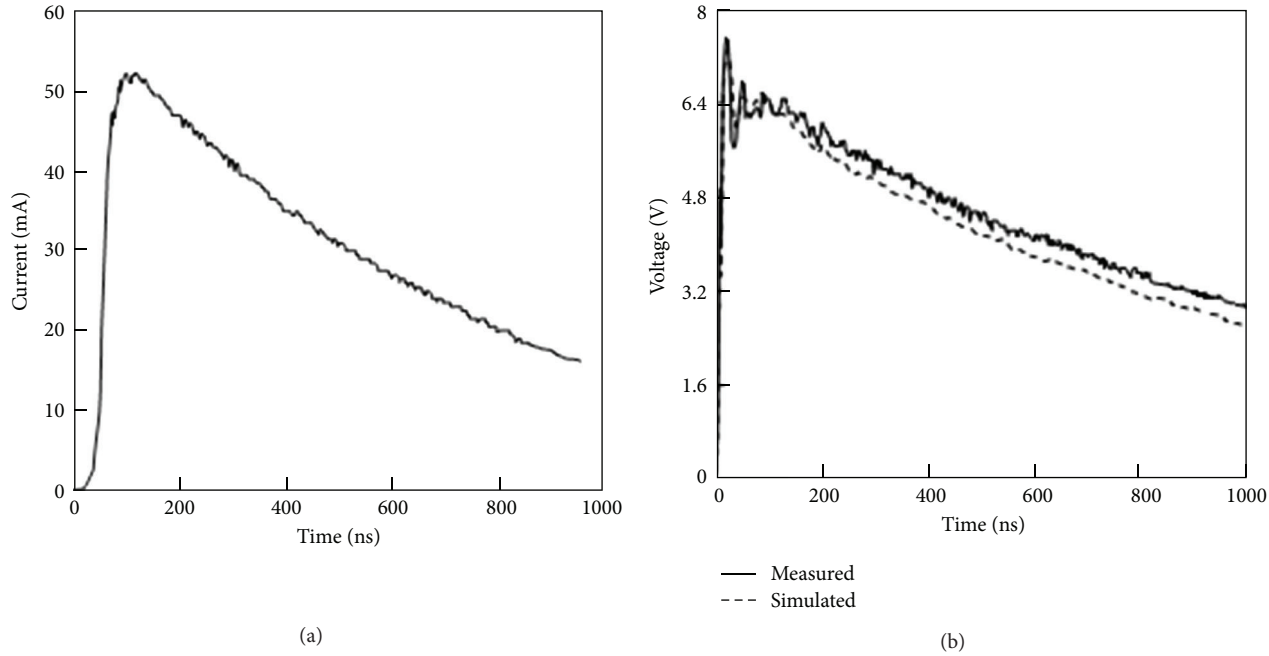

Figure 8: Measured and simulated waveforms: (a) injected current waveform and (b) potential waveform at the top of the tower.

3. Simulation of Lightning Transients

By means of the electrical parameters obtained previously, a branch unit with M coupled branches is represented by a coupled π-type circuit formed by resistances, inductances, and capacitances. A coupled π-type circuit representing three coupled branches ($M = 3$) is shown in Figures 6(a) and 6(b). Expression of the electrical parameters in matrix form gives a simplified circuit, as shown in Figure 6(c). With a time discretization treatment for the inductance and capacitance elements, these two kinds of circuit elements are replaced by current sources and parallel equivalent resistances [12, 13]. Thus, Figure 6(c) is further converted into a discretization π-type circuit, as shown in Figure 6(d), where Δt is the time step size, $\mathbf{I}_{RL}(t - \Delta t)$ and $\mathbf{I}_C(t - \Delta t)$ are the current source vectors determined by the current and voltage values from previous time steps, and $\mathbf{R}_{RL}$ and $\mathbf{R}_C$ are the equivalent resistance matrices determined by the electrical parameters and the time step size. The formulas for calculating $\mathbf{I}_{RL}(t - \Delta t)$, $\mathbf{I}_C(t - \Delta t)$, $\mathbf{R}_{RL}$, and $\mathbf{R}_C$ have been given in [13, 14]. For M ($M > 3$) coupled branches, the discretization π-type circuit is similar to that in Figure 6(d). After all the branch units in the multiconductor system are replaced by the discretization π-type circuits, the tower body can be converted into an equivalent discretization network. The lightning current source is injected to the top nodes of the equivalent discretization network. According to the topology connection mode of the equivalent resistances and current sources, the node voltage equations are formed and then solved numerically at each time step. The solving process has been described in detail in [13, 14]. As a result, lightning transient responses can be obtained in different parts on the tower body.

If the blade and the conducting path in the nacelle are taken into account, the former can be converted into a series circuit unit consisting of a few π-type circuits and the latter into a parallel resistance-capacitance unit. In the parallel unit, the resistance is the contact one of the brush and the sliding contact system, while the capacitance represents the main shaft bearings [2, 15]. After the two circuit units are serially connected to the equivalent discretization network of the tower, the complete circuit model can be built for the WT. However, the two circuit units in the complete circuit model do not change the lightning current and transient potential distributions on the tower body due to their series connection to the tower. Thus, their removal from the complete circuit model will not make a significant influence on calculation of the potential responses on the tower body.

4. Verification of the Proposed Algorithm with Laboratory Measurement

An experimental setup was built in the laboratory space, as shown in Figure 7. The reduced-scale tower is made of the iron sheet, whose dimensions are taken as $r_1 = 0.0283$ m, $r_2 = 0.067$ m, $h = 2$ m, and $\delta = 0.002$ m (see Figure 1). The potential measurement wire and the current lead wire are orthogonal to weaken the electromagnetic induction between them.

The potential measurement wire is grounded, that is, connected to the steel plate, at a point 9 m apart from the tower. Five resistances of 5 Ω, representing the grounding resistances, are connected between the tower bottom and steel plate. The impulse current with fast wavefront is injected to the top of the tower. Under the excitation of the injected

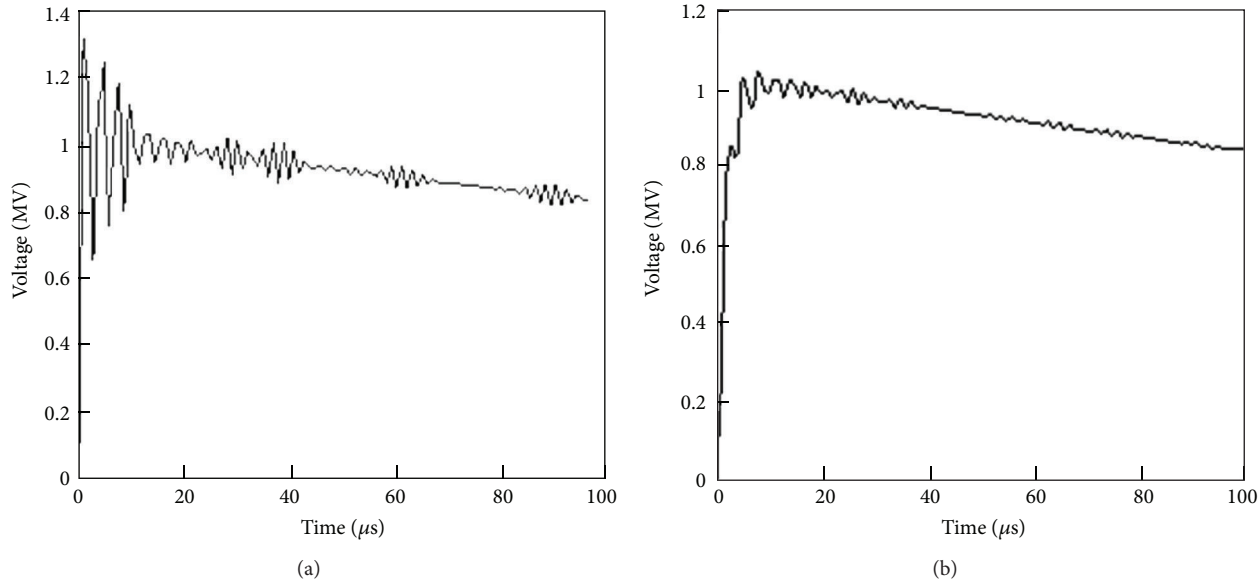

Figure 9: Transient potential waveforms: (a) potential waveforms at the top of the tower and (b) potential waveforms at the bottom of the tower.

current, the transient potential response is measured at the top of the tower. The frequency bandwidth of the potential probe is 0~500 MHz and that of the current probe 20 kHz~ 500 MHz, which is competent to measure the fast transient responses. The measured waveforms of the injected current and the transient potential are shown in Figure 8, where the corresponding waveform simulated by the proposed algorithm is given simultaneously for comparison. It can be found that a better agreement appears between measured and simulated waveforms. This agreement confirms the validity of the proposed algorithm.

5. Application Example

This example takes into account an actual WT with a rated power of 2.5 MW. The dimensions of the WT tower are $r_1 = 1.35$ m, $r_2 = 2.17$ m, $h = 82$ m, and $\delta = 0.025$ m, and the grounding resistance R_g is 4 Ω (see Figure 1). The parameter of the injected lightning current is taken as 10/350 μs, 100 kA according to the technical specification of lightning protection [16]. By using the proposed algorithm to perform transient simulation, the transient potential responses are obtained on the tower body. The potential waveforms at the top and the bottom of the tower are shown in Figure 9, and the peak potential distribution along the height of the tower is also plotted in Figure 10. As seen in Figures 9 and 10, the transient potential rise on the tower body is extremely serious and may do damage to the facilities installed inside the tower under lightning stroke.

In an actual wind farm, individual WT earth-termination systems are usually connected by the metallic armor of the power cable running between the WTs. An interconnected grounding system consisting of 5 WTs and a substation is shown in Figure 11. The distance between two successive WTs is 380 m. The substation (SS) is located 390 m away from

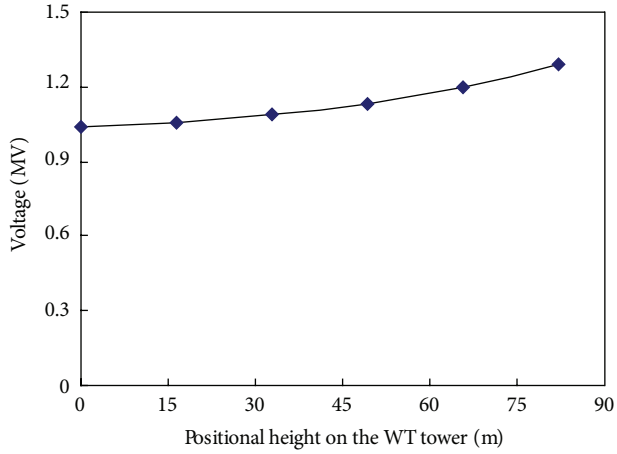

Figure 10: Peak potential distribution along the height of the tower.

WT5. Inner and outer radii of the power cable are 0.0135 m and 0.016 m, respectively. The burial depth of the power cable is 1 m, and the grounding grid of the substation has a grounding resistance of 10 Ω. The power cable between two successive WTs or SS and WT5 is divided into 5 segments. Each segment is represented by a π-type circuit [17]. The peak earth potential distribution in the interconnected grounding system is shown in Figure 12, where the peak earth potential at each WT or SS is expressed by the percentage of the maximum earth potential. As expected, the maximum earth potential always appears at WT3, where the lightning strikes. The earth potential rise at WT2 and WT4 is more serious than that at WT1 and WT5, for WT2 and WT4 are adjacent to WT3. This transferred overvoltage is very harmful to the neighboring WT transformers and the power cables.

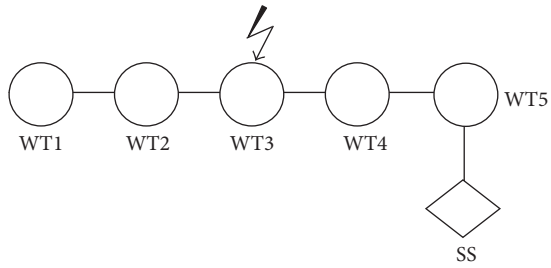

Figure 11: Layout of the interconnected grounding system.

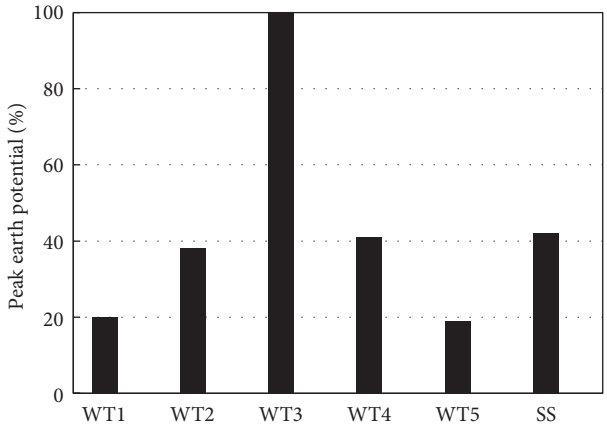

Figure 12: Earth potential distribution in the interconnected grounding system.

In view of the results obtained above, the efficient protective measures against the transient potential rise on the tower body and the transferred overvoltage in the interconnected grounding system need to be taken for the multimegawatt WTs [18].

6. Conclusions

The lightning transient analysis has been carried out in this paper for the WT towers. The subdividing treatment of the large-sized continuous conducting shell allows a WT tower to be converted into a discrete multiconductor system. For calculating the electrical parameters of the branches in the multiconductor system, a set of analytical formulas have been given. These formulas have the capability of considering the electromagnetic coupling between the branches in different space positions. By means of the electrical parameters, the branch units are represented by the coupled π-type circuits and the equivalent discretization network is further built for the multiconductor system. The solution of lightning transients is then obtained from the equivalent discretization network. The proposed algorithm can take into account the structural feature of actual large-sized WT towers and give the lightning transient responses in different parts on the tower body. The laboratory measurement has been made by a reduced-scale tower. A better agreement appears between simulated and measured potential waveforms. The applicability of the proposed algorithm to the lightning transient analysis has also been examined by an actual example of a 2.5 MW WT tower and its interconnected grounding system.

Acknowledgments

This work was financially supported by the National Natural Science Foundation of China under Award no. 509770926 and the Fundamental Research Funds for the Central Universities under Award no. 2012JBZ006. The author expresses his thanks to the foundation committees.

References

[1] P. Sarajcev and R. Goic, "A review of current issues in state-of-art of wind farm overvoltage protection," *Energies*, vol. 4, no. 4, pp. 644–668, 2011.

[2] D. Romero, J. Montany, and A. Candela, "Behavior of the wind-turbines under lightning strikes including nonlinear grounding system," in *Proceedings of the International Conference on Renew Energy and Power Quality*, September 2004.

[3] Z. Haixiang and W. Xiaorong, "Overvoltage analysis of wind turbines," *Power System Technology*, vol. 24, no. 5, pp. 27–29, 2006.

[4] X. Zhang and C. Liu, "Lightning transient modeling of wind turbine towers," *International Review of Electrical Engineering*, vol. 7, no. 1, pp. 3505–3511, 2012.

[5] X. Wang and X. Zhang, "Calculation of electromagnetic induction inside a wind turbine tower struck by lightning," *Wind Energy*, vol. 13, no. 7, pp. 615–625, 2010.

[6] C. R. Paul, *Inductance-Loop and Partial*, John Wiley & Sons, New York, NY, USA, 2010.

[7] P. L. Kalantrarov and L. A. Ceitlin, *Inductance Calculation*, Energy Press, Moscow, Russia, 1992.

[8] M. M. Al-Asadi, A. P. Duffy, A. J. Willis, K. Hodge, and T. M. Benson, "A simple formula for calculating the frequency-dependent resistance of a round wire," *Microwave and Optical Technology Letters*, vol. 19, no. 2, pp. 84–87, 1998.

[9] M. B. Kostenko, *Analysis of Lightning Protection Reliability of Substations*, Science Press, Moscow, Russia, 1991.

[10] U. Y. Iosseli, A. S. Kothanov, and M. G. Stlyrski, *Capacitance Calculation*, Energy Press, Moscow, Russia, 1990.

[11] X. Zhang, "A circuit approach to the calculation of lightning transients in cage-like multiconductor systems," *International Journal of Electrical Engineering Education*, vol. 47, no. 2, pp. 213–222, 2010.

[12] J. Beiza, S. H. Hosseinian, and B. Vahidi, "Multiphase transmission line modeling for voltage sag estimation," *Electrical Engineering*, vol. 92, no. 3, pp. 99–109, 2010.

[13] H. W. Dommel, *Electromagnetic Transients Program Theory Book*, BPA, Portland, Ore, USA, 1995.

[14] W. Shi, *Overvoltage Calculation in Power Systems*, High Education Press, Beijing, China, 2009.

[15] F. Napolitano, M. Paolone, A. Borghetti et al., "Models of wind-turbine main-shaft bearings for the development of specific lightning protection systems," *IEEE Transactions on Electromagnetic Compatibility*, vol. 53, no. 1, pp. 99–107, 2011.

[16] National Standard GB, 50057-2010, *Design Code for Lightning Protection of Structures*, China Planning Press, Beijing, China, 2010.

[17] E. Pyrgioti and V. Bokogiannis, "Lightning impulse performance of a wind generator grounding grid considering soil ionization," in *Proceedings of the 7th Asia-Pacific International Conference on Lightning (APL '11)*, pp. 103–107, November 2011.

[18] IEC61400-24, "Wind Turbine Generation System-24: Lightning Protection," Ed. 1.0, IEC, Geneva, Switzerland, 2010.

Hindawi Publishing Corporation
Mathematical Problems in Engineering
Volume 2013, Article ID 461983, 8 pages
http://dx.doi.org/10.1155/2013/461983

Research Article

Multistep Wind Speed Forecasting Based on Wavelet and Gaussian Processes

Niya Chen,[1] Zheng Qian,[2] and Xiaofeng Meng[2]

[1] *Key Laboratory of Precision Opto-Mechatronics Technology, Ministry of Education, Beihang University, Beijing 100191, China*
[2] *School of Instrument Science and Opto-Electronics Engineering, Beihang University, Beijing 100191, China*

Correspondence should be addressed to Niya Chen; pekiny@aspe.buaa.edu.cn

Received 19 April 2013; Revised 10 July 2013; Accepted 10 July 2013

Academic Editor: Ming-Hung Hsu

Accurate wind speed forecasts are necessary for the safety and economy of the renewable energy utilization. The wind speed forecasts can be obtained by statistical model based on historical data. In this paper, a novel W-GP model (wavelet decomposition based Gaussian process learning paradigm) is proposed for short-term wind speed forecasting. The nonstationary and nonlinear original wind speed series is first decomposed into a set of better-behaved constitutive subseries by wavelet decomposition. Then these subseries are forecasted respectively by GP method, and the forecast results are summed to formulate an ensemble forecast for original wind speed series. Therefore, the previous process which obtains wind speed forecast result is named W-GP model. Finally, the proposed model is applied to short-term forecasting of the mean hourly and daily wind speed for a wind farm located in southern China. The prediction results indicate that the proposed W-GP model, which achieves a mean 13.34% improvement in RMSE (Root Mean Square Error) compared to persistence method for mean hourly data and a mean 7.71% improvement for mean daily wind speed data, shows the best forecasting accuracy among several forecasting models.

1. Introduction

Wind power is one of the fastest-developing renewable energy sources of which the current total capacity around the world is approximately 282 gig watts (GW) till the end of 2012, with a growing rate around 20% [1]. However, the variable and uncontrollable characteristics of wind pose several operational challenges. Thus, the wind power forecasting is an essential process for the wind farm units' maintenance and energy reserves scheduling [2, 3].

Since wind power is a function of wind speed, the wind power forecasts basically depend on wind speed forecasts. The short-term wind speed forecasting, of which the prediction horizon is from 1 hour to 3 days, is critical to minimize scheduling errors which impact grid reliability and market based ancillary service costs. Broadly speaking, there are two statistical approaches for short-term wind speed prediction: regression models contain Numerical Weather Prediction (NWP) data as inputs and time series based methods which only use historical data to obtain prediction results. The former downscales information from global meteorological model to wind farm location therefore got inputs to regression model which estimate the future wind and have advantages in multihour (from several hours to dozens of hours) ahead prediction [4–6], while the latter use only historical wind speed data to build models and perform better in multistep ahead (usually 1–4 hours ahead for mean hourly wind data or several days ahead for mean daily data) prediction. Since the combination of NWP data requires long computational time (usually several hours) and does not show advantage in multistep ahead forecasts, models built only based on historical data are preferred for this prediction horizon. Time series based models for multistep wind forecasting have been investigated deeply and developed based on different methodologies, such as autoregressive integrated moving average [7, 8], Kalman filter [9, 10], artificial neural network [11, 12], and support vector machine methods [13].

Recently, wavelet decomposition method has been applied to establish different hybrid wind speed forecasting models. The main contribution of wavelet transform is to decompose and reconstruct a wind speed series into a set

of better-behaved constitutive series. Then each sub-series can be separately predicted by a suitable model according to its feature; hence, the new hybrid model improves the forecasting accuracy. Wavelet combined methods can be found in [14–16]. Liu et al. proposed a hybrid method based on the methods of wavelet and classical time series analyses to predict short-term wind speed and wind power, which gained more accurate simulation results than classical time series method and BP network method, especially with multistep forecasting and jumping data [14]. Catalão et al. presented a novel forecasting method by combining artificial neural networks with wavelet transform. Results from a real-world case study, which used wind speed data in Portugal, show the efficiency of this model [15]. An et al. proposed a prediction model for wind farm power forecasting by combining the wavelet transform, chaotic time series, and GM(1,1) method [16].

As an effective statistical method, Gaussian Process (GP) has been applied broadly in many domains, including wind energy prediction. Jiang et al. focused on very short-term (<30 min) wind speed prediction using GPs [17]. They evaluated their model on real-world datasets and found that the GP performs better than ARMA (a simpler variant of ARIMA) and Mycielski algorithms [18].

In this paper, a novel hybrid forecasting approach is proposed based on wavelet method and Gaussian Processes (GPs) for multiple steps ahead wind speed prediction. Compared with earlier work, this paper has the following contributions. First, the novel combination of wavelet method and GP (W-GP model) managed to improve forecasting accuracy, especially when forecast step grows. Second, lots of simulation work was done to determine the best W-GP model by comparing the forecasting error of several W-GP models decomposed by different levels. Third, not only mean hourly wind speed but also mean daily wind speed is forecasted by proposed model in this paper.

Actual wind speed data of 1 year from a wind farm in southern China is used to examine the proposed W-GP model. The proposed model is compared with persistence, MLP (Multilayer Perceptron) neural network, and the original GP approaches to demonstrate its effectiveness regarding forecast accuracy. The forecasting results are given and discussed hereinafter.

This paper is organized as follows. Section 2 presents the proposed W-GP approach to forecast wind speed. Section 3 first presents a case study of detailed forecast process based on W-GP model and then introduces three different criterions used to evaluate the forecasting accuracy, based on which the most suitable model for our database is finally chosen. Section 4 presents the large-scale simulation results for a real wind speed data set from a wind farm in southern China. Finally, Section 5 outlines the conclusions.

2. The Proposed W-GP Model

The proposed W-GP approach to forecast short-term wind speed is based on the hybrid of GP with wavelet method. The wavelet method is used to decompose the original wind speed series into a set of sub-series which can be analyzed easier. Then, GP method is used to forecast the future values for all those sub-series. In turn, through the inverse wavelet decomposition, finally the wind speed forecast value can be obtained by aggregating the forecast value of sub-series.

2.1. Wavelet Method. The wavelet method used here is to decompose a wind speed series into a set of sub-series. With the filtering effect of the wavelet decomposition, these sub-series present a better behaviour than the original wind power series and therefore can be analyzed clearer and predicted more accurately.

Wavelet method can be divided in two categories: continuous wavelet transform (CWT) and discrete wavelet transform (DWT) [19]. In CWT, a wavelet can be defined as function $\psi(t)$ with a zero mean:

$$\int_{-\infty}^{+\infty} \psi(t)\, dt = 0. \tag{1}$$

A signal can be decomposed into many series of wavelets with different scales a and translation b:

$$\psi_{a,b}(t) = \frac{1}{\sqrt{a}} \psi\left(\frac{t-b}{a}\right). \tag{2}$$

Thus, the wavelet transform of a signal $f(t)$ at translation b and scale a is defined by

$$wf(b,a) = \frac{1}{\sqrt{a}} \int_{-\infty}^{+\infty} f(t)\, \psi\left(\frac{t-b}{a}\right) dt. \tag{3}$$

The original signal $f(t)$ can be reconstructed by inverse wavelet transform:

$$f(t) = \int_{0}^{+\infty} \int_{-\infty}^{+\infty} \frac{1}{a^2} wf(b,a)\, \psi_{b,a}(t)\, dbda. \tag{4}$$

Different from CWT, when the mother wavelet is scaled and translated using certain scales and positions, it is known as the DWT, which is more efficient and just as accurate as the CWT. The definition is as follows:

$$W(m,n) = 2^{-(m/2)} \sum_{t=0}^{T-1} f(t)\, \phi\left(\frac{t - n\cdot 2^m}{2^m}\right), \tag{5}$$

where T is the length of the signal $f(t)$. The functions of the integer variables m and n ($a = 2^m$, $b = n\cdot 2^m$) are scaling and translation parameters, and t is the discrete time index.

2.2. Gaussian Process. Recently, there has been much activity concerning the application of Gaussian process to machine learning tasks. The systematic and detailed explanation of Gaussian process regression can be found in Rasmussen's book [20]; here we only provide a brief illustration on GP applied in regression.

A Gaussian process $f(x)$ can be completely specified by its mean function and covariance function, written as $f(x) \sim \mathrm{GP}(m(x), k(x,x'))$, where the mean function $m(x)$ and covariance function $k(x,x')$ are defined as follows:

$$\begin{aligned} m(x) &= E[f(x)] \\ k(x,x') &= E\left[(f(x) - m(x))\left(f(x) - m\left(x'\right)\right)\right]. \end{aligned} \tag{6}$$

Usually, the mean function is assumed to be zero, and the target variables are normalised to have zero mean.

Consider GP in a classic regression problem, assume x_i represents a feature vector of input space with dimension N, y_i represents the output value to be estimated, based on the training vectors' set $D = \{(x_i, y_i), i = 1, \ldots, n\}$, and the key point of GP regression method is to model the relationship between inputs and targets, that is, to build a function to satisfy

$$y_i = f(x_i) + \varepsilon_i. \tag{7}$$

The observed value y is assumed to be different from the function value $f(x)$ by additive noise ε, which is assumed to be an independent and identically distributed Gaussian distribution with zero mean and variance σ_n^2, that is, $\varepsilon \sim N(0, \sigma_n^2)$.

Note that y is a linear combination of Gaussian variables and, hence, is itself Gaussian. The prior on y becomes as follows:

$$\begin{aligned} E[y] &= E[f + \varepsilon] = 0, \\ \operatorname{cov}[y] &= K(X, X) + \sigma_n^2 I, \end{aligned} \tag{8}$$

where K is a matrix with elements $K_{ij} = k(x_i, x_j)$, which is also known as the kernel function.

Given a training set $D = (X, y)$, our goal is to make predictions of the target variable f_* for a new input x_*. Since we already have $p(y \mid X, k) = N(0, K + \sigma_n^2 I)$, the distribution with new input can be written as follows:

$$\begin{bmatrix} y \\ f_* \end{bmatrix} \sim \left(0, \begin{bmatrix} K(X, X) + \sigma_n^2 I & k(X, x_*) \\ k(x_*, X) & k(x_*, x_*) \end{bmatrix}\right), \tag{9}$$

where $k(X, x_*) = [k(x_1, x_*), \ldots, k(x_n, x_*)]$, and it can be shortened to k_*. Then according to the principle of joint Gaussian distribution, the prediction result of target is given by

$$\begin{aligned} \overline{f}_* &= k_*^T \left(K + \sigma_n^2 I\right)^{-1} y \\ V[f_*] &= k(x_*, x_*) - k_*^T \left(K + \sigma_n^2 I\right)^{-1} k_*. \end{aligned} \tag{10}$$

Now, the whole regression model based on Gaussian process is completed.

In the GP model for wind speed forecasting, we define the wind speed series as $\{d_n, n = 1, \ldots\}$, then the input vector x_i is constructed as $\{d_i, d_{i+1}, \ldots, d_{i+t-1}\}$; correspondingly the output value y_i is d_{i+t}. Therefore, the GP model can estimate the wind speed value at next time period based on historical data.

2.3. Process of W-GP Modelling. Most researches use symmetric WTs such as Symlet or Morlet for decomposition. However, this type of WT is not suitable for forecasting problem because in symmetric wavelet future information is also needed as well as previous information [19]. In this paper, a wavelet function of type Daubechies of order 4 (abbreviated as Db4), which is an asymmetric WT, is used to solve this problem.

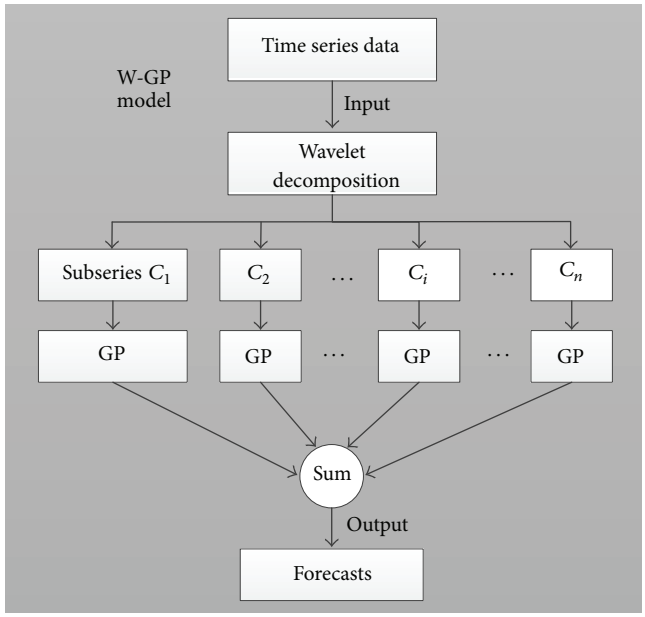

Figure 1: Structure of proposed W-GP model.

Table 1: Information of wind farm and its wind turbines.

Location	Installed capacity	Height	Number
Fujian	2000 kW	80 m	15

As shown in Figure 1, the modelling steps of the proposed W-GP method are described as follows.

(1) Use wavelet method to decompose original wind speed data series into a number of different sub-series (depending on level of decomposition) which can be analyzed and separately predicted. Denote these sub-series as $C_1, \ldots, C_n$.

(2) Build the prediction models for each sub-series based on GP method and estimate the multistep forecasting results.

(3) Through the inverse wavelet decomposition, attain final forecasting results for original wind speed series by aggregating the forecasting value of sub-series.

(4) Calculate the root mean square error (RMSE), the mean absolute error (MAE), and the mean absolute percentage error (MAPE) of forecasting results.

3. A Case Study of W-GP Model

A real-world dataset based on wind farm is used in this paper to evaluate our approach. The dataset is from a wind farm in Fujian province, a coastal area located in very southern China, where wind source is sufficient and variable, and the integration of wind farm is important.

As shown in Table 1, the tested wind farm contains 15 wind turbines, of which installed capacity is 2000 kW and

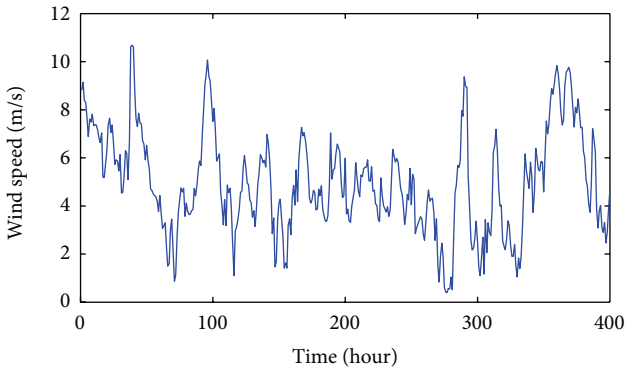

Figure 2: Original time series of wind speed.

turbine height is 80 m. With wind speed being measured consistently on different heights (70 m, 35 m, and 10 m) by a wind tower located in the centre of the wind farm, the data from the 70 m high sensor is chosen for calculation, since it is the nearest to turbine height. The original measured data has an interval of 10 mins, which we averaged into mean hourly and daily data for different forecast targets.

To illustrate the specific process of modelling and analyze the performance of W-GP model, in this section, we use the 1st-400th hours' data of each month as training set to build the model, the later ones as test set, and we obtain multihour ahead forecasting results.

3.1. Wavelet Decomposition. According to Section 2, if Daubechies-4 wavelet is employed to do n level discrete wavelet decomposition in simulation, the original wind speed series would be decomposed to $n + 1$ sub-series: one low-frequency section and other n high-frequency series. To facilitate the latter modelling, the low-frequency section is recorded as $\{x_{1t}\}$ series; correspondingly, the other high-frequency sub-series are recorded as $\{x_{2t}\} \cdots \{x_{(n+1)t}\}$.

Here, we decompose the actual wind speed data in February 2012 to the 3rd level as an example. The original wind speed series is shown in Figure 2, while the sub-series $(\{x_{1t}\}, \ldots, \{x_{4t}\})$ are plotted in Figure 3.

As shown in the figures previously, the original wind speed series is decomposed into a set of better-behaved constitutive series. Therefore, it is easier for sub-series to obtain better performance in forecasting and eventually get results with higher accuracy.

3.2. Wind Speed Forecasting. According to Section 2.3, after obtaining the sub-series by wavelet method, the prediction models for each sub-series should be built based on GP method. Then the final forecast value of original wind speed series can be attained by aggregating the forecasting results of sub-series.

Consequently, we calculate 1-hour-ahead forecasting based on GP model for $x_{1t}(1 \cdots 400)$, the result is recorded as $\widehat{x}_{1t}(1)$. Similarly, and we obtain 1-hour-ahead forecasting results of, $\{x_{2t}\} \cdots \{x_{4t}\}$, recorded as $\widehat{x}_{2t}(1), \ldots, \widehat{x}_{4t}(1)$. Then we aggregate the forecast value of sub-series by

$$\widehat{x}_t(1) = \widehat{x}_{1t}(1) + \widehat{x}_{2t}(1) + \cdots + \widehat{x}_{4t}(1), \tag{11}$$

where $\widehat{x}_t(1)$ represents the forecast result of the original wind speed series; thus, the final forecasting value is attained.

Correspondingly, calculate 1-hour-ahead forecasting for $x_t(2 \cdots 401), \ldots, x_t(60 \cdots 459)$; these 60 forecast values are shown in Figure 4(a), plotted by green star line.

Meantime, the basic GP model is applied on the same original wind speed data to obtain 60 forecast values. By subtracting from the actual wind speed value, the absolute value of forecasting error can be calculated. The comparison of the GP model and W-GP model's forecasting errors at each hour is shown in Figure 4(b).

As shown in Figure 4, it can be observed that W-GP model performs a better wind speed forecasting than the basic GP model at most of the time.

Since now we have one-hour-ahead forecasting value, it could be useful in the case of attaining several-hour-ahead forecasting value, based on $\{x_{1t}(2), \ldots, x_{1t}(400), \widehat{x}_{1t}(1)\}$ series to rebuild the GP model and calculate 1-hour-ahead forecasting again, that is, the 2-hour-ahead forecasting for $\widehat{x}_{1t}(1 \cdots 400)$, recorded as $\widehat{x}_{1t}(2)$. Similarly obtain 3-hour-ahead forecasting results based on $\{x_{1t}(3), \ldots, x_{1t}(400), \widehat{x}_{1t}(1), \widehat{x}_{1t}(2)\}$ series and multi-hour-ahead forecasting likewise.

The performance of multihour forecasting by proposed W-GP model can be observed in Figure 5, of which the upper part displays 2-hour-ahead forecasting curve, while the lower part presents the corresponding forecast error (absolute value).

It is clearly seen that at most of the forecast points, the W-GP model decreases forecast error of GP model, even more obvious than 1-hour-ahead prediction displayed previously. Therefore, it is reasonable to say that the hybrid W-GP model is effective and applicable in wind speed forecasting problem and has greater advantage when forecast step grows.

3.3. Forecasting Accuracy Evaluation. Clearly, accuracy is the most important criterion to compare the efficiency of alternative forecasting approaches. Therefore, different criteria are used here to evaluate the accuracy of the proposed approach. This accuracy is computed in function of the actual wind speed that occurred.

Three forecast error measures were employed for model evaluation and model comparison: the root mean square error (RMSE), the mean absolute error (MAE), and the mean absolute percentage error (MAPE). The error is defined as follows:

$$\begin{aligned} e_t &= y_t - \widehat{y}_t, \\ \text{RMSE} &= \sqrt{\frac{1}{n}\sum_{i=1}^{n} e_i^2}, \\ \text{MAE} &= \frac{1}{n}\sum_{i=1}^{n} |e_i|, \\ \text{MAPE} &= \frac{1}{n}\sum_{i=1}^{n} \left| \frac{y_i - \widehat{y}_i}{y_i} \times 100 \right|, \end{aligned} \tag{12}$$

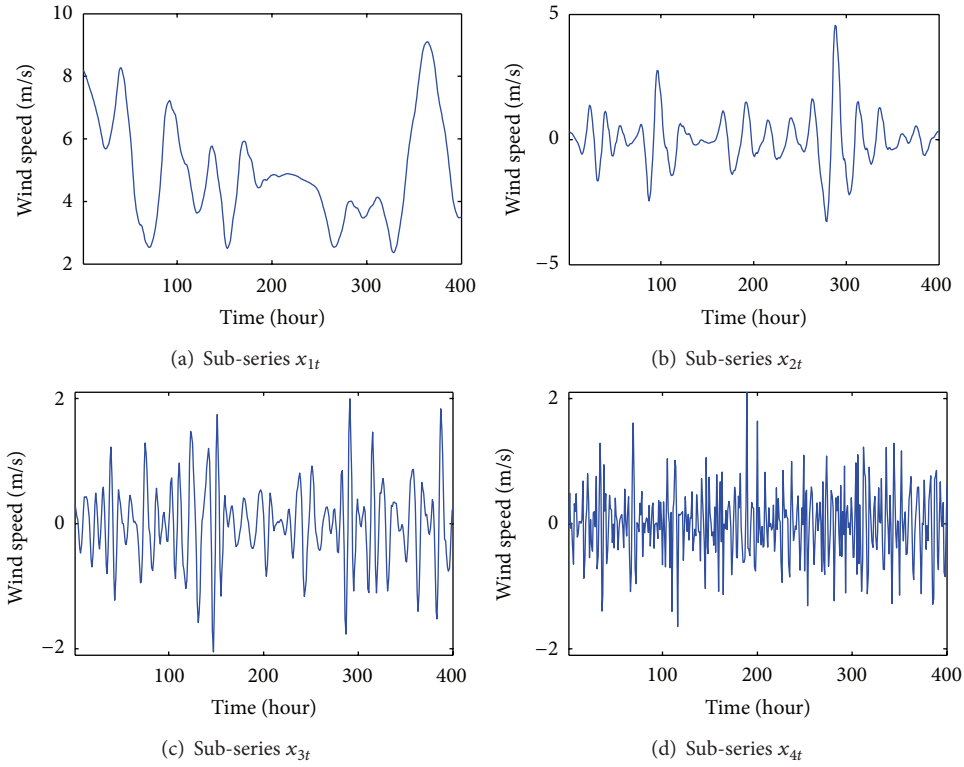

FIGURE 3: Decomposition results of the original series.

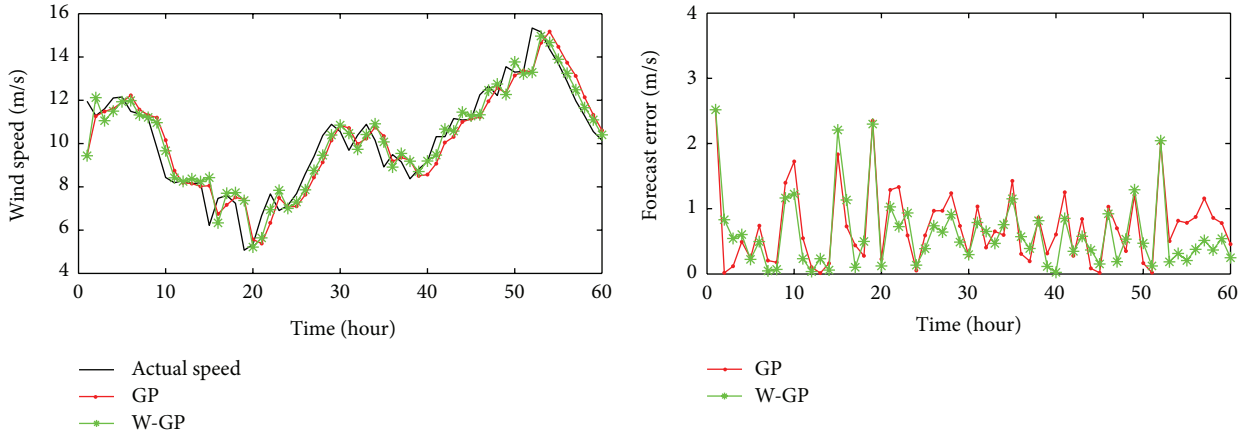

FIGURE 4: One-hour-ahead forecast results.

where y_t represents the actual observation value at hour t and $\hat{y}_t$ represents the forecast value for the same period. n is the number of forecasted hours.

3.4. Comparison of Different Decomposition Levels. Currently, there is still no specific principle of determining wavelet decomposition level of W-GP model yet, though various decomposition levels of proposed forecast model may lead to different forecasting performances. Therefore, we should recognise the most adequate decomposition level for our database by analyzing simulation results.

As shown in Figure 6, it is obvious that the forecasting error is highly relevant to decomposition level. Furthermore, the error is the minimum while the discrete wavelet decomposition level of Daubechies-4 wavelet is 3. Therefore, in this paper, the 3 level decomposed W-GP model is applied through the whole simulation process.

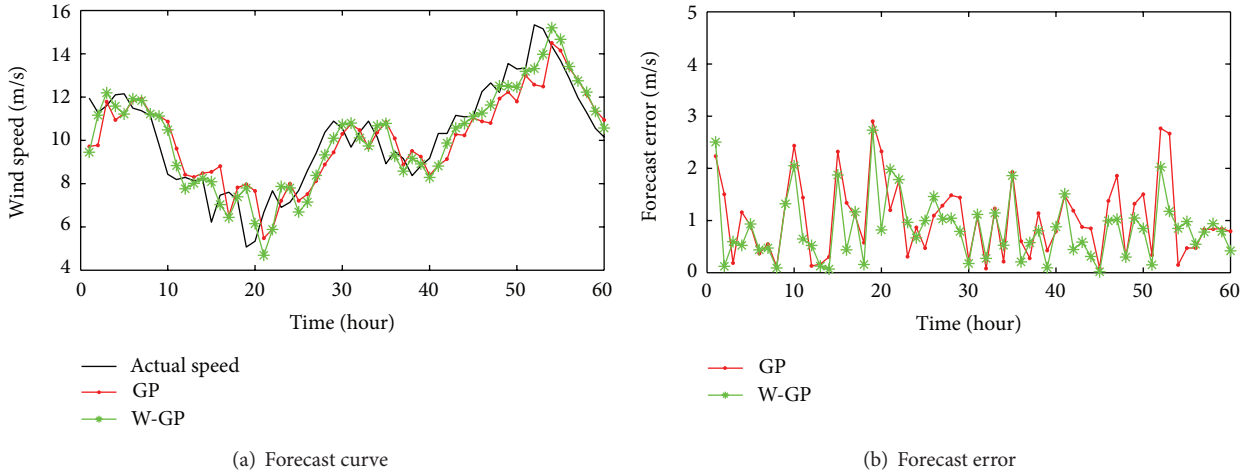

(a) Forecast curve (b) Forecast error

Figure 5: Two-hour-ahead forecast results.

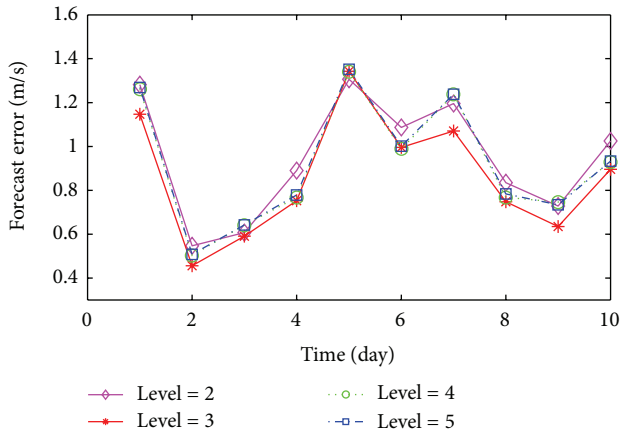

Figure 6: One-hour-ahead forecast error (averaged by 24 hour).

4. Wind Speed Forecasting Results

The actual measured wind speed data from a wind farm in southern China through a whole year has been applied in simulation. Since sometimes the wind speed data may be invalid because of anemometer fault, a preprocess was taken to modify invalid speed data by interpolation, after which the whole dataset contains 2 sub-sets: D1, 8700 points of mean hourly data and D2, 362 points of mean daily data. In order to reasonably testify the performance of proposed model, the sub-set D1 was divided into 12 parts; each part was separately modeled, using the first 400 data as training set and the rest as test set. Similarly, the sub-set D2 was divided into 2 parts, using the first 160 data of each part as training set, with the rest as test set. The short-term forecasting results, of both mean hourly and mean daily wind speed, are presented and analyzed in the following.

Besides the basic GP method, the other models represented as comparison in this paper are persistence and MLP methods. Persistence method is a quite simple method which only uses the current value as forecast and is impressively effective for short-term prediction and therefore is considered as the most classical benchmark in wind forecasting area. The MLP network is a very popular machine learning method and has been applied in wind power forecasting widely. We established MLP model based on the same wind speed dataset and obtained simulation results to compare with the proposed W-GP model.

Table 2: Comparison of forecast accuracy for mean hourly wind speed.

	Number of forecasting steps (hour)				
	1	2	3	4	Average
	RMSE (m/s)				
Persistence	1.0028	1.5272	1.9233	2.2231	1.6691
MLP	1.0075	1.5697	1.8911	2.1545	1.6557
GP	1.0305	1.4741	1.8219	2.1572	1.6209
W-GP	0.9605	1.2672	1.6041	1.9539	1.4464
	MAE (m/s)				
Persistence	0.7431	1.1399	1.5271	1.7293	1.2849
MLP	0.7647	1.2168	1.4515	1.7095	1.2856
GP	0.7675	1.1280	1.4200	1.7035	1.2548
W-GP	0.7204	0.9565	1.2093	1.5320	1.1046
	MAPE (%)				
Persistence	11.0534	16.9723	26.3192	26.7187	20.2659
MLP	11.9014	19.0887	22.3889	27.7471	20.2815
GP	11.2190	17.4187	23.1315	28.4284	20.0494
W-GP	11.2430	14.3263	18.3666	23.9891	16.9812

According to Section 3.3, the evaluation index applied in this paper is the root mean square error (RMSE), the mean absolute error (MAE), and the mean absolute percentage error (MAPE). The comparison among the forecasting accuracy of persistence method, MLP, basic GP, and W-GP models is shown in Tables 2 and 3.

Table 2 shows the forecasting errors of persistence method, MLP, basic GP, and proposed W-GP models for mean hourly wind speed data. It can be observed that though

Table 3: Comparison of forecast accuracy for mean daily wind speed.

	Number of forecasting steps (day)			
	1	2	3	Average
	RMSE (m/s)			
Persistence	1.6069	2.2461	2.2985	2.0505
MLP	2.2651	2.5642	2.4331	2.4208
GP	1.9024	2.1317	2.0892	2.0411
W-GP	1.6110	2.0241	2.0421	1.8924
	MAE (m/s)			
Persistence	1.2979	1.8150	1.8368	1.6499
MLP	1.6953	1.9832	2.0775	1.9187
GP	1.4838	1.7028	1.7227	1.6364
W-GP	1.2775	1.6355	1.6357	1.5162
	MAPE (%)			
Persistence	29.9989	49.0180	42.9931	40.6700
MLP	47.7015	52.4184	56.1476	52.0892
GP	40.8972	38.6730	47.5696	42.3799
W-GP	30.2413	39.4201	44.0601	37.9072

forecast performance gets worse when prediction time grows, normally basic GP method shows a better forecast accuracy than MLP model, and comparing with GP method, the proposed W-GP model presents positive error improvements over the entire forecast horizon:

$$\text{Improvement} = \frac{\left(e_{\text{Persistence}} - e_{\text{proposed}}\right)}{e_{\text{Persistence}}} \times 100\%. \quad (13)$$

With respect to the basic persistence method, the improvement of W-GP model in RMSE, computed by formula (13), ranges from a maximum of 17.02% to a minimum of 4.22% with a mean value of 13.34%.

Table 3 shows the forecasting errors of the same models for mean daily wind speed data. Here, the MLP model works the worst, which is understandable because of the small scale of training set. Fortunately, Gaussian process based models maintain a stable performance without needing large-scale dataset to train appropriate parameters that is why the proposed model still shows an obvious advantage than the other forecasts. Comparing with the basic persistence method, the improvement of W-GP model in RMSE, computed by formula (13), ranges from a minimum of −0.26% to a maximum of 11.16% with a mean value of 7.71%. Although for 1-day-ahead forecast, the W-GP model is slightly worse than persistence method, the other results with larger forecast step strongly reveal the efficiency of proposed W-GP model.

Since the wavelet method decomposes the original wind speed series into a set of better-behaved constitutive series, the proposed W-GP model achieves a higher level of accuracy at short-term wind speed forecast. What is more, the improvement approached by wavelet decomposition is getting more obvious as forecast step grows. However, as the prediction time grows, the forecast accuracy of each model decreases severely. Anyway, it is completely natural that models based only on historical data would behave this way considering the uncontrollable and unstable inhesion of wind.

Though due to the variable nature of wind, the forecast performance of all the models listed in the tables decade as the predict time grows, the proposed W-GP model continuously shows a better forecasting accuracy and, eventually, represents an obvious advantage.

5. Conclusion

In this paper, first, a novel historical forecast model is proposed based on the wavelet method and Gaussian Process (GP) method in order to predict multistep ahead wind speed. Second, based on analysis of W-GP model's forecasting error series, an appropriate level of wavelet decomposition is chosen to get the most accurate model. Finally, real-world dataset is applied with the proposed model to validate its efficiency.

The simulation results convincingly reveal the effectiveness and accuracy of proposed model for short-term wind speed forecasting, which achieves a mean 13.34% improvement in RMSE comparing to persistence method for mean hourly data and a mean 7.71% improvement for mean daily wind speed data.

Considering the unstability of wind, there must be a limit on single historical methodology. A tendency of future method is combinatorial models, of which the effective way of combination between methods is worth more research.

Acknowledgment

This study is supported by the National Fund for Creative Groups of China (Grant no. 61121003).

References

[1] Global Wind Energy Council, Global wind statistics 2012, http://www.gwec.net/wp-content/uploads/2013/02/GWEC-PRstats-2012_english.pdf.

[2] A. Costa, A. Crespo, J. Navarro, G. Lizcano, H. Madsen, and E. Feitosa, "A review on the young history of the wind power short-term prediction," *Renewable and Sustainable Energy Reviews*, vol. 12, no. 6, pp. 1725–1744, 2008.

[3] M. Lei, L. Shiyan, J. Chuanwen, L. Hongling, and Z. Yan, "A review on the forecasting of wind speed and generated power," *Renewable and Sustainable Energy Reviews*, vol. 13, no. 4, pp. 915–920, 2009.

[4] M. G. De Giorgi, A. Ficarella, and M. Tarantino, "Assessment of the benefits of numerical weather predictions in wind power forecasting based on statistical methods," *Energy*, vol. 36, no. 7, pp. 3968–3978, 2011.

[5] J. Ignacio, L. Alfredo, M. Claudio et al., "Comparison of two new short-term wind-power forecasting systems," *Renewable Energy*, vol. 34, no. 7, pp. 1848–1854, 2009.

[6] S. Salcedo-Sanz, A. M. P. Ángel M. Pérez-Bellido, E. G. Ortiz-García, A. Portilla-Figueras, L. Prieto, and D. Paredes, "Hybridizing the fifth generation mesoscale model with artificial neural networks for short-term wind speed prediction," *Renewable Energy*, vol. 34, no. 6, pp. 1451–1457, 2009.

[7] E. Erdem and J. Shi, "ARMA based approaches for forecasting the tuple of wind speed and direction," *Applied Energy*, vol. 88, no. 4, pp. 1405–1414, 2011.

[8] H. Liu, E. Erdem, and J. Shi, "Comprehensive evaluation of ARMA-GARCH approaches for modeling the mean and volatility of wind speed," *Applied Energy*, vol. 88, no. 3, pp. 724–732, 2011.

[9] D. Pan, H. Liu, and Y. Li, "Optimization algorithm of short-term multi-step wind speed forecast," *Proceedings of the Chinese Society of Electrical Engineering*, vol. 28, no. 26, pp. 87–91, 2008 (Chinese).

[10] P. Louka, G. Galanis, N. Siebert et al., "Improvements in wind speed forecasts for wind power prediction purposes using Kalman filtering," *Journal of Wind Engineering and Industrial Aerodynamics*, vol. 96, no. 12, pp. 2348–2362, 2008.

[11] E. Cadenas and W. Rivera, "Short term wind speed forecasting in La Venta, Oaxaca, México, using artificial neural networks," *Renewable Energy*, vol. 34, no. 1, pp. 274–278, 2009.

[12] S. A. P. Kani and M. M. Ardehali, "Very short-term wind speed prediction: a new artificial neural network-Markov chain model," *Energy Conversion and Management*, vol. 52, no. 1, pp. 738–745, 2011.

[13] S. Sancho, G. Emilio, M. Angel et al., "Short term wind speed prediction based on evolutionary support vector regression algorithms," *Expert Systems with Applications*, vol. 38, no. 4, pp. 4052–4057, 2011.

[14] H. Liu, H. Tian, C. Chen, and Y. Li, "A hybrid statistical method to predict wind speed and wind power," *Renewable Energy*, vol. 35, no. 8, pp. 1857–1861, 2010.

[15] J. P. S. Catalão, H. M. I. Pousinho, and V. M. F. Mendes, "Short-term wind power forecasting in Portugal by neural networks and wavelet transform," *Renewable Energy*, vol. 36, no. 4, pp. 1245–1251, 2011.

[16] X. An, D. Jiang, C. Liu, and M. Zhao, "Wind farm power prediction based on wavelet decomposition and chaotic time series," *Expert Systems with Applications*, vol. 38, no. 9, pp. 11280–11285, 2011.

[17] X. Jiang, B. Dong, L. Xie, and L. Sweeney, "Adaptive Gaussian process for short-term wind speed forecasting," in *Proceedings of the 19th European Conference on Artificial Intelligence (ECAI '10)*, H. Coelho, R. Studer, and M. Wooldridge, Eds., Lisbon, Portugal, August 2010.

[18] F. O. Hocaoğlu, M. Fidan, and O. N. Gerek, "Mycielski approach for wind speed prediction," *Energy Conversion and Management*, vol. 50, no. 6, pp. 1436–1443, 2009.

[19] H. T. Nguyen and I. T. Nabney, "Short-term electricity demand and gas price forecasts using wavelet transforms and adaptive models," *Energy*, vol. 35, no. 9, pp. 3674–3685, 2010.

[20] C. E. Rasmussen and C. K. I. Williams, *Gaussian Processes for Machine Learning*, MIT Press, Cambridge, Mass, USA, 2006.

Hindawi Publishing Corporation
Mathematical Problems in Engineering
Volume 2013, Article ID 982597, 13 pages
http://dx.doi.org/10.1155/2013/982597

Review Article

Modeling and Control of Wind Turbine

Luis Arturo Soriano,[1] Wen Yu,[1] and Jose de Jesus Rubio[2]

[1] *Departamento de Control Automático, CINVESTAV, National Polytechnic Institute, 07360 Mexico City, DF, Mexico*
[2] *Sección de Estudios de Posgrado e Investigación, ESIME Azcapotzalco, National Polytechnic Institute, 02250 Mexico City, DF, Mexico*

Correspondence should be addressed to Wen Yu; yuw@ctrl.cinvestav.mx

Received 15 April 2013; Revised 23 June 2013; Accepted 26 June 2013

Academic Editor: Ming-Hung Hsu

In recent years, the energy production by wind turbines has been increasing, because its production is environmentally friendly; therefore, the technology developed for the production of energy through wind turbines brings great challenges in the investigation. This paper studies the characteristics of the wind turbine in the market and lab; it is focused on the recent advances of the wind turbine modeling with the aerodynamic power and the wind turbine control with the nonlinear, fuzzy, and predictive techniques.

1. Introduction

Wind energy is gaining increasing importance worldwide. The processes of industrialization and economic development require energy. Fuels are the main energy resource in the world and are at the center of the energy demands [1–4]. Wind turbines using aerodynamic lift can be divided according to the orientation of the axis of rotation on the horizontal axis and vertical axis turbines. The horizontal axis or propeller-type approach currently dominates wind turbine applications [5]. A horizontal axis wind turbine comprises a tower; a nacelle is mounted on top of the tower. The nacelle contains the generator, gearbox, and rotor. There are several mechanisms to signal the gondola to the wind direction or to move the nacelle of the wind in the case of high wind speeds. In small turbines, the rotor and nacelle are oriented into the wind with a tail vane. In larger turbines, the gondola with the rotor is electrically yawed out of the wind in or in response to a signal from a vane.

Horizontal axis wind turbines typically use a different number of blades, depending on the purpose of the wind turbine. Turbines with two sheets or three blades are generally used for power generation. The most common design of modern turbines is based on the horizontal shaft structure. This design of wind turbine towers is assembled as shown in Figure 1. The role of the tower is to raise the wind turbine above the ground to intercept the strongest winds to get more energy. Wind energy has evolved rapidly during the past three decades with increasing diameters of the rotor and the use of sophisticated power electronics to allow operation at rotor speed varies; see Figure 2.

These turbines are operated such tightly that when you turn the rotor plane to be positioned directly upwind of the tower through the use of a yaw motor, that rotates the entire nacelle (housing for all components in the upper tower). Wind passes through the turbine blades and this then produces lift inducing a torque [2, 6]. The aerodynamic torque captured by the blades is transferred to the hub which connects the blades to a power train and after a generator. Typically, the drive train includes a scale gearbox rotation speed and torque levels that are suitable for the configuration of the generator. Although the gearbox is still used in most turbines, direct drive wind turbines developed to connect the shaft of the generator directly with one axis to increase reliability and reduce maintenance costs are largely associated with gearbox failures.

The aim of this survey is to address all the aspects involved in wind turbines. Compared to the previous reviews, this literature discusses the dynamic modeling of wind turbines, actuators, and wind turbines-actuator combined system in detail using both linear and nonlinear methods. The paper deals with different control strategies including the nonlinear,

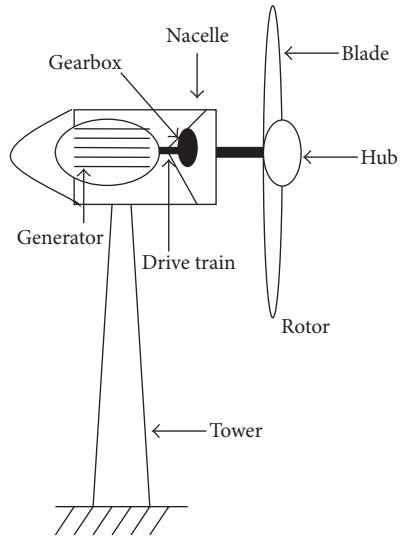

Figure 1: A horizontal axis wind turbine [7, 8].

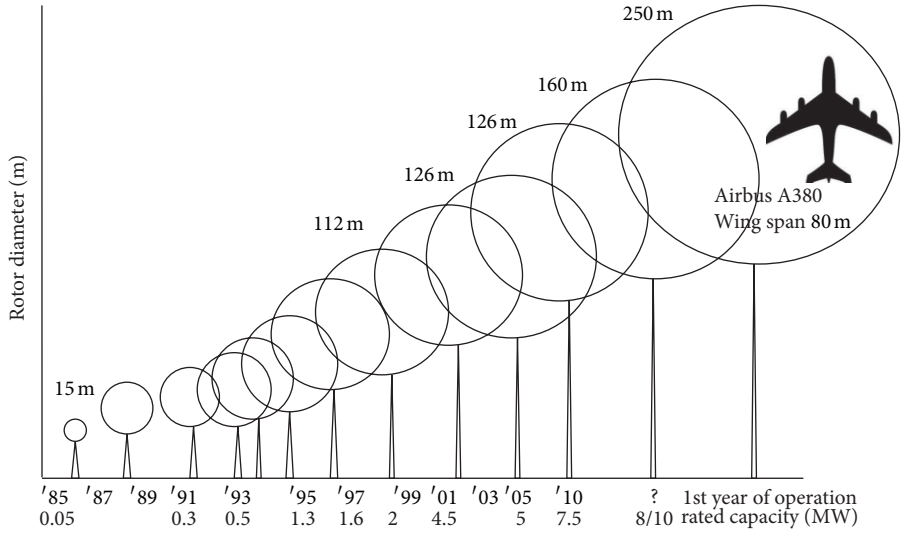

Figure 2: Evolution of the wind turbine dimensions.

fuzzy logic, and predictive control techniques. The survey concludes with some of the observations noticed throughout the review.

2. Wind Turbine Structure

The wind turbines can be classified based on thier orientation and thier axis of rotation, into horizontal axis wind turbines (HAWT) and vertical axis wind turbines (VAWT), which can be installed on the land or sea [1, 3]. The HAWT feature higher wind energy conversion efficiency due to the blade design and access to stronger wind, but they need a stronger tower to support the heavy weight if the nacelle and its installation cost is higher. The VAWT have the advantage of lower installation; however, their wind energy conversion efficiency is lower due to the weaker wind on the lower portion of the blades and limited aerodynamic performance of the blades [9]. A comparison between the horizontal and vertical axis wind turbines is summarized in Table 1.

Another form to classify the wind turbines is by speed control methods and power control methods. The wind energy conversion is divided into fixed and variable speeds [10]. As the name suggests, fixed speed wind turbines (FSWT) rotate at almost a constant speed, which is determined by the gear ratio, grid frequency, and number of poles of the generator. The maximum conversion efficiency can be achieved only at a given wind speed, and the system efficiency degrades at other wind speeds. The wind turbine is protected by aerodynamic control of the blades from possible damage caused by high wind gusts. On the other hand, variable speed wind turbines (VSWT) can achieve maximum energy conversion efficiency over a wide range of wind speeds. The turbine can continuously adjust its rotational speed according to the wind speed. In doing so, the tip speed radio which is the

Table 1: Properties of HAWT over VAWT.

	Advantages
HAWT	(i) Higher wind energy conversion efficiency (ii) Access to stronger wind due to high tower
VAWT	(i) Lower installation cost and easier maintenance due to the ground level gearbox and generator (ii) Operation independent of wind direction
	Disadvantages
HAWT	(i) Higher installation cost, stronger tower to support heavy weight of nacelle (ii) The orientation is required
VAWT	(i) Lower wind energy conversion efficiency (ii) Higher torque fluctuations and prone to mechanical vibrations

ratio of the blade tip speed to the wind speed can be kept at an optimal value to achieve the maximum power conversion efficiency at different wind speeds. A comparison between the fixed speed wind and variable speed turbines is summarized in Table 2.

2.1. Generator. Basically, a wind turbine can be equipped with any type of three-phase generator. Today, the demand for the grid-compatible electric current can be met by frequency converters when the generator supplies the alternating current (AC) of variable frequency or direct current (DC). Synchronous and asynchronous generators are the most common devices that are used in wind turbines [1, 3, 5, 11–14], as shown in Figures 3, 4, 5, and 6. They are classified into four types:

(1) asynchronous (induction) generator:

  (i) squirrel cage induction generator (SCIG) [15, 16]; see Figure 3,
  (ii) wound rotor induction generator (WRIG) [11, 17, 18]; see Figure 4,

(2) synchronous generator:

  (i) permanent magnet synchronous generator (PMSG) [19]; see Figure 5,
  (ii) wound rotor synchronous generator (WRSG) [20]; see Figure 6,

(3) other types of potential interest:

  (i) high-voltage generator (HVG) [21, 22],
  (ii) switch reluctance generator (SRG) [23, 24],
  (iii) transverse flux generator (TFG) [25, 26].

Wind turbine configurations can also be classified with both the speed control and power control criterion [10]; see Table 3.

The advantages and disadvantages of these typical wind turbine configurations are as follows:

Table 2: Advantages and disadvantages of FSWT and VSWT [9].

	Advantages
FSWT	(i) Simple, robust, reliable (ii) Low cost and maintenance
VSWT	(i) High energy conversion, efficiency (ii) Improved power quality (iii) Reduced mechanical stress
	Disadvantages
FSWT	(i) Relatively low energy conversion efficiency (ii) High mechanical stress (iii) High power fluctuations to the grid
VSWT	(i) Additional cost and losses due to use of converters (ii) More complex control system

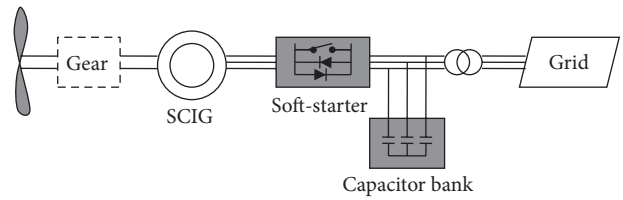

Figure 3: A. Wind Turbine with a Squirrel Cage Induction Generator [5].

(A) *Fixed speed*: This configuration denotes the fixed speed wind turbine with an SCIG directly connected to the grid via a transformer [21, 23].

  (A0) *Passive Stall Control*: This is the conventional concept applied by many Danish wind turbine manufacturers during the years 1980 and 1990, that is, a postwindward-regulated three-bladed wind turbine concept. It has been very popular because of its relatively low cost, its simplicity, and robustness. Passive stall controlled wind turbines cannot start assisted conduct, which means that the power of the turbine cannot be controlled during the connection sequence [18, 20].

  (A1) *Pitch control*: This also has been present in the market. The main advantage is that it facilitates power control capacity, the start, and emergency stop control. Its main drawback is that, at high wind speeds, even small variations in wind speed result in large variations in output power. The pitch mechanism is not fast enough to avoid such power fluctuations. For releasing the sheet, the slow variations in wind can compensate; nevertheless, this is not possible in the case of gusts [17, 25].

  (A2) *Active stall control*: It has recently become popular. This configuration basically maintains all the features of power quality controlled system shutdown. The improvements are in a better utilization of the overall system as a result of using active stall control. The flexible coupling of the

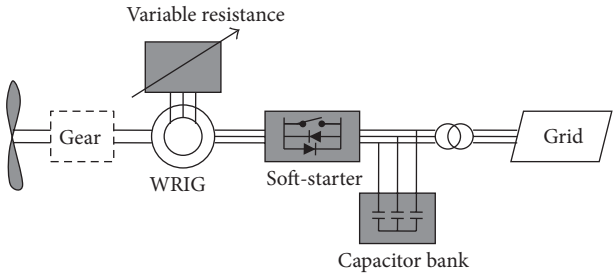

Figure 4: B. Wind Turbine with a Wound Rotor Induction Generator [5].

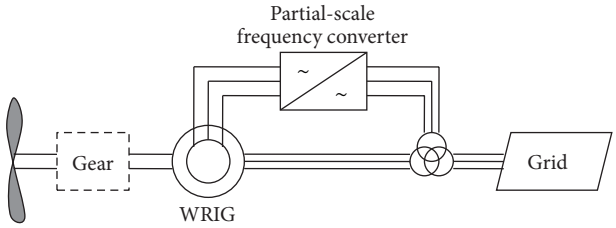

Figure 5: C. Wind Turbine with a Permanent Magnet Synchronous Generator [5].

blades to the hub also facilitates emergency stop and startups. A disadvantage is the highest price that raises the pitch mechanism and controller [15, 24].

(B) *Limited variable speed*: This configuration corresponds to the limited variable speed wind turbine with variable generator rotor resistance. It uses a WRIG [26].

(C) *Variable speed with partial-scale frequency converter*: This configuration, known as the DFIG, corresponds to the limited variable speed of the wind turbine with a WRIG and partial-scale frequency converter on the rotor circuit [19].

(D) *Variable speed with full-scale frequency converter*: This configuration corresponds to the full variable speed wind turbine, with the generator being connected to the grid through a full-scale frequency converter. The frequency converter performs the reactive power compensation and the smoother grid connection. The generator can be excited electrically by a WRSG, WRIG, or PMSG [11].

Therefore, as illustrated in Table 3, Type B0, Type B2, Type C0, Type C2, Type D0, and Type D2 are not used in today's wind turbine industry [5].

2.2. Soft Starter. The soft starter is a component of simple and inexpensive electrical power used in fixed speed wind turbines during grid connection; see Figures 3 and 4. The soft starter function is to reduce the input current, limiting disruptions to the network. Without a smooth start, the input current can be up to 7-8 times of the rated current, which can

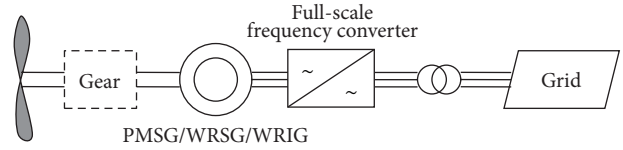

Figure 6: D. Wind Turbine with a Wound Rotor Synchronous Generator [5].

Table 3: Wind turbine classification [5].

Speed control		Power control		
		Passive stall	Pitch	Active stall
Fixed speed	A	A0	A1	A2
Variable speed	B	B0	B1	B2
	C	C0	C1	C2
	D	D0	D1	D2

cause serious disturbances in the network voltage. The soft starter contains two thyristors as switching devices in each phase [5].

They are connected antiparallel to each phase. The smooth connection of the generator to the network over a predefined number of grating periods is accomplished by adjusting the firing angle α of the thyristors. The relationship between the firing angle and the resulting amplification of the soft starter is highly nonlinear and is also a function of the power factor connected element. After the in-rush, thyristors are bridged to reduce overall system losses.

2.3. Capacitor Bank. The capacitor bank is used in fixed speed wind turbines or limited variable speed; see Figures 3 and 4. It is an electrical component that supplies power to the induction generator reactive. Thus, the reactive power absorbed by the generator of the grid is minimized [27]. The wind turbine generators may have a full load dynamic compensation, where a number of capacitors are connected or disconnected continuously, depending on the reactive power demand of the generator during a predefined time period.

The capacitor banks are usually mounted in the bottom of the tower or the nacelle, that is, at the top of the wind turbine. They can be very charged and damaged in the event of surges on the network and, consequently, it may increase the cost of maintenance.

2.4. Rectifiers and Inverters. Diodes can only be used in the rectification mode, while the electronic switches can be used in the rectification and inversion mode [23, 28]. The most common solution is the rectifier diode rectifier, because of its simplicity, low cost, and low losses. It is nonlinear in nature and accordingly generates harmonic currents. Another drawback is that it permits only unidirectional power flow and cannot control the voltage or current generator [5]. Therefore, it is only used with a generator which can control the tension and with an inverter (e.g., one IGBT) that can control the flow.

The thyristor (grid-commutated) based solution is cheap investor, with low losses, and, as the name suggests, must be connected to the network to be able to operate. Unfortunately, consuming reactive power and harmonics produces a large increasing demand of power quality and makes the self-commutated thyristor less attractive for the investors than the GTO or IGBT converters. The advantage of a GTO inverter is that it can handle more power than the IGBT; nevertheless, this feature is less important in the future due to the rapid development of the IGBT. The disadvantage of this is that the control circuit of the GTO valve is more complicated.

The generator and the rectifier must be selected as a combination (i.e, a solution), while the investor can choose almost independently of the generator and the rectifier. A rectifier diode or a thyristor rectifier can be used only together with a synchronous generator, as it requires no reactive current magnetization. In opposition to this, rectifiers GTO IGBT have to be used with induction generators variable speed because they are able to control the reactive power. However, despite the IGBT is a very attractive option; has the disadvantages of high cost and high losses. The synchronous generator with a diode rectifier, for example, has a much lower total cost than equivalent induction generator IGBT inverter or a rectifier.

2.5. Frequency Converters. A traditional frequency converter, also called an adjustable speed drive, consists of

(i) a rectifier (AC-DC conversion unit) to convert alternating current into direct current, while the energy flows into the DC system;

(ii) energy storage (capacitors);

(iii) an inverter (DC-AC with controllable frequency and voltage) to convert direct current into alternating current, while the energy flows to the AC side.

There are different ways to combine a rectifier and an inverter into a frequency converter. In recent years, different converter topologies have been investigated as to whether it can be applied in wind turbines:

(i) back-to-back converters [26],

(ii) multilevel converters [26],

(iii) tandem converters [11],

(iv) matrix converters [11],

(v) resonant converters [11].

3. Modeling of the Wind Turbine

Since vertical axis wind turbines have very low starting torque, as well as dynamic stability problems they are commonly found in small wind applications. On the other hand, horizontal axis wind turbines are the most common wind turbines and are most commonly used for wind farms, community wind projects, and small wind applications. In this paper, we only discuss the modeling and control methods of horizontal axis wind turbines.

3.1. Modeling Based on the Aerodynamic. The aerodynamic modeling of the wind turbine has been studied and is presented in several research papers as [1, 10, 11, 26, 28–32]. The kinetic energy obtained by the blades of the wind is transformed into mechanical torque at the rotor shaft of the wind turbine the model can be described of in spoiler see Figure 7.

The blades are attached to the rotor with the tip speed $\omega_{\text{rot}} \cdot r$, where r is the length of the blade [33]. The profile of the blade experiences a relative wind speed generated by overlapping the tip speed and wind speed v_w. Wind is introduced from the lift profile (L) and drag forces (D) on the blade, resulting in the movement of these forces blade wind energy which is called the aerodynamic power P_w given as follows [1]:

$$P_w = \frac{1}{2}\rho_{\text{air}} \cdot A_r \cdot c_p(\lambda, \vartheta) \cdot v_w^3, \tag{1}$$

where ρ_{air} is the air density, v_w is the free wind speed experienced by the rotor, A is the swept rotor area, and c_p is the power coefficient.

The power coefficient depends upon the pitch angle ϑ and the tip-speed-ratio λ [1]:

$$\lambda = \frac{\omega_{\text{rot}} \cdot r}{v_w}. \tag{2}$$

The power coefficient c_p is typically given in a form of Figure 8 [30, 34].

The torque on the rotor shaft (see Figure 9), which is important for the axis model, can be calculated from the power with the aid of the rotational speed [33, 35]:

$$T_A = \frac{P_w}{\omega_r}, \tag{3}$$

where ω_r is the wind turbine speed (velocity of the rotor) and T_A is the aerodynamic torque.

3.2. Modeling Based on the Mechanical Property. In the power system analysis, the following four types of drive train models are usually used for the wind turbine available:

(i) six-mass drive train model [29],

(ii) three-mass drive train model [29],

(iii) two-mass shaft model [11],

(iv) one-mass or lumped model [36].

The simplified model of the power train is shown in Figure 9. In this model, all masses are grouped into low and high speed shaft [1, 35]. This model is sufficient for transient stability analysis with a fixed speed. The inertia of the low speed shaft comes mainly from the rotating blades and the inertia of the high speed shaft. It is important to include all small masses of high speed shaft, since they have an important influence on the dynamic system due to the transformation of the transmission ratio. The stiffness and damping of the shaft are combined in equivalent stiffness and damping placed

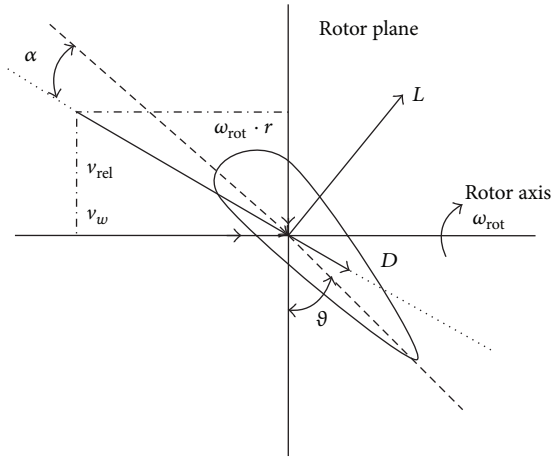

Figure 7: Aerodynamic model [1].

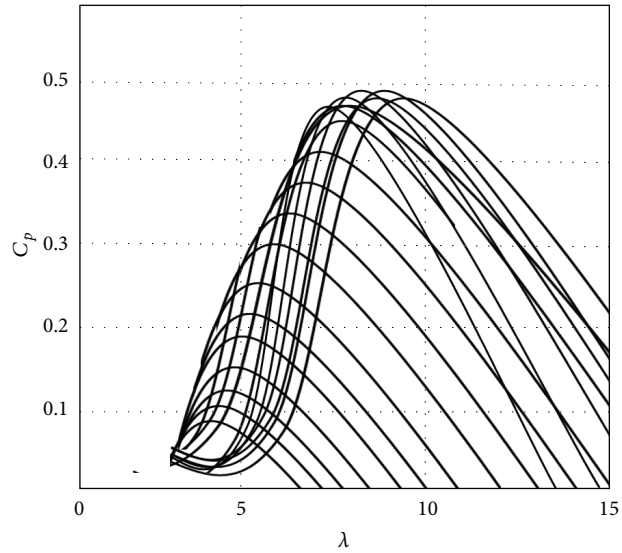

Figure 8: The power coefficient c_p versus the tip speed ratio [34].

on the low speed side. The mass of the gearbox itself is insignificant and abandoned.

The input to the model for a two-mass system is defined as torque T_A, which is obtained by the aerodynamic system and the generator reaction torque T_e. The output is the changes in the rotor speed ω_r and generator speed ω_g.

The dynamic of high speed generator can be expressed as a machine model. The differences in the mechanical drive torque T_m, the generator torque reaction T_e, and torque losses due to friction T_{fric}, cause the change of angular velocity $\dot{\omega}_g$ [29]:

$$T_m - T_e - T_{\text{fric}} = J_g \cdot \dot{\omega}_g,$$
$$\dot{\omega}_g = \ddot{\varphi}_g. \tag{4}$$

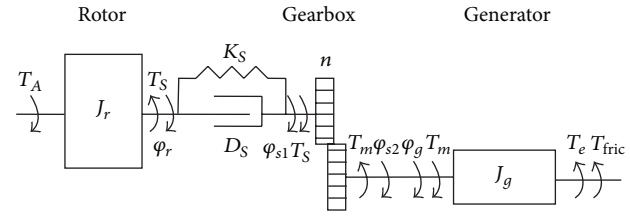

Figure 9: Drive train schematic for the modelling of a wind turbine [34].

The change of the angular speed $\dot{\omega}_r$ is caused by the difference of the aerodynamic torque T_A and shaft torque T_s at the low speed [29]:

$$T_A - T_S = J_r \cdot \dot{\omega}_r,$$
$$\dot{\omega}_r = \ddot{\varphi}_r. \tag{5}$$

The mechanical driving torque T_m and shaft torque T_s are connected by the gear ratio [29]:

$$T_m = \frac{T_s}{n}. \tag{6}$$

The dynamics of the shaft can be described by [29]:

$$T_s = K_s \cdot \Delta\varphi + D_s \cdot \Delta\dot{\varphi},$$
$$\Delta\dot{\varphi} = \dot{\varphi}_r - \frac{\dot{\varphi}_g}{n} = \omega_r - \frac{\omega_g}{n}. \tag{7}$$

The final drive train dynamics is as follows [29]:

$$\dot{\omega}_r = \frac{1}{J_r}\left(T_A - D_S \cdot \omega_r + \frac{D_s}{n}\omega_g - K_s \int \left(\omega_r - \frac{\omega_g}{n}\right) dt\right),$$
$$\dot{\omega}_g = \frac{1}{J_g}\left(-T_e - \left(D_g + \frac{D_s}{n^2}\right)\omega_g + \frac{D_s}{n}\omega_r - \frac{K_s}{n} \int \left(\omega_r - \frac{\omega_g}{n}\right) dt\right), \tag{8}$$

where K_s is the stiffness constant and D_s is the damping constant of the shaft. To obtain the stiffness constant, the eigen frequency of the drive train has to be known. Consider a two-mass free swinging system; the eigen frequency is as follows [29]:

$$\omega_{0S} = 2\pi f_{0S} = \sqrt{\frac{K_s}{J_{\text{ges}}}}. \tag{9}$$

The total inertia of the free swinging system on the low speed is calculated by [29]:

$$J_{\text{ges}} = \frac{J_r \cdot J_g \cdot n^2}{J_r + J_g \cdot n^2}. \tag{10}$$

Consequently, the stiffness constant of the low speed shaft is [29]:

$$K_s = J_{\text{ges}} \cdot (2\pi f_{0S})^2. \tag{11}$$

The damping constant D_s can be calculated by [29]:

$$D_s = 2\xi_s \cdot \sqrt{\frac{K_s \cdot J_{\text{ges}}}{\xi_s^2 + 4\pi^2}}, \tag{12}$$

where ξ_s is the logarithmic decrement.

3.3. Linearized Model. The aerodynamic torque, T_A,must be opposed by an equal and opposite load torque, T_L, for the turbine to operate at steady speed. If T_A is greater than T_L, the turbine will accelerate, while if T_A is less than T_L, the turbine will decelerate. Equation (13) gives this mathematical description where J_T is the equivalent combined moment of inertia of the rotor, gear reducer and both the low speed and high speed shafts [37]:

$$J_T \dot{\omega}_T = T_A - T_L. \tag{13}$$

T_L is the mechanical torque necessary to turn the generator and was assumed to be a constant value derived from the wind turbine plant physical properties. The aerodynamic torque, T_A, is represent by (5). The power extracted from the wind is shown in (1). This equation is nonlinear, because the power coefficient c_p is highly nonlinear [37]. To simplify the analysis and design linear controllers, we should linearize this model.

Assuming $T_A|_{OP} \approx T_L|_{OP}$, the linearization of (1) is [37]

$$J_T \dot{\omega} = J_T \left.\frac{\partial \dot{\omega}}{\partial u}\right|_{OP} \Delta u + J_T \left.\frac{\partial \dot{\omega}}{\partial \omega}\right|_{OP} \Delta\omega + J_T \left.\frac{\partial \dot{\omega}}{\partial \beta}\right|_{OP} \Delta\beta. \tag{14}$$

In a simple form (14) becomes [37]:

$$\dot{\omega} = \alpha\Delta u + \gamma\Delta\omega + \delta\Delta\beta, \tag{15}$$

where $\Delta\omega_T, \Delta u$, and $\Delta\beta$ are the derivations at the operating points ω_{TOP}, u_{OP}, and β_{OP}. The parameters α, γ, and δ are coefficients.

α, γ, and δ represent the wind turbine dynamics at the linearization point. Their quantities depend on the wind speed and the partial derivatives of the coefficient of torque c_p with respect to λ and β. The magnitudes of α and δ are the relative weight of the effect wind speed u and pitch angle β on the wind turbine angular speed, respectively. Equation (15) is the linear equation describing the wind turbine dynamics.

The linear model (15) can be transformed by the Laplace transformation as follows [37]:

$$\Delta\omega(s) = \left[\alpha\Delta u(s) + \delta\Delta\beta(s)\right] \frac{1}{s-\gamma}. \tag{16}$$

The linearized model is at the angular rotation speed ω_{TOP}, the wind speed u_{OP}, and the pitch angle β_{OP}. It represents the change of rotor speed $\Delta\omega$ with respect to the inputs Δu and $\Delta\beta$. Therefore, the wind turbine is represented by the first order transfer function $G_p(s)$ [37]:

$$G_p(s) = \frac{\Delta\omega(s)}{\alpha\Delta u + \delta\Delta\beta} = \frac{\Delta\omega(s)}{(\Delta T_A/J_T)} = \frac{1}{s-\gamma}. \tag{17}$$

4. Control of the Wind Turbine

There are many results on wind turbines control from the aerodynamic to generator energy. In this paper, we only discuss the horizontal axis wind turbine and doubly fed induction generator (DFIG). This type of wind turbine is the most used in the market [1].

The performance of the wind turbine depends not only on hardware, also on the wind turbine control technique [38]. The main control objectives of the wind turbine are as follows [39, 40]:

(i) capture the wind power as possible as it can,

(ii) maximize the wind harvested power in partial load zone,

(iii) guarantee a certain level of resilience of the mechanical parts by alleviating the variable loads,

(iv) meet strict power quality standards (power factor, harmonics, flicker, etc.),

(v) transfer the electrical power to the grid at an imposed level in wide range of wind velocities.

The control system has three subsystems: aerodynamic control, variable speed control, and grid connection control; see Figure 10. In the following sections several popular control techniques will be discussed [41].

4.1. Aerodynamic Control. The wind turbine aerodynamics are very similar to the airplane. The blade rotates in the wind, because the air flowing along the surface moves faster than the upwind surface. This creates a lifting force to remove the sheet to rotate [30]. The attack angle of the blade plays a critical role in determining the amount of force and torque generated by the turbine. Therefore, it is an effective means to control the amount of power. There are three methods to aerodynamically control for large wind turbines: passive stall, active stall, and pitch control.

(i) Passive stall control: the blade is fixed on the rotor hub in an optimum (nominal) attack angle. When the wind speed is less than or equal to the nominal value, the turbine blades with the nominal attack angle capture the maximum possible power wind. With wind speed above the nominal value, the strong wind can cause turbulence on the surface of the blade, which faces away from the wind. As a result, the lifting force is reduced and eventually disappears with increasing wind speed by reducing the speed of rotation of the turbine. This phenomenon is called stall. The passive stall control does not need complex pitch mechanisms; however, the blades need a good aerodynamic design.

(ii) Active stall control: the stall phenomenon can be induced not only by higher wind speeds, but also by increasing the attack of the blade. Thus, active stall wind turbines have blades with adjustable pitch control mechanism. When the wind speed exceeds the rated value, the blades are controlled towards the

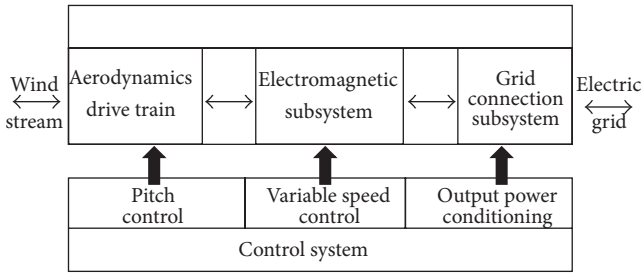

Figure 10: Main control subsystems of a wind turbine [38].

wind to reduce the captured power. Consequently, the captured power can remain at the nominal value by adjusting the blade angle of attack.

(iii) Pitch control: for the light and medium wind, the pitch control can optimize the operation of the wind turbine in the sense of maximizing rotor power. For the strong wind that exceeds the nominal level, pitch control maintains a desired operating condition [26]. The optimization operation by the pitch control can increase rotor power up to 2% [42]. This accuracy of the pitch angel is important but is not relevant for the stability investigations of short-term stress. Therefore, the steady-state angle of inclination can be adjusted to zero when the incoming wind is below the normal level. For strong wind, the steady-state angle is greater than zero and increases with increasing wind speed. Similar to the active stall control, the wind turbines with pitch control have adjustable blade in the rotor hub. When wind speed exceeds nominal value, the pitch controller reduces the attack angle, turning the blades (pitching) from wind gradually. The difference pressure in front and in the rear of the blade is reduced. The pitch control reacts faster than active stall control and provides better controllability.

4.2. Linear Control. Since the drive train is very rigid, its train dynamics do not need to be included. Furthermore, the drive system used in the turbine pitch is very fast. The actuator dynamics are not required. Without considering viscous damping, the dynamic of the direct drive turbine is as follows [1, 29, 37]:

$$T_{\text{aero}} - T_{\text{gen}} = I\dot{\omega}, \tag{18}$$

where T_{aero} is the aerodynamic torque generated by the rotor, T_{gen} is the generator torque, I is the inertia of the rotating system, and $\dot{\omega}$ is the rate of change of rotor speed.

Considering T_{gen} as a constant in the power regulation region, the derivative of (18) is [1, 29, 37]

$$\dot{T}_{\text{aero}} = I\ddot{\omega}. \tag{19}$$

The aerodynamic torque change depends on the change in wind speed, the change in the pitch angle of the rotor blades, and also the change at the current operating point of the turbine. For this representation of the turbine dynamics, the transfer function of the change rate of aerodynamic torque to the rotor speed is a double integrator. It is scaled by the inverse of the rotational inertia. Thus, this linear system is the control model.

The proportional integral derivative technique (PID) is the most popular and powerful linear control, because it is robust with respect to uncertainties and it has a simple form. PID control for the rotational speed error is [37]

$$u = K_p e(t) + K_i \int_0^t e(\tau)\, d\tau + K_d \frac{de(t)}{dt}, \tag{20}$$

where $e(t)$ is the rotational speed error and K_p, K_i, and K_d are the proportional, integral, and derivative gains of the PID controller, respectively.

Wind turbine PID control works quite well for speed regulation in low winds and has oscillations in pitch control of high winds [37]. To realize linear PID control, a traditional approach is to linearize the nonlinear turbine dynamics in a specified operating point [43]. The transfer function $G_C(s)$ for the PID controller between the input rotational speed error and the output pitch angle is [37]

$$G_c(s) = \frac{\Delta\beta_c(s)}{\Delta\omega(s)} = \frac{k_d s^2 + k_p s + k_i}{s}. \tag{21}$$

How to select the PID gains is not an easy job. In [37] a systematic approach with a visualization of the potential performance is presented. However, it still relies on the experience and the intuition of control engineers.

In certain operating points, a set of controllers can now be determined using LQ control [44]. To have a good tracking performance for both DC tracking problems in each integrator, the tracking error is included; see Figure 11. Here the controller gain K is calculated at each operating point for minimizing the cost J_c of [37]:

$$\begin{aligned} J_c &= \int_{t=0}^{\infty} z(t)^T Q z(t) + u(t)^T R u(t)\, dt, \\ z &= \left[Q_{\text{sh}} \;\; x_\omega \;\; x_Q\right]^T, \\ u &= \left[\beta_{\text{ref}} \;\; Q_{g,\text{ref}}\right]^T, \end{aligned} \tag{22}$$

where β_{ref} is the pitch reference, ω_r is the velocity of the rotor, Q_g is the generator torque, ω_g is the output angular on the high speed side, and Q_{sh} is the torsion between the two inertias [37].

It should be noted that with the approach of interpolating controller gains, a good behavior cannot be guaranteed in terms of stability and performance for intermediate operating conditions. In practice, however, the method has shown various application areas [44]. One way of overcoming this problem is to apply LPV technique, such that the model is provided in a time-varying parameter, which is a prior unknown and measurable.

4.3. Nonlinear Control. Sliding mode control is a robust nonlinear feedback control technique. It can be applied for the wind turbine control [45, 46]; see Figure 12.

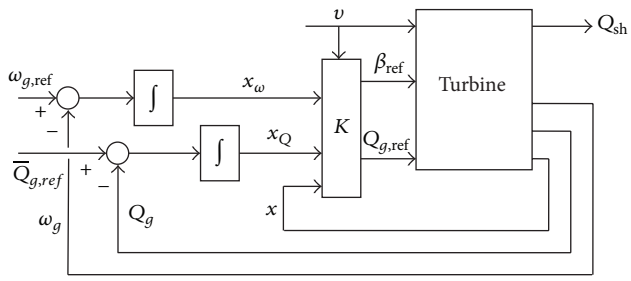

Figure 11: Block diagram of controller formulation [37].

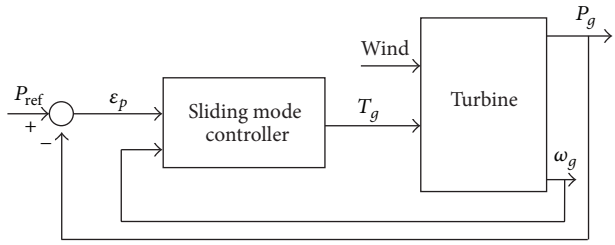

Figure 12: Sliding mode control for wind turbine [45].

The tracking error ε_p is defined as $\varepsilon_p = P_{\mathrm{ref}} - P_w$, where P_w is the aerodynamic power (rotor power) defined in (1) and (3)and P_{ref} is the reference power. The derivative of ε_p is [45]

$$\dot{\varepsilon}_p = \dot{P}_{\mathrm{ref}} - T_A\dot{\omega}_r - \dot{T}_A\omega_r. \tag{23}$$

The dynamic sliding mode controller is defined as follows [45]:

$$\dot{T}_A = \frac{(B+\lambda)}{\omega_r}\,\mathrm{sgn}\left(\varepsilon_p\right), \tag{24}$$

where $\dot{B}= |\varepsilon_p|$, λ is the tip-speed-ratio defined in (2) and ω_r is the wind turbine speed (velocity of the rotor) defined in (3):

$$\mathrm{sgn}\,(s) = \begin{cases} 1 & \text{if } s > 0, \\ -1 & \text{if } s < 0. \end{cases} \tag{25}$$

The closed-loop system is [45]

$$\dot{\varepsilon}_p = \dot{P}_{\mathrm{ref}} - T_A\dot{\omega}_r - (B+\lambda)\,\mathrm{sgn}\left(\varepsilon_p\right). \tag{26}$$

The uncertainty is defined as $d = \dot{P}_{\mathrm{ref}} - T_A\dot{\omega}_r$, and it is bounded as $|d| < B_1$; B_1 is a positive constant. Then, (26) is rewritten as follows [45]:

$$\dot{\varepsilon}_p = -(B+\lambda)\,\mathrm{sgn}\left(\varepsilon_p\right) + d. \tag{27}$$

A Lyapunov function is defined as follows [45]:

$$V = \frac{1}{2}\varepsilon^2 + \frac{1}{2}\left(B - B_1\right)^2. \tag{28}$$

It is not difficult to see that its time derivative satisfies [45]

$$\dot{V} \le -\lambda\,|\varepsilon|\,. \tag{29}$$

By the LaSalle theorem, it is concluded that the tracking error converges asymptotically to zero.

Since the sliding mode control system provides dynamic invariant property with uncertainties, it has to increase gains when tracking error is not zero. The main problem of the sliding mode control is the chattering. To decrease this behavior the sign function can be approximated as $\mathrm{sgn}(\varepsilon_p) \approx \varepsilon_p/(|\varepsilon_p| + a_0)$; a_0 is small positive constant. This prevents from increased mechanical stress due to strong torque variations. Another chattering reduction method is to use the boundary layer $m\,\mathrm{sgn}(s)$ around the switching surface as follows [45]:

$$m\,\mathrm{sgn}\,(s) = \begin{cases} \mathrm{sgn}\,(s) & \text{if } s \ge \delta, \\ \dfrac{s}{\delta} & \text{if } s = \delta. \end{cases} \tag{30}$$

4.4. Intelligent Control. Neural control for the wind turbine is shown in Figure 13. Here the adaptive controller has the learning ability [50–53]. The objective is to train the neural network so that the controller will allow the plant to produce the desired result [47]. To accomplish this, the neural network must be trained so that the input error $\varepsilon_p = e(t) = P_{\mathrm{ref}} - P_w = x_d(t) - x_n(t)$ produces the proper control parameter $T_A = u(t)$ to be applied to the plant to produce the aerodynamic power $P_w = x_n(t)$ [54].

Fuzzy control for the wind turbine is shown in Figure 14. $\varepsilon_p = \Delta Q = P_{\mathrm{ref}} - P_w = Q^* - Q$ is the tracking error, $P_{\mathrm{ref}} = Q^*$ is the reference, $P_w = Q$ is the aerodynamic power, and $T_A = Vdr^*$ is the control input. Here each input is evaluated by the triangular or trapezoidal membership functions [48, 55–57]. The degree of membership of the fuzzy sets is associated with each input. The defuzzification is obtained by averaging each output membership function [58, 59].

In [48], each input/output variable that is used in the controller design is expressed in fuzzy set using linguistic variables. Seven linguistic variable are used for LLP, CII, and the flow change rate. The rules are expressed by IF-THEN rules. The defuzzification uses the center gravity technique.

4.5. Generalized Predictive Control. Model predictive control (MPC) usually represents the behavior of complex dynamic systems. It is also applied to the wind turbines [60, 61]. It appears in the form of generalized predictive control (GPC) [62] and bias estimation model (BEM) [49].

GPC uses the estimations of future output to calculate current control [38]. A discrete model of wind turbine is shown in Figure 15. It is a finite difference approximation of the double integrator model. Here Δ_p is the change in the angle of the blade pitch, Δ_v is the wind speed change, and ω is the rotor speed. The coefficients b and c are obtained by a recursive least squares filter.

This model can predict the rotor speed with varying ratios and wind speed. The coefficients b and c increase with the wind speed increasing. The GPC method can be summarized as follows.

The cost function J is [49]

$$J = \left(W - W_D\right)^T Q\left(W - W_D\right) + \sigma u^T u, \tag{31}$$

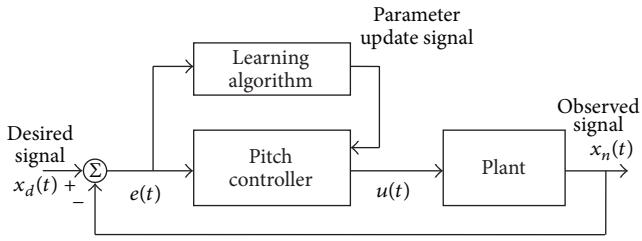

Figure 13: Neural network controller [47].

where Q is the weighting matrix, W_D is the desired response vector, which is known for all time from the desired rotor speed, and σ is the deciding factor that weights the use of control against error in the desired response. For positive semidefinite cost function Q, the control law u is [49]

$$u = \left(\sigma I + G^T Q G\right)^{-1} G^T Q \left(W_D - F\right). \tag{32}$$

To calculate the inverse, Q is chosen as a diagonal matrix. The above can be written as follows [49]:

$$W = Gu + F, \tag{33}$$

where

$$W = \begin{pmatrix} \omega(n+1) \\ \omega(n+2) \\ \Delta\omega(n+1) \\ \Delta\omega(n+1) \end{pmatrix},$$

$$u = \begin{pmatrix} \Delta u(n) \\ \Delta u(n+1) \end{pmatrix},$$

$$G = \begin{pmatrix} 0 & 0 \\ b & 0 \\ 0 & 0 \\ b & 0 \end{pmatrix},$$

$$F = \begin{pmatrix} 2\omega(n) + \omega(n-1) + b\Delta p(n+1) + c\Delta v(n+1) \\ 2F(1) - G\omega(n) + c\Delta v(n) \\ \Delta\omega(n) + b\Delta p(n+1) + c\Delta v(n+1) \\ F(3) + c\Delta v(n) \end{pmatrix}. \tag{34}$$

The transient response of this method is not good, because of the double integrator and short control horizon. The term $\Delta\omega$ is added to provide derivative-type control to improve the transient response.

The desired change in the pitch for the current time step is given by the first element of u. The GPC method is able to adjust the control system as the coefficients vary with changing conditions. However, the change in control is not the preferred change. As wind speed and b increase, the method utilizes the additional gain to obtain a more accurate rotor speed. To enable the system to perform similarly for all wind speeds, the deciding factor σ is scaled by $b, \sigma = \sigma_0 b$, where σ_0 is a constant.

BEM can estimate the unmodelled disturbances acting on the system with additional equations. This method is investigated because the wind speed over the rotor disk cannot be measured exactly [38]. Consequently, the bias term estimation is useful for the effect of changes in wind speed acting on the turbine.

BEM uses the same model as GPC; see Figure 16. Here the coefficients b and c are determined for 12 m/s wind speed and the average values of b_M and c_M. The estimate of Δ_v is included in the control law to cancel the disturbance.

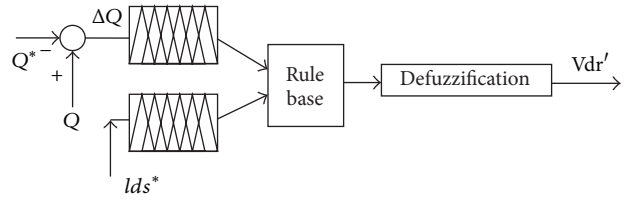

Figure 14: The block diagram of reactive power fuzzy logic controller [48].

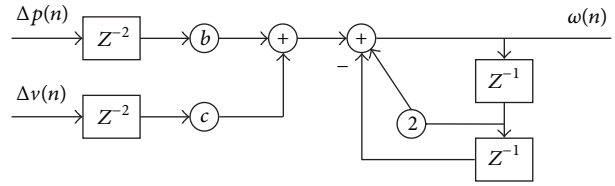

Figure 15: Wind turbine model [49].

5. Offshore Floating Wind Turbines

The growing demand for wind energy offshore installed in recent years has been motivated primarily by reduced space for installation in the land and the great advantages to mention a few [63]:

(i) better energy production,

(ii) reduced turbulence intensity,

(iii) higher capacity factor,

(iv) avoids size limits.

Currently investigating this type of turbine is focused not only on controlling wind energy production, but also in three groups, namely, the design [64, 65], installation, and electrical infrastructure and maintenance [66]. This is because the material from which the turbine should be constructed to be resistant to salinity and big changes suffered from the sea climate; secondly because there is no restriction on the dimensions of the turbine, the installation makes it expensive and difficult because it is in the sea; once installed, the turbine in the sea faces another major challenge which is the operation of the network generation; this is done at long distance including wiring, substations, and connecting to the network. Once designed, installed, and put into operation only a challenge remains to cover which is maintenance; this maintenance is usually very expensive due to the conditions under which it is done in some cases in the depth of the sea in other weather conditions [67].

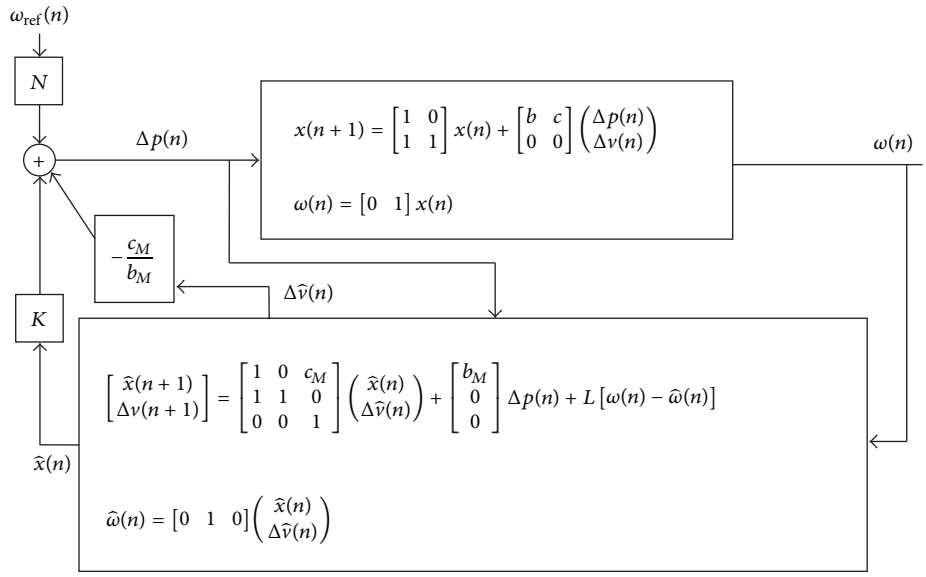

Figure 16: BEM control system [38].

6. Conclusions

Green energy has opened an important branch and shows in the rise of technology. The wind turbines and related techniques, environment, structure, and control methodology, are paid more attention recently. This paper presents the most common used wind turbine models which are classified with respect to different objectives as are more production energy, safety of turbine, connection to grid; consequently, the wind turbine dimensions are increased and the control methods are required to respond quickly and effectively to the important task of the power generation. The previous fact results in high cost of the sensors as well as the instability of the system; therefore, more complex identification techniques are required to help the control.

References

[1] S. M. Bolik, *Modelling and Analysis of Variable Speed Wind Turbines with Induction Generator during Grid Fault [Ph.D. thesis]*, Alborg University, Denmark, 2004.

[2] P. J. Moriarty and S. B. Butterfield, "Wind turbine modeling overview for control engineers," in *Proceedings of the American Control Conference (ACC '09)*, pp. 2090–2095, St. Louis, Mo, USA, June 2009.

[3] O. Anaya-Lara, *Wind Energy Generation: Modelling and Control*, John Wiley & Sons, New York, NY, USA, 2009.

[4] Q. Hernández-Escobedo, F. Manzano-Agugliaro, and A. Zapata-Sierra, "The wind power of Mexico," *Renewable and Sustainable Energy Reviews*, vol. 14, no. 9, pp. 2830–2840, 2010.

[5] T. Ackermann, *Wind Power in Power Systems*, John Wiley & Sons, New York, NY, USA, 2005.

[6] J. Aho, A. Buckspan, J. Laks et al., "A tutorial of wind turbine control for supporting grid frequency through active power control," in *Proceedings of the National Renewable Energy Laboratory (NREL) Control Conference*, pp. 27–29, Golden, Colo, USA, 2012.

[7] J. D. J. Rubio-Avila, A. Ferreyra-Ramírez, F. B. Santillanes-Posada, M. Salazar-Pereyra, and G. Deloera-Flores, "Topics related with the wind turbine," *WSEAS Transactions on Computers*, vol. 7, no. 8, pp. 1169–1178, 2008.

[8] J. J. Rubio, M. Figueroa, J. Pacheco, and M. Jimenez-Lizarraga, "Observer design based in the mathematical model of a wind turbine," *International Journal of Innovative Computing, Information and Control*, vol. 7, no. 12, pp. 6711–6725, 2011.

[9] B. Wu, Y. Lang, N. Zargari, and S. Kouro, *Power Conversion and Control of Wind Energy Systems*, John Wiley & Sons, New York, NY, USA, 2011.

[10] G. Ofualagba and E. U. Ubeku, "Wind energy conversion system-Wind turbine modeling," in *Proceedings of the IEEE Power and Energy Society General Meeting: Conversion and Delivery of Electrical Energy in the 21st Century, PES*, pp. 1–8, July 2008.

[11] G. Michalke and A. D. Hansen, "Modelling and control of variable speed wind turbines for power system studies," *Wind Energy*, vol. 13, no. 4, pp. 307–322, 2010.

[12] F. Zhang, W. E. Leithead, and O. Anaya-Lara, "Wind turbine control design to enhance the fault ride-through capability," in *Proceedings of the IET Conference on Renewable Power Generation (RPG '11)*, p. P31, September 2011.

[13] H.-L. Fu and W.-C. Chang, "Win turbine control moniter syestem simulation and validation," in *Proceedings of the International Symposium on Computer, Communication, Control and Automation (3CA' 10)*, pp. 6–9, May 2010.

[14] I. Pourfar, H. A. Shayanfar, H. M. Shanechi, and A. H. Naghshbandy, "Controlling PMSG-based wind generation by a locally available signal to damp power system inter-area oscillations," *European Transaction on Electrical Power*, 2012.

[15] F. Wu, X.-P. Zhang, and P. Ju, "Modeling and control of the wind turbine with the direct drive permanent magnet generator integrated to power grid," in *Proceedings of the 3rd International Conference on Deregulation and Restructuring and Power Technologies (DRPT '08)*, pp. 57–60, Nanjuing, China, April 2008.

[16] M. Andriollo, M. De Bortoli, G. Martinelli, A. Morini, and A. Tortella, "Control strategy of a wind turbine drive by an integrated model," *Wind Energy*, vol. 12, no. 1, pp. 33–49, 2009.

[17] J. Zhao, W. Zhang, Y. He, and J. Hu, "Modeling and control of a wind-turbine-driven DFIG incorporating core saturation during grid voltage dips," in *Proceedings of the 11th International Conference on Electrical Machines and Systems (ICEMS '08)*, pp. 2438–2442, October 2008.

[18] A. Petersson, T. Thiringer, L. Harnefors, and T. Petrů, "Modeling and experimental verification of grid interaction of a DFIG wind turbine," *IEEE Transactions on Energy Conversion*, vol. 20, no. 4, pp. 878–886, 2005.

[19] G. Quinonez-Varela and A. Cruden, "Modelling and validation of a squirrel cage induction generator wind turbine during connection to the local grid," *IET Generation, Transmission and Distribution*, vol. 2, no. 2, pp. 301–309, 2008.

[20] S. K. Salman, B. Badrzadeh, and J. Penman, "Modelling wind turbine-generators for fault ride-through studies," in *Proceedings of the 39th International Universities Power Engineering Conference (UPEC '04)*, pp. 634–638, September 2004.

[21] H.-S. Ko, G.-G. Yoon, N.-H. Kyung, and W.-P. Hong, "Modeling and control of DFIG-based variable-speed wind-turbine," *Electric Power Systems Research*, vol. 78, no. 11, pp. 1841–1849, 2008.

[22] L. B. Shi, C. Wang, L. Z. Yao, L. M. Wang, and Y. X. Ni, "Analysis of impact of grid-connected wind power on small signal stability," *Wind Energy*, vol. 14, no. 4, pp. 517–537, 2011.

[23] Z. Qiu, K. Zhou, and Y. Li, "Modeling and control of diode rectifier fed PMSG based wind turbine," in *Proceedings of the 4th International Conference on Electric Utility Deregulation and Restructuring and Power Technologies (DRPT '11)*, pp. 1384–1388, July 2011.

[24] L. Peng, Y. Li, and B. Francois, "Modeling and control of doubly fed induction generator wind turbines by using causal ordering graph during voltage dips," in *Proceedings of the 11th International Conference on Electrical Machines and Systems (ICEMS '08)*, pp. 2412–2417, October 2008.

[25] Y. He, J. Hu, and R. Zhao, "Modeling and control of wind-turbine used DFIG under network fault conditions," in *Proceedings of the 8th International Conference on Electrical Machines and Systems (ICEMS '05)*, pp. 986–991, September 2005.

[26] V. Akhmatov, "Modelling and ride-through capability of variable speed wind turbines with permanent magnet generators," *Wind Energy*, vol. 9, no. 4, pp. 313–326, 2006.

[27] S. M. Muyeen, S. Shishido, M. H. Ali, R. Takahashi, T. Murata, and J. Tamura, "Application of energy capacitor system to wind power generation," *Wind Energy*, vol. 11, no. 4, pp. 335–350, 2008.

[28] A. B. Cultura II and Z. M. Salameh, "Modeling and simulation of a wind turbine-generator system," in *Proceedings of the IEEE PES General Meeting: The Electrification of Transportation and the Grid of the Future*, pp. 1–7, July 2011.

[29] S. M. Muyeen, J. Tamura, and T. Murata, *Stability Augmentation of a Grid-Connected Wind Farm*, Green Energy and Technology, Springer, New York, NY, USA, 2009.

[30] W. Hongbin and D. Ming, "Modeling and control of distribution system with wind turbine generators," in *Proceedings of the 3rd International Conference on Deregulation and Restructuring and Power Technologies (DRPT '08)*, pp. 2498–2503, April 2008.

[31] X. Q. Ma, V. Chopra, S. H. H. Zargarbashi, and J. Angeles, "Wind turbine control using a gearless epicyclic transmission," in *Proceedings of the 1st International Conference on Applied Robotics for the Power Industry (CARPI '10)*, October 2010.

[32] S. Heier, *Grid Integration of Wind Energy Conversion System*, Chichester, UK, John Wiley & Sons, 1998.

[33] C. Pournaras, V. Riziotis, and A. Kladas, "Wind turbine control strategy enabling mechanical stress reduction based on dynamic model including blade oscillation effects," in *Proceedings of the 18th International Conference on Electrical Machines (ICEM '08)*, pp. 1–6, September 2008.

[34] A. Rolán, Á. Luna, G. Vázquez, D. Aguilar, and G. Azevedo, "Modeling of a variable speed wind turbine with a permanent magnet synchronous generator," in *Proceedings of the IEEE International Symposium on Industrial Electronics (IEEE ISIE '09)*, pp. 734–739, July 2009.

[35] J. G. Stuart, A. D. Wright, and C. P. Butterfield, "Wind turbine control systems: dynamyc model devel opment using system identification and the fast structural dynamics code," in *Proceedings of the American Society of Mechanical Engineers wind energy symposium*, Reno, Nev, USA, 1997.

[36] A. Rolán, Á. Luna, G. Vázquez, D. Aguilar, and G. Azevedo, "Modeling of a variable speed wind turbine with a permanent magnet synchronous generator," in *Proceedings of the IEEE International Symposium on Industrial Electronics (IEEE ISIE '09)*, pp. 734–739, July 2009.

[37] B. Malinga, "Modeling and control of a wind turbine as a distributed resource," in *Proceedings of the 35th Southeastern Symposium on System Theory*, pp. 108–112, 2003.

[38] K. Pierce and L. Jay, "Wind turbine control system modeling capabilities," in *Proceedings of the American Controls Conference*, pp. 24–26, Philadelphia, Pa, USA, June1998.

[39] I. Munteanu, N. A. Cutululis, A. I. Bratcu, and E. CeangA, *Optimal Control of Wind Energy Systems Advances in Industrial Control*, Springer, New York, NY, USA, 2008.

[40] W. E. Holley, "Wind turbine dynamics and control—issues and challenges," in *Proceedings of the American Control Conference*, pp. 3794–3795, June 2003.

[41] G. E. Van Baars, "Wind turbine control design and implementation based on experimental models," in *Proceedings of the 31st IEEE Conference on Proceedings of the Decision and Control*, vol. 2, pp. 2454–2459, 1992.

[42] M. Yin, G. Li, M. Zhou, and C. Zhao, "Modeling of the wind turbine with a permanent magnet synchronous generator for integration," in *Proceedings of the IEEE Power Engineering Society General Meeting (PES '07)*, pp. 1–6, June 2007.

[43] J. Wang, N. Tse, and Z. Gao, "Synthesis on PI-based pitch controller of large wind turbines generator," *Energy Conversion and Management*, vol. 52, no. 2, pp. 1288–1294, 2011.

[44] K. Z. Østergaard, P. Brath, and J. Stoustrup, "Gain-scheduled linear quadratic control of wind turbines operating at high wind speed," in *Proceedings of the 16th IEEE International Conference on Control Applications (CCA '07)*, pp. 276–281, October 2007.

[45] B. Beltran, T. Ahmed-Ali, M. E. H. Benbouzid, and A. Haddoun, "Sliding mode power control of variable speed wind energy conversion systems," in *Proceedings of the IEEE International Electric Machines and Drives Conference (IEMDC '07)*, pp. 943–948, May 2007.

[46] V. I. Utkin, *Sliding Modes in Control and Optimization*, Communications and Control Engineering Series, Springer, Berlin, Germany, 1992.

[47] S. Kélouwani and K. Agbossou, "Nonlinear model identification of wind turbine with a neural network," *IEEE Transactions on Energy Conversion*, vol. 19, no. 3, pp. 607–612, 2004.

[48] T. Ustuntas and A. D. Şahin, "Wind turbine power curve estimation based on cluster center fuzzy logic modeling," *Journal of Wind Engineering and Industrial Aerodynamics*, vol. 96, no. 5, pp. 611–620, 2008.

[49] D. Castaignet, N. K. Poulsen, T. Buhl, and J. J. Wedel-Heinen, "Model predictive control of trailing edge flaps on a wind turbine blade," in *Proceedings of the American Control Conference (ACC '11)*, pp. 4398–4403, July 2011.

[50] L. Fausett, *Fundamentals of Neural Networks: Architectures, Algorithms and Applications*, Prentice-Hall, New York, NY, USA, 2009.

[51] F. L. Luo and R. Unbehaben, *Applied Neural Networks for Signal Processing*, Cambridge University Press, New York, NY, USA, 1997.

[52] A. S. Yilmaz and Z. Özer, "Pitch angle control in wind turbines above the rated wind speed by multi-layer perceptron and radial basis function neural networks," *Expert Systems with Applications*, vol. 36, no. 6, pp. 9767–9775, 2009.

[53] X. Yao, X. Su, and L. Tian, "Wind turbine control strategy at lower wind velocity based on neural network PID control," in *Proceedings of the International Workshop on Intelligent Systems and Applications (ISA '09)*, May 2009.

[54] H. M. Hasanien and S. M. Muyeen, "Speed control of grid-connected switched reluctance generator driven by variable speed wind turbine using adaptive neural network controller," *Electric Power Systems Research*, vol. 84, no. 1, pp. 206–213, 2012.

[55] L. A. Zadeh, "Fuzzy logic computing with words," *IEEE Transactions on Fuzzy Systems*, vol. 4, no. 2, pp. 103–111, 1996.

[56] R. Bayindir, I. Colak, E. Kabalci, and E. Irmak, "The fuzzy logic control of a multilevel converter in a variable speed wind turbine," in *Proceedings of the International Conference on Machine Learning and Applications (ICMLA '09)*, pp. 787–7790, Miami Beach, Fla, USA, 2009.

[57] M. Jafarian and A. M. Ranjbar, "Fuzzy modeling techniques and artificial neural networks to estimate annual energy output of a wind turbine," *Renewable Energy*, vol. 35, no. 9, pp. 2008–2014, 2010.

[58] S. Chiu, "Fuzzy model identification based on cluster estimation," *Intelligent Fuzzy Systems*, vol. 2, pp. 267–278, 1994.

[59] H. H. Lee, P. Q. Dzung, L. M. Phuong, L. D. Khoa, and N. H. Nhan, "A new fuzzy logic approach for control system of wind turbine with doubly fed induction generator," in *Proceedings of the International Forum on Strategic Technology (IFOST '10)*, pp. 134–139, October 2010.

[60] D. Q. Dang, S. Wu, Y. Wang, and W. Cai, "Model predictive control for maximum power capture of variable speed wind turbines," in *Proceedings of the 9th International Power and Energy Conference (IPEC '10)*, pp. 274–279, October 2010.

[61] Y. S. Qudaih, M. Bernard, Y. Mitani, and T. H. Mohamed, "Model predictive based load frequency control design in the presence of DFIG wind turbine," in *Proceedings of the 2nd International Conference on Electric Power and Energy Conversion Systems (EPECS '11)*, November 2011.

[62] L. C. Henriksen, "Model predictive control of a wind turbine," *Technical University of Denmark Informatics and Mathematical Modelling*, pp. 7–38, 2007.

[63] E. Hau, "Offshore wind energy utilisation," *Wind Turbines*, pp. 677–718, 2013.

[64] T. Sebastian and M. A. Lackner, "Development of a free vortex wake method code for offshore floating wind turbines," *Renewable Energy*, vol. 46, pp. 269–275, 2012.

[65] T. Sebastian and M. A. Lackner, "Analysis of the induction and wake evolution of an offshore floating wind turbine," *Energies*, vol. 5, pp. 968–1000, 2012.

[66] Z. Hameed, J. Vatn, and J. Heggset, "Challenges in the reliability and maintainability data collection for offshore wind turbines," *Renewable Energy*, vol. 36, no. 8, pp. 2154–2165, 2011.

[67] I. Erlich, F. Shewarega, C. Feltes, F. W. Koch, and J. Fortmann, "Offshore wind power generation technologies," *Proceedings of the IEEE*, vol. 101, pp. 891–905, 2013.

Hindawi Publishing Corporation
Mathematical Problems in Engineering
Volume 2013, Article ID 163565, 5 pages
http://dx.doi.org/10.1155/2013/163565

Research Article

Wind Farm Power Forecasting

Nabiha Haouas[1,2] and Pierre R. Bertrand[1]

[1] *Laboratoire de Mathématiques (UMR CNRS 6620), Université Blaise Pascal (Clermont-Ferrand II), 63177 Aubière Cedex, France*
[2] *Computational Mathematics Laboratory, Monastir, Tunisia*

Correspondence should be addressed to Nabiha Haouas; nabiha.haouas@math.univ-bpclermont.fr

Received 19 April 2013; Accepted 4 July 2013

Academic Editor: Wei-Jen Lee

Forecasting annual wind power production is useful for the energy industry. Until recently, attention has only been paid to the mean annual wind power energy and statistical uncertainties on this forecasting. Recently, Bensoussan et al. (2012) have pointed that the annual wind power produced by one wind turbine is a Gaussian random variable under a reasonable set of assumptions. Moreover, they can derive both mean and quantiles of annual wind power produced by one wind turbine. The novelty of this work is the obtainment of similar results for estimating the annual wind farm power production. Eventually, we study the relationship between the power production for each turbine of the farm in order to avoid interaction between them.

1. Introduction

The energy industry is one of the most important types of modern industries. In recent years, wind power has become increasingly popular as a renewable energy source that can both develop the economy and protect the environment. Thereby, the development of suitable mathematical models becomes necessary. A detailed review on the existing tools used in wind power prediction is provided by [1], which proposes a perspective of future developments. A more recent update can be found in [2] where they used two alternative numerical prediction models: an empirical one and a computational one, in order to forecast the power output of two Greek wind farms before their installation. Different models for monitoring and forecasting the turbine output are considered such as those in the studies by the authors of [3–7] or [8] and recently in [9]. But, to our knowledge, the performance of a wind power farm has not been adequately studied. In this work, we suggest a statistical analysis based on central limit theorem as in [9]. Firstly, by using the wind speed, as input variables, we can forecast the annual energy production and its quantiles. Secondly, we study the relationship between the power outputs for each turbine in the farm to avoid the effect of interaction between them.

The rest of this paper is organized as follows. In Section 2, we present the dataset. In Section 3, we first recall the state on the art on the wind farm power forecasting, then we give the theoretical results for the forecasting of the annual wind power production, and we apply these results to real datasets. Moreover, we study the relationship between the power outputs for each turbine in the farm. Finally, discussions are available in Section 4.

2. Data Presentation

In this case study, we have processed ten-minute wind speed and ten-minute wind power production corresponding to a wind farm with four turbines. The duration of observation is 29 months leading to large series. The wind farm is located in a flat area close to the sea.

The wind farm power production depends on wind speed. Thus we begin with data representation. The wind speed series is intermittent; that is, it presents very irregular variations, as shown in Figure 1. This intermittency induces forecasting difficulties. A different approach has been considered, but also with a different horizon of time; see, for example, [10, 11] or [12]. Let us point out that the previous methods take only into account the absolute value of wind speed, leading to 1D time series. Other modern methods include the 2D or 3D behavior of wind; see, for example, [13] or [14].

By a simple calculation, the average wind speed over the period is equal to 7.25 m/s, which is enough to guarantee a

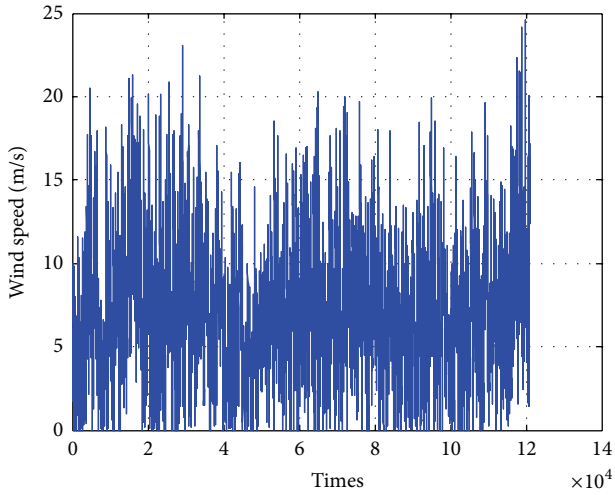

Figure 1: Mean wind speed in the farm.

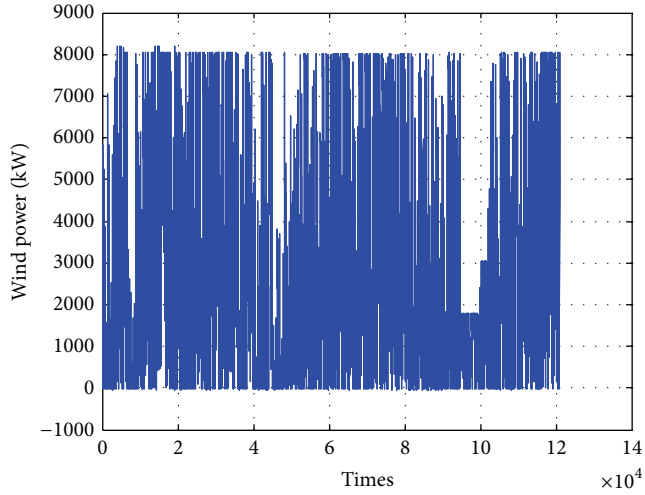

Figure 2: Average wind farm power every ten minutes.

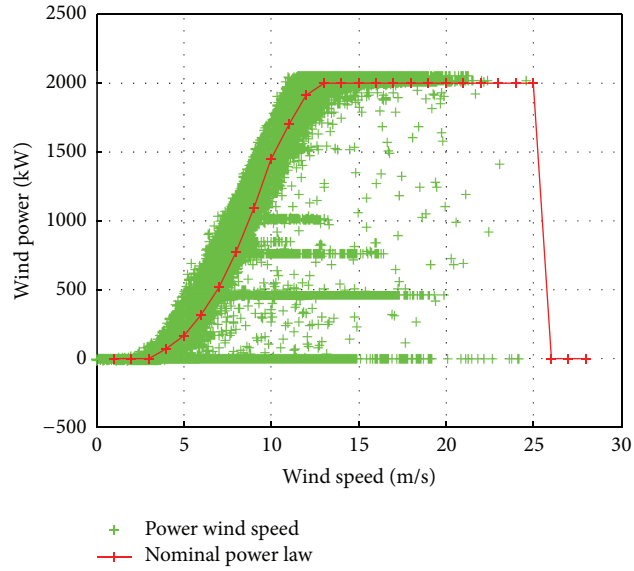

Figure 3: Wind power versus wind speed for turbine 1.

good profitability of the project but does not allow a detailed forecast.

Regarding the energy output, we can note the large amount generated by this wind farm which reaches 2870 kW on average every ten minutes. This perfectly fits the building of a wind farm on a flat area close to a windy sea. We can also plot the ten-minute wind speed versus the ten-minute power; see Figure 3. We then get a cloud of points around the nominal power law. Let us recall that the nominal power law is provided by the manufacturer and indicates the power P produced for a given wind speed v, which corresponds to the map $v \mapsto P(v)$ (see Figure 2).

Moreover, the turbine is cut for wind speed outside the interval $(V_{\text{cut.in}}, V_{\text{cut.off}})$. The large dispersion in Figure 3 around the nominal power law is due to outliers and error of measurement. We see that the power

(i) is null if the wind speed is less than the starting speed ($V_{\text{cut.in}} = 3.5$ m/s) and beyond the cut out speed $V_{\text{cut.off}} = 25$ m/s,

(ii) is proportional to the wind speed rise between $V_{\text{cut.in}}$ and the rated speed (about 13 m/s),

(iii) is constant between the rated speed and the cut out speed.

Let us remark that the energy output is not the same for each of the four turbines. Indeed, there is a turbine that produces on average less than the others although the four turbines have the same power law, being of the same type. A possible explanation is the wake effect. In this frame, modeling by 2D wind series could enhance wind power forecasting (see Table 1).

Table 1: Mean wind power for ten-minute by each turbine.

Turbine	T_1	T_2	T_3	T_4
Mean wind power (kW)	756	712	684	717

3. Wind Farm Power Forecasting

3.1. State of the Art. The traditional method is based on modeling ten-minute wind speed probability density function (pdf) and then calculating the average ten-minute wind power production as $\mathscr{P} = (1 - p_0) \int_{V_{\text{cut.in}}}^{V_{\text{cut. off}}} P(v) f(v) dv$, where p_0 denotes the probability of zero wind; $V_{\text{cut.in}}$, $V_{\text{cut. off}}$ denote the wind speed for cutting in and cutting off the turbine; $v \mapsto P(v)$ denotes the nominal power law; $f(v)$ denotes the wind speed probability density function (pdf). Most often the ten-minute wind speed is assumed to follow a Weibull distribution, or a hybrid Weibull law; see, for example, [15, 16], or [7]. This model gives a good estimation of both mean ten-minute wind speed and mean ten-minute wind power production and after that provides us with a good forecasting of the mean annual wind power production. However, this traditional method discards the time structure of wind speed

and wind power and thus it does not allow to forecast the variance, nor the quantiles of annual wind power production.

Recently, the authors of [9] have proposed a new method which takes into account the dynamical structure of the annual wind power production. This method provides forecasting not only of the mean annual wind power production, but also of its variance and the quantiles of annual wind power production. The techniques rely on the central limit theorem (CLT) which asserts that the pdf of annual wind power production is almost Gaussian under natural assumptions. In the next section, we slightly adapt this method to the case of a wind farm.

3.2. Forecasting Wind Farm Power. The annual wind power production of the farm is defined by

$$\mathscr{P}^F_{\text{annual}} = \sum_{t=1}^{T} P_t^F, \tag{1}$$

where $T = 52,560$ denotes the number of ten-minute periods during one year. The farm production is the sum of the individual production of the J turbines, that is, $P_t^F = \sum_{j=1}^{J} P_t^{(j)}$. The most simple but quite large model is to assume that each series P_t is wide sense stationary. Wide sense stationary means that on the one hand both mean $\mathscr{P}^{(j)}$ and variance $\mathscr{V}^{(j)}$ are not depending on time and that on the other hand the dynamical structure read on the covariance does not depend on the time t. As a corollary, the farm production series P_t^F is also wide sense stationary with mean $\mathscr{P}^F = \mathbb{E}(P_t^F) = \sum_{j=1}^{J} \mathscr{P}^{(j)}$ and variance as follows:

$$\mathscr{V}^F = \operatorname{Var}\left(P_t^F\right) = \sum_{i,j=1}^{J} \operatorname{cov}\left(P_t^{(i)}, P_t^{(j)}\right) \tag{2}$$

and correlation coefficient $\rho_P^F(k) = \operatorname{cov}(P_t^F, P_{t+k}^F)/\operatorname{Var}(P_t^F)$ which does not depend on the time t. Moreover, the family of random variables P_t^F is weakly dependent, and it admits a finite second-order moment (i.e., $\mathbb{E}(\mathscr{P}_t^F) < \infty$ for each $t \geq 1$). In addition, the annual wind production $\mathscr{P}^F_{\text{annual}}$ is also random with mean $\mathbb{E}(\mathscr{P}^F_{\text{annual}}) = T \times \mathscr{P}^F$ and variance as follows:

$$\operatorname{var}\left(\mathscr{P}^F_{\text{annual}}\right) = \operatorname{var}\left(\sum_{t=1}^{T} P_t^F\right) = T \times \mathscr{V}^F \times \left(\Gamma_T^F\right)^2, \tag{3}$$

where $\Gamma_T^F = \{1 + 2\sum_{k=1}^{T}[\rho_p^F(k) \times (1 - k/T)]\}^{1/2}$ with $\rho_P^F(k) = \operatorname{cov}(P_t^F, P_{t+k}^F)/\operatorname{Var}(P_t^F)$ which was introduced to variance analysis for characterizing wind energy conversion as in [17].

Let us stress that the variance of annual production of the farm depends both on the variance of ten-minute wind power $\mathscr{V}^F$ and its correlogram $\rho_p^F(k)$, which corresponds to the time structure of the series. We will also need the two following assumptions.

(A1) The second-order moment of P_t is finite, that is, size $\mathscr{V} = \mathbb{E}((P_t)^2) < \infty$;

(A2) The family of random variables P_t is weakly dependent.

After having made precise assumptions and notation, by using the same tricks as in Proposition 3.1 in [9], we can deduce the following CLT.

Theorem 1 (CLT for wind farm annual production).

(i) *If the family of r.v. P_t is wide sense stationary, and assumptions (A1) and (A2) are fulfilled, then one has*

$$\mathscr{P}^F_{annual} = T \times \mathscr{P}^F + T^{1/2} \times \left(\mathscr{V}^F\right)^{1/2} \cdot \Gamma_T^F \times \varepsilon_T, \tag{4}$$

where

$$\mathscr{P}^F = \sum_{j=1}^{J} \mathscr{P}^{(j)},$$

$$\mathscr{V}^F = \operatorname{Var}\left(P_t^F\right) = \sum_{i,j=1}^{J} \operatorname{cov}\left(P_t^{(i)}, P_t^{(j)}\right), \tag{5}$$

$$\Gamma_T^F = \left\{1 + 2\sum_{k=1}^{T}\left[\rho_p^F(k) \times \left(1 - \frac{k}{T}\right)\right]\right\}^{1/2}$$

and ε_T is a zero mean r.v. with variance 1 which converges towards a standard Gaussian law; that is, $\varepsilon_T \to \mathcal{N}(0,1)$ when $T \to \infty$.

(ii) *Moreover, one can deduce the quantiles of annual production as follows:*

$$\begin{aligned} Q_{0.05} &= T \times \mathscr{P}^F - 1.65 \times T^{1/2} \times \left(\mathscr{V}^F\right)^{1/2} \times \Gamma_T^F, \\ Q_{0.95} &= T \times \mathscr{P}^F + 1.65 \times T^{1/2} \times \left(\mathscr{V}^F\right)^{1/2} \times \Gamma_T^F. \end{aligned} \tag{6}$$

Remark 2. Theorem 1 is warrant under the assumptions (A1) and (A2), which correspond to the stationarity of wind series and consequently of power series P_t. However, this result can be enhanced by taking into account the wind direction as in [13, 14] or by replacing the stationarity assumption by seasonality.

To sum up, the quantiles and the mean annual wind power production depend on three parameters, that is $\mathscr{P}^F$ the mean of ten-minute wind power of the farm, $\mathscr{V}^F$ the variance of ten-minute wind power, and Γ_T^F which depends on the correlation structure of the wind power time series. Before starting the estimation procedures, we check the correlation coefficient $\rho_X(k)$ as described previously, which proves that wind speed and the average wind farm power of four turbines are strongly correlated at a time scale smaller than ten hours and become uncorrelated at scale 48 hours (confirmed by Ljung-Box test; see e.g., [18]) as shown in the following Figure 4.

3.3. Results. In order to carry out the overestimation of the mean wind farm power production, first, we take again

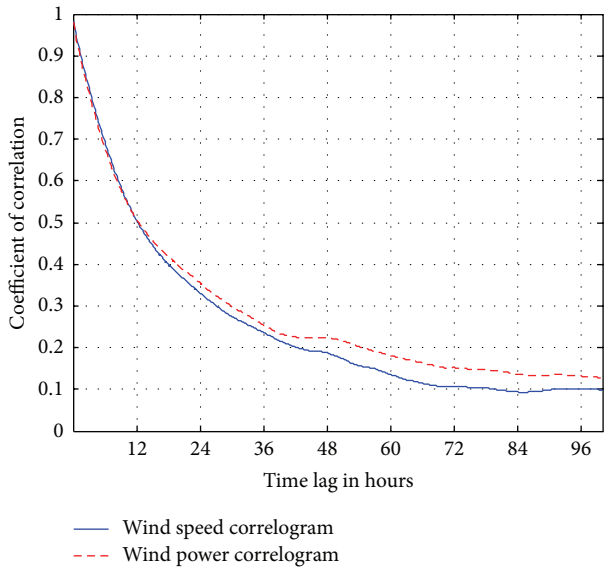

Figure 4: Correlogram of mean wind speed and mean wind farm power, duration 19 months.

the nominal power law proposed in [9] based on the use of a numerical sample of the ten-minute wind power derived from the sample of wind speed. Secondly, we use the traditional method which is modeled by a Weibull distribution law described in Section 3.1. We compare the overestimation rate for each turbine and for all the farm as illustrated in Table 2.

We should note that the overestimation of the mean power farm production based on a Weibull model is 10.43% and with the numerical wind power series it becomes 1.8%. The sources of this overestimation are out of the scope of this article. However, starting from the estimation of the autocorrelation coefficient, defined in Section 3.2, we proceed to calculate the mean and the quantiles of the annual power production for the whole farm. It is based on a sample of ten-minute wind power as a postproduction approach. Then, we use the new method, that is, the preproduction approach which has already been used in the computed precedents.

3.3.1. The Postproduction Approach. For the measurements P_t^F of the existing turbines, we calculate the quantity Γ_T^F provided by the entire farm and $\Gamma_T^{E_j}$ for each turbine, that is, $j = 1, \ldots, 4$, and we get the values stored in Table 3.

Then, we can deduce the mean and the quantiles of the annual power production (see Table 4).

3.3.2. The Preproduction Approach. First, we calculate $P_t^{E_1}$, $P_t^{E_2}$, $P_t^{E_3}$, and $P_t^{E_4}$ based on the wind speed measurements provided by each turbine through power law. Thereafter, we follow the same procedure as mentioned previously. We get Table 5.

Then, from these values, we obtained the mean and the quantiles by using Theorem 1 for each turbine and for the farm, for the annual wind power production (see Table 6).

We can also forecast the twenty-year wind farm power production (20yPP), which corresponds to the lifespan of some turbines (see Table 7).

Table 2: The overestimation rate.

	E_1	E_2	E_3	E_4	Farm
Power law	−4.4	−3.8	−0.7	+2.1	−1.8
Weibull law	−1.8	−0.2	−46.3	+4.7	−10.43

Table 3: Estimated values of Γ for existing turbines.

Γ_T^F	$\Gamma_T^{E_1}$	$\Gamma_T^{E_2}$	$\Gamma_T^{E_3}$	$\Gamma_T^{E_4}$
9.159	10.068	10.015	9.891	10.008

Table 4: The annual mean power production and its quantiles (GWH).

	T_1	T_2	T_3	T_4	Farm
$E(\mathscr{P}_{\text{annual}})$	6.62	6.24	6.0	6.29	25.14
$Q_{0.05}$	6.18	5.82	5.58	5.86	23.47
$Q_{0.95}$	7.06	6.67	6.41	6.71	26.82
Spread (%)	13.4	13.6	13.9	13.5	13.3

Table 5: Estimated values of Γ obtained by the preproduction approach.

Γ_T^F	$\Gamma_T^{E_1}$	$\Gamma_T^{E_2}$	$\Gamma_T^{E_3}$	$\Gamma_T^{E_4}$
10.095	10.085	9.995	9.904	10.026

Table 6: Forecasting power production for one year and its quantiles (GWH).

	T_1	T_2	T_3	T_4	Farm
$\mathbb{E}(\mathscr{P}_{\text{annual}})$	6.33	6.0	5.95	6.42	24.70
$Q_{0.05}$	5.89	5.58	5.53	5.58	23
$Q_{0.95}$	6.77	6.42	6.37	6.85	26.41
Spread (%)	14	14	14.1	13.5	13.8

Table 7: Forecasting of twenty-year power production and its quantiles (GWH).

	T_1	T_2	T_3	T_4	Farm
20yPP	127	120	119	128	494
$Q_{0.05}$	125	118	117	126	486
$Q_{0.95}$	129	122	121	130	502
Spread (%)	3.1	3.1	3.1	3	3

We find that the uncertainties decrease with the length of the forecast period, rising from 13.8% for one year to 3% for twenty years on total wind farm power, whereas it is decreased from 14% for one year to 3% for twenty years at each turbine.

3.4. The Relationship between the Measurements of Each Turbine in the Farm. To achieve a good characterization of the relationship between the power output and the wind speed for the four turbines, we calculate the correlation coefficients of wind power production (denoted by P_1, P_2, P_3, and P_4) and the correlation coefficients of wind speed (denoted by S_1, S_2, S_3, and S_4) of the four turbines. Let us recall that the correlation coefficient for two series X and Y is

Table 8: Correlation coefficients for P_1, P_2, P_3, and P_4.

	P_1	P_2	P_3	P_4
P_1	1	0.91	0.90	0.91
P_2	0.91	1	0.92	0.90
P_3	0.90	0.92	1	0.90
P_4	0.91	0.90	0.90	1

Table 9: Correlation coefficients using numerical sample for P_1, P_2, P_3, and P_4.

	P_1	P_2	P_3	P_4
P_1	1	0.96	0.94	0.96
P_2	0.96	1	0.97	0.96
P_3	0.94	0.97	1	0.97
P_4	0.96	0.96	0.97	1

Table 10: Correlation coefficients for S_1, S_2, S_3, and S_4.

	S_1	S_2	S_3	S_4
S_1	1	0.97	0.91	0.97
S_2	0.97	1	0.92	0.97
S_3	0.91	0.92	1	0.92
S_4	0.97	0.97	0.92	1

calculated as $\rho(X, Y) = \mathrm{cov}(X, Y)/\sigma_X\sigma_Y$. The correlations for the existing turbines can be summarized in Table 8.

Let us point out that the coefficient correlation is always superior to 0.9 for the wind power production of the four turbines. This assessment is of importance to appreciate the quality of the location of the turbines. We should take into account the effect of interactions between neighbour turbines which can eventually present loss in wind power production. The results obtained by the data generated through the power law are very close to this one. This once again underlines the contribution of the proposed approach to study the relationship that may exist between the energy outputs of wind turbines on a farm before their installation.

Similarly, regarding the correlation between the four wind speeds (denoted by S_1, S_2, S_3, and S_4), we can distinguish the strong correlation between all the turbines which is nearly equal to 1 (see Tables 9 and 10).

4. Discussion

The grouping of several wind turbines on the same site reduces the investment costs. However, it is important to make an optimal configuration of the turbines locations. For this wind farm site, there will be certain directions for which other turbines affect the production of single wind turbine. A more detailed analysis of this dependence will be made in further work.

References

[1] I. Colak, S. Sagiroglu, and M. Yesilbudak, "Data mining and wind power prediction: a literature review," *Renewable Energy*, vol. 46, pp. 241–247, 2012.

[2] C. Chourpouliadis, E. Ioannou, A. Koras, and A. I. Kalfas, "Comparative study of the power production and noise emissions impact from two wind farms," *Energy Conversion and Management*, vol. 60, pp. 233–242, 2012.

[3] L. Landberg, "Short-term prediction of the power production from wind farms," *Journal of Wind Engineering and Industrial Aerodynamics*, vol. 80, no. 1-2, pp. 207–220, 1999.

[4] G. Giebel, L. Landberg, G. Kariniotakis, and R. Brownsword, "Stateof- the-art methods and software tools for short-term prediction of wind energy production," in *Proceedings of European Wind Energy Conference and Exhibition (EWEC 03)*, Madrid, Spain, 2003, CD-ROM.

[5] P. Ramírez and J. A. Carta, "The use of wind probability distributions derived from the maximum entropy principle in the analysis of wind energy. A case study," *Energy Conversion and Management*, vol. 47, no. 15-16, pp. 2564–2577, 2006.

[6] A. Costa, A. Crespo, J. Navarro, G. Lizcano, H. Madsen, and E. Feitosa, "A review on the young history of the wind power short-term prediction," *Renewable and Sustainable Energy Reviews*, vol. 12, no. 6, pp. 1725–1744, 2008.

[7] J. A. Carta, P. Ramírez, and S. Velázquez, "A review of wind speed probability distributions used in wind energy analysis. Case studies in the Canary Islands," *Renewable and Sustainable Energy Reviews*, vol. 13, no. 5, pp. 933–955, 2009.

[8] A. Kusiak, H. Zheng, and Z. Song, "Wind farm power prediction: a data-mining approach," *Wind Energy*, vol. 12, no. 3, pp. 275–293, 2009.

[9] A. Bensoussan, P. R. Bertrand, and A. Brouste, "Forecasting the energy produced by a windmill on a yearly basis," *Stochastic Environmental Research and Risk Assessment*, vol. 26, pp. 1109–1122, 2012.

[10] A. Sfetsos, "A comparison of various forecasting techniques applied to mean hourly wind speed time series," *Renewable Energy*, vol. 21, no. 1, pp. 23–35, 2000.

[11] J. M. Sloughter, T. Gneiting, and A. E. Raftery, "Probabilistic wind speed forecasting using ensembles and Bayesian model averaging," *Journal of the American Statistical Association*, vol. 105, no. 489, pp. 25–35, 2010.

[12] P. Pinson, "Very-short-term probabilistic forecasting of wind power with generalized logit-normal distributions," *Journal of the Royal Statistical Society. Series C*, vol. 61, no. 4, pp. 555–576, 2012.

[13] D. P. Mandic, S. Javidi, S. L. Goh, A. Kuh, and K. Aihara, "Complex-valued prediction of wind profile using augmented complex statistics," *Renewable Energy*, vol. 34, no. 1, pp. 196–201, 2009.

[14] C. C. Took, G. Strbac, K. Aihara, and D. P. Mandic, "Quaternion-valued short-term joint forecasting of three-dimensional wind and atmospheric parameters," *Renewable Energy*, vol. 36, no. 6, pp. 1754–1760, 2011.

[15] O. A. Jaramillo and M. A. Borja, "Wind speed analysis in La Ventosa, Mexico: a bimodal probability distribution case," *Renewable Energy*, vol. 29, no. 10, pp. 1613–1630, 2004.

[16] M. Li and X. Li, "MEP-type distribution function: a better alternative to Weibull function for wind speed distributions," *Renewable Energy*, vol. 30, no. 8, pp. 1221–1240, 2005.

[17] R. B. Corotis, A. B. Sigl, and M. P. Cohen, "On a measure of lack of fit in time series models," *Journal of Applied Meteorology*, vol. 16, no. 11, pp. 1149–1157, 1977.

[18] G. M. Ljung and G. E. P. Box, "On a measure of lack of fit in time series models," *Biometrika*, vol. 65, no. 2, pp. 297–303, 1978.

Hindawi Publishing Corporation
Mathematical Problems in Engineering
Volume 2013, Article ID 396740, 12 pages
http://dx.doi.org/10.1155/2013/396740

Research Article

Robust Active Disturbance Rejection Control Approach to Maximize Energy Capture in Variable-Speed Wind Turbines

Horacio Coral-Enriquez, John Cortés-Romero, and Germán A. Ramos

Universidad Nacional de Colombia, Departamento de Ingeniería Eléctrica y Electrónica, Carrera 45 No. 26-85, Bogotá, Colombia

Correspondence should be addressed to Horacio Coral-Enriquez; hacorale@unal.edu.co

Received 19 April 2013; Accepted 30 May 2013

Academic Editor: Ming-Hung Hsu

This paper proposes an alternative robust observer-based linear control technique to maximize energy capture in a 4.8 MW horizontal-axis variable-speed wind turbine. The proposed strategy uses a generalized proportional integral (GPI) observer to reconstruct the aerodynamic torque in order to obtain a generator speed optimal trajectory. Then, a robust GPI observer-based controller supported by an active disturbance rejection (ADR) approach allows asymptotic tracking of the generator speed optimal trajectory. The proposed methodology controls the power coefficient, via the generator angular speed, towards an optimum point at which power coefficient is maximum. Several simulations (including an actuator fault) are performed on a 4.8 MW wind turbine benchmark model in order to validate the proposed control strategy and to compare it to a classical controller. Simulation and validation results show that the proposed control strategy is effective in terms of power capture and robustness.

1. Introduction

The use of wind energy has a history of over a hundred years. Its applications include agriculture, milling, water pumping, and power production. In the 1970s, this technology started developing as an experimental technology. Nowadays, the conversion of wind energy into electrical energy by wind turbines is a mature technology that exhibits the highest growth rates among the renewable energy sources [1] and can be considered as the most promising option for replacing a significant part of the electricity produced by conventional sources [2].

The main objective of wind turbines is to convert efficiently wind energy into electrical power. There are wind turbines available in a different number of configurations (vertical axis, horizontal axis, fixed speed, variable speed, etc.). The most used type for large-scale power production is the variable-speed horizontal-axis wind turbine (HAWT) with a two- or three-blade rotor [3]. HAWTs are commonly equipped with blade-pitch actuators, generator torque control and many sensors for use in real time control [4]. HAWTs operate in different control regions, and the region considered in the present work is a low-to-medium wind speeds operation (also called partial load operation or operation in region 2) where the main objective is to extract the maximum power from the wind.

Modern wind turbines are machines that require big efforts when maximizing wind energy capture, not only because of their highly nonlinear aerodynamics, but also because of the high efficiency required even when model uncertainties, external perturbations, or system faults are present. As a consequence, the efficiency of both power capture and power generation is strongly dependent on the selected control method [5]. This situation provides a motivation to consider new alternative control techniques that improve the performance of HAWT without any structural change.

A large number of control schemes to find the best way of solving the energy capture maximization problem for wind turbines at low-to-medium wind speeds have been proposed (see, e.g., [6–12]). The control techniques range from standard torque control [6], disturbance tracking control [7], maximum power point tracking [8], and aerodynamic torque feedforward [9] to complex nonlinear strategies [5, 10–12]. Most of these techniques deal with the wind turbine complexity using linearization techniques or nonlinear control. Following a different approach, some of the active-disturbance-rejection- (ADR-) based techniques allow linear control

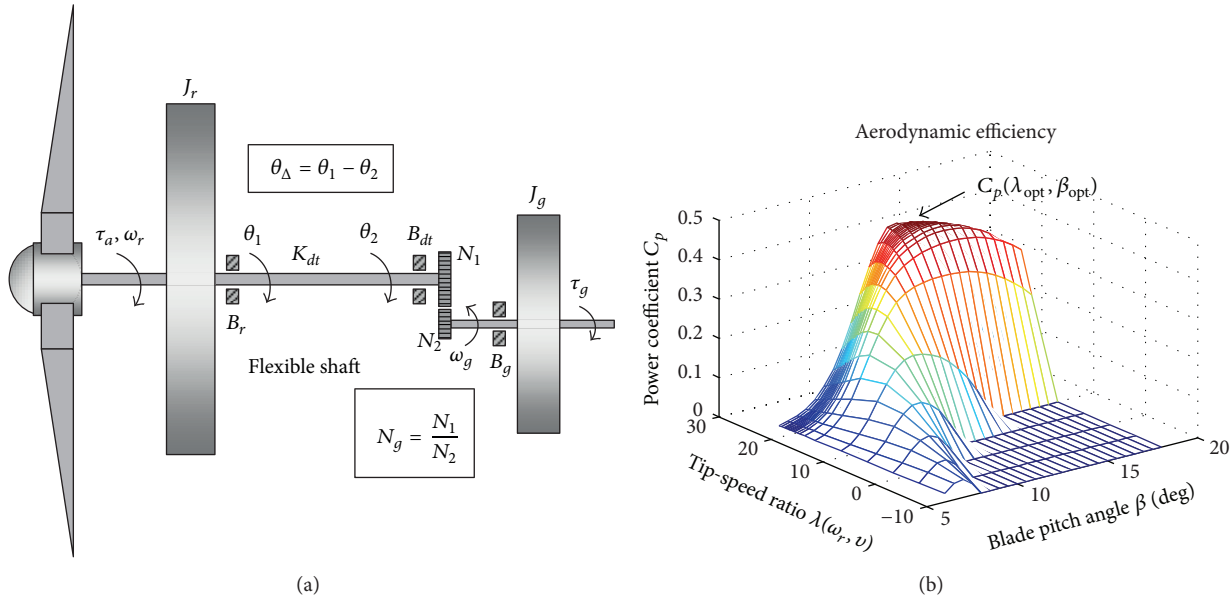

Figure 1: Mechanical and aerodynamical characteristics of the wind turbine.

solutions for some class of uncertain complex nonlinear systems and could offer a linear, simpler, and robust solution to the wind energy capture maximization problem. This is the case of the ADR philosophy-based technique called generalized proportional integral (GPI) Control [13] and its GPI observer-based control extensions [14, 15].

Generalized proportional integral (GPI) control technique was started in 2000 by Fliess et al. [13, 16] and involves in its design the active rejection of disturbances. The dual counterpart of the generalized proportional integral controller, called GPI observer, was introduced in [15], in the context of sliding mode observers for flexible robotics systems. The nonsliding version appears in [14] applied to chaotic systems synchronization. The GPI control strategies have been adapted, extended, and applied successfully in areas other than wind energy, such as induction motor control [17], chaotic systems control [18], and power converters control [19]. Therefore, it is interesting to adapt, evaluate, and determine the scope of this control method in partial load wind turbine operation.

GPI observer-based control of nonlinear uncertain systems is very much related to methodologies known as disturbance accommodation control (DAC) and active disturbance rejection control (ADRC). These approaches deal with the problem of cancelling, from the controller's actions, endogenous and exogenous unknown additive disturbance inputs affecting the system. Perturbation effects are made available via a suitable linear or nonlinear estimation. The reader is invited to read the works by Johnson [20], Han [21], and Gao et al. [22, 23].

This work presents an alternative linear control technique based on GPI observers to maximize wind energy capture in variable-speed wind turbines operating at partial load. The proposed strategy uses a GPI observer to reconstruct the aerodynamic torque in order to provide a generator speed optimal trajectory to a robust GPI observer-based controller that regulates the power coefficient, via the generator torque, towards an optimum point at which the power coefficient is maximum. It is expected that the proposed GPI observer-based control technique adds robustness to the system and solves the control problem through linear active estimation and rejection of nonlinearities and perturbations of the wind energy conversion system (WECS).

This paper is organized as follows. In Section 2, a wind turbine dynamic model for control purposes is presented. Section 3 formulates the control problem and presents the proposed methodology to solve it. Section 4 describes the benchmark and the tests model used to validate the proposed methodology. Section 5 presents the simulations and validations results of the proposed control strategy. Finally, Section 6 contains the conclusions and suggestions for further work.

2. Wind Turbine Model

Consider a wind turbine represented by a two-mass mechanical system as shown in Figure 1(a), where the aerodynamic power captured by the rotor is given by [24]

$$P_a(t) = \frac{1}{2}\rho\pi R^2 C_p(\lambda, \beta)\, \upsilon(t)^3, \tag{1}$$

where R is the rotor radius, ρ is the air density, $\upsilon(t)$ is the wind velocity, and $C_p(\lambda, \beta)$ is the power coefficient which denotes the aerodynamic efficiency of the wind energy conversion system. The power coefficient curve $C_p(\lambda, \beta)$ of the wind turbine considered in this work is shown in Figure 1(b). This curve was taken from the benchmark model published in [25]. The power coefficient $C_p(\lambda, \beta)$ depends on both

the blade pitch angle β and the tip-speed ratio λ. The latter is defined as

$$\lambda = \frac{\omega_r(t) R}{v(t)}, \tag{2}$$

where $\omega_r(t)$ is the rotor angular speed. The aerodynamic power $P_a(t)$ can also be expressed in function of both the aerodynamic torque $\tau_a(t)$ and the rotor speed $\omega_r(t)$ as follows [24]:

$$P_a(t) = \omega_r(t)\,\tau_a(t). \tag{3}$$

The aerodynamic torque $\tau_a(t)$ is given by

$$\tau_a(t) = \frac{1}{2}\rho\pi R^3 C_q(\lambda,\beta)\, v(t)^2, \tag{4}$$

where C_q is the torque coefficient and is defined as follows:

$$C_q(\lambda,\beta) = \frac{C_p(\lambda,\beta)}{\lambda}. \tag{5}$$

The mechanical system of the wind turbine is modeled using Newton's laws, and the following system is derived [25]:

$$\begin{aligned} \frac{d}{dt}\mathbf{x_{wt}}(t) &= \mathbf{A_{wt}}\mathbf{x_{wt}}(t) + \mathbf{B_{wt}}\tau_g(t) + \mathbf{F_{wt}}\tau_a(t), \\ y(t) &= \mathbf{C_{wt}}\mathbf{x_{wt}}(t) \end{aligned} \tag{6}$$

with

$$\mathbf{x_{wt}}(t) = \begin{bmatrix} \omega_r(t) \\ \omega_g(t) \\ \theta_\Delta(t) \end{bmatrix},$$

$$\mathbf{A_{wt}} = \begin{bmatrix} \dfrac{-B_{dt}-B_r}{J_r} & \dfrac{B_{dt}}{J_r N_g} & \dfrac{-K_{dt}}{J_r} \\ \dfrac{B_{dt}\eta_{dt}}{J_g N_g} & \dfrac{-\left(B_g + \left(B_{dt}\eta_{dt}/N_g^2\right)\right)}{J_g} & \dfrac{K_{dt}\eta_{dt}}{J_g N_g} \\ 1 & \dfrac{-1}{N_g} & 0 \end{bmatrix}, \tag{7}$$

$$\mathbf{B_{wt}} = \begin{bmatrix} 0 \\ \dfrac{-1}{J_g} \\ 0 \end{bmatrix}, \qquad \mathbf{F_{wt}} = \begin{bmatrix} \dfrac{1}{J_r} \\ 0 \\ 0 \end{bmatrix}, \qquad \mathbf{C_{wt}} = \begin{bmatrix} 0 & 1 & 0 \end{bmatrix},$$

where $\omega_g(t)$ is the generator side angular speed, $\theta_\Delta(t)$ is the torsion angle of the drive train, J_r is the moment of inertia of the low speed shaft, J_g is the moment of inertia of the high speed shaft, K_{dt} is the torsion stiffness of the drive train, B_{dt} is the torsion damping coefficient of the drive train, B_r is the viscous friction of the low speed shaft, B_g is the viscous friction of the high speed shaft, N_g is the gear ratio, η_{dt} is the efficiency of the drive train, and $\tau_g(t)$ is the generator torque.

The power converter and generator dynamics are given by [25]

$$\frac{d}{dt}\tau_g(t) = -\alpha_{\mathrm{gc}}\tau_g(t) + \alpha_{\mathrm{gc}}\tau_{g,\mathrm{ref}}(t), \tag{8}$$

$$P_g(t) = \eta_g \omega_g(t)\,\tau_g(t), \tag{9}$$

respectively, where $\tau_{g,\mathrm{ref}}(t)$ is the desired generator torque (control input), $P_g(t)$ is the produced power by the generator, α_{gc} denotes the dynamic coefficient of the generator/converter, and η_g is the generator efficiency.

3. Active Disturbance Rejection Design for Wind Turbine Control

The following assumptions in relation to the system (1)–(9) are stated.

Assumption 1. All the parameters of the WECS are known.

Assumption 2. The pair $(\mathbf{A_{wt}}, \mathbf{C_{wt}})$ is completely observable.

Assumption 3. The generator angular speed $\omega_g(t)$ as well as the generated generator torque $\tau_g(t)$ is available to be used in the control system.

Assumption 4. For sufficiently large positive integer p, the disturbance input $\tau_a(t)$ exhibits uniformly absolute bounded time derivative of order p. This condition assures the existence of an unknown but finite constant, K_{τ_a}, such that $\sup_{t\geq 0}|\tau_a^{(p)}(t)| \leq K_{\tau_a}$.

3.1. Problem Formulation. For a partial load-operating regime (operation in region 2), the main control objective is the maximization of wind power capture. This objective has a strong relation with the wind turbine power coefficient curve $C_p(\lambda,\beta)$, which has a unique maximum point that corresponds to the optimal capture of the wind power:

$$C_p\left(\lambda_{\mathrm{opt}},\beta_{\mathrm{opt}}\right) = C_{p_{\mathrm{opt}}}, \tag{10}$$

where

$$\lambda_{\mathrm{opt}} = \frac{\omega_{g_{\mathrm{opt}}}(t)\, R}{N_g v(t)}. \tag{11}$$

Accordingly, in order to maximize wind power capture, the blade pitch angle β is fixed to its optimal value β_{opt}, and in order to maintain λ at its optimal value λ_{opt}, the generator speed must be adjusted to track the optimal reference $\omega_{g_{\mathrm{opt}}}(t)$, given by

$$\omega_{g_{\mathrm{opt}}}(t) = \frac{N_g \lambda_{\mathrm{opt}}}{R} v(t). \tag{12}$$

Then, it is desired to force the output $\omega_g(t)$ to accurately track the given trajectory $\omega_{g_{\mathrm{opt}}}(t)$, independently of the aerodynamic torque input and possible unmodeled perturbation inputs in the WECS, using the desired generator torque $\tau_{g,\mathrm{ref}}(t)$ as the control input and the generator angular speed $\omega_g(t)$ as the feedback signal.

3.2. GPI Observer Design for Aerodynamic Torque Estimation. In order to obtain the optimal reference $\omega_{g_{\mathrm{opt}}}(t)$, (4), (5), and

(12) are combined. The wind velocity $v(t)$ is easily represented as a function of $\tau_a(t)$ and C_p using (4) and (5):

$$v(t) = \sqrt{\frac{2\lambda\tau_a(t)}{\rho\pi R^3 C_p(\lambda,\beta)}}. \tag{13}$$

Then, by replacing (13) in (12), setting λ and C_p to its optimal values, and changing $\tau_a(t)$ to its estimated version $\widehat{\tau}_a(t)$, the following expression is obtained for the optimal reference trajectory:

$$\widehat{\omega}_{g_{\text{opt}}}(t) = \frac{N_g\lambda_{\text{opt}}}{R}\sqrt{\frac{2\lambda_{\text{opt}}\widehat{\tau}_a(t)}{\rho\pi R^3 C_{p_{\text{opt}}}}}. \tag{14}$$

According to (14), it is necessary to estimate the aerodynamic torque $\tau_a(t)$. For that purpose, an extended Luenberger-like linear observer is developed, here referred as GPI observer. The proposed observer uses an approximated internal model of the unknown input disturbance to compose an augmented model for the plant and the disturbance input. Inherent to this kind of observer, a state estimation is also provided. This estimation will be used in the establishment of the GPI observer-based control for $\omega_{g_{\text{opt}}}(t)$ tracking.

Given a positive integer p, the unknown input perturbation $\tau_a(t)$ can be modeled by the approximation of its internal model given by

$$\frac{d^p\tau_a(t)}{dt^p} \approx 0. \tag{15}$$

Consider the following disturbance states, related to (15):

$$\mathbf{x_d}(t) = \left[\tau_a(t) \;\; \dot{\tau}_a(t) \;\; \cdots \;\; \tau_a^{(p-2)}(t) \;\; \tau_a^{(p-1)}(t)\right]^T, \tag{16}$$

where its corresponding dynamics is given by

$$\begin{aligned}\frac{d}{dt}\mathbf{x_d}(t) &= \mathbf{A_d}\mathbf{x_d}(t) + \mathbf{B_d}\tau_a^{(p)}(t),\\ \tau_a(t) &= \mathbf{C_d}\mathbf{x_d}(t)\end{aligned} \tag{17}$$

with

$$\mathbf{A_d} = \begin{bmatrix} 0 & 1 & 0 & \cdots & 0\\ 0 & 0 & 1 & \cdots & 0\\ \vdots & \vdots & \vdots & \ddots & \vdots\\ 0 & 0 & 0 & \cdots & 1\\ 0 & 0 & 0 & \cdots & 0 \end{bmatrix},$$
$$\mathbf{B_d} = \begin{bmatrix} 0\\ 0\\ \vdots\\ 0\\ 1 \end{bmatrix}, \qquad \mathbf{C_d} = \begin{bmatrix} 1 & 0 & 0 & \cdots & 0 \end{bmatrix}, \tag{18}$$

where $\mathbf{x_d}(t) \in \mathbb{R}^{p\times 1}$, $\mathbf{A_d} \in \mathbb{R}^{p\times p}$, $\mathbf{B_d} \in \mathbb{R}^{p\times 1}$, and $\mathbf{C_d} \in \mathbb{R}^{1\times p}$.

Now, the disturbance states $\mathbf{x_d}(t)$ can be added to the system state vector $\mathbf{x_{wt}}(t)$ to form the following augmented system:

$$\begin{aligned}\frac{d}{dt}\mathbf{x}(t) &= \mathbf{A}\mathbf{x}(t) + \mathbf{B}\tau_g(t) + \mathbf{B_a}\tau_a^{(p)}(t),\\ y(t) &= \mathbf{C}\mathbf{x}(t)\end{aligned} \tag{19}$$

with

$$\mathbf{x}(t) = \begin{bmatrix}\mathbf{x_{wt}}(t)\\ \mathbf{x_d}(t)\end{bmatrix}, \qquad \mathbf{A} = \begin{bmatrix}\mathbf{A_{wt}} & \mathbf{F_{wt}}\mathbf{C_d}\\ \mathbf{0} & \mathbf{A_d}\end{bmatrix},$$
$$\mathbf{B} = \begin{bmatrix}\mathbf{B_{wt}}\\ \mathbf{0}\end{bmatrix}, \qquad \mathbf{B_a} = \begin{bmatrix}\mathbf{0}\\ \mathbf{B_d}\end{bmatrix}, \qquad \mathbf{C} = \begin{bmatrix}\mathbf{C_{wt}} & \mathbf{0}\end{bmatrix}, \tag{20}$$

where $\mathbf{x}(t) \in \mathbb{R}^{(p+3)\times 1}$, $\mathbf{A} \in \mathbb{R}^{(p+3)\times(p+3)}$, $\mathbf{B}, \mathbf{B_a} \in \mathbb{R}^{(p+3)\times 1}$, and $\mathbf{C} \in \mathbb{R}^{1\times(p+3)}$.

The next step is to design a GPI observer for the composite system in (19) regarding the approximated internal model given in (15). The estimated augmented state vector $\mathbf{x}(t)$ contains a real-time estimate of $\mathbf{x_d}(t)$, which is used along with $\mathbf{C_d}$ to recover $\tau_a(t)$.

Remark 5. ADR-GPI observer-based controllers use an internal model approximation of the perturbation functions to reconstruct and reject the perturbations. Under this disturbance model approximation setting, several authors have applied it to different areas. Parker and Johnson used a first-order perturbation approximation to model wind speed perturbations in a wind turbine operating in region 3 [26]. Freidovich and Khalil [27] used a first-order perturbation model approximation to estimate the model uncertainty and disturbance on a nonlinear system. Zhao and Gao also used a first-order internal model disturbance approximation to estimate the resonance in two-inertia systems [28] and a first- and second-order approximation to estimate the nonlinearities of an actuator [29]. Zheng et al. also used disturbance model approximation applied to disturbance decoupling control [30].

Remark 6. The parameter p is related to the complexity of the signal to estimate, as in the case of Taylor polynomial approximation. A first-order perturbation model approximation means that the internal model approximation is capable to converge towards a constant disturbance. Equation (15) is a more generalized extension of the internal model perturbation function which provides extra information and increases the ability to track different types of disturbances. For example, $p = 2$ allows convergence to a disturbance with a constant derivative, $p = 3$ allows convergence to a disturbance with a constant acceleration, and so forth.

Theorem 7. *Supposing that Assumptions 1–4 are valid, for the augmented WECS represented by* (19) *and* (20)*, the following GPI observer is proposed:*

$$\frac{d}{dt}\widehat{\mathbf{x}}(t) = \mathbf{A}\widehat{\mathbf{x}}(t) + \mathbf{B}\tau_g(t) + \boldsymbol{\alpha}\left(y - \mathbf{C}\widehat{\mathbf{x}}(t)\right), \tag{21}$$

where $\widehat{\mathbf{x}}(t) = \left[\widehat{\mathbf{x}}_{\mathbf{wt}}(t)^{\mathbf{T}} \ \widehat{\mathbf{x}}_{\mathbf{d}}(t)^{\mathbf{T}}\right]^T = \left[\widehat{\omega}_r(t) \ \widehat{\omega}_g(t) \ \widehat{\theta}_\Delta(t) \ \widehat{\tau}_a(t) \ \dot{\widehat{\tau}}_a(t) \ \cdots \ \widehat{\tau}_a^{(p-2)}(t) \ \widehat{\tau}_a^{(p-1)}(t)\right]^T$ *is the augmented system state estimation and* $\boldsymbol{\alpha} = \left[\alpha_{p+3} \ \alpha_{p+2} \ \cdots \ \alpha_2 \ \alpha_1\right]^T$ *are the observer gains. The GPI observer* (21) *asymptotically and exponentially reconstructs the system states* $\omega_r(t)$, $\omega_g(t)$, $\theta_\Delta(t)$, *and the perturbation inputs* $\tau_a(t)$, $\dot{\tau}_a(t), \ldots, \tau_a^{(p-1)}$ *forcing the state estimation error* $\widetilde{\mathbf{e}}_{\mathbf{x}}(t) = \mathbf{x}(t) - \widehat{\mathbf{x}}(t)$ *to converge towards the interior of a disk centered in the origin of the corresponding estimation error phase space, as long as the set of coefficients* $\{\alpha_{p+3}, \ldots, \alpha_2, \alpha_1\}$ *is chosen in such a way that the characteristic polynomial defined by*

$$\det(s\mathbf{I} - \mathbf{A} + \boldsymbol{\alpha}\mathbf{C}) = 0 \tag{22}$$

is a Hurwitz polynomial, with roots located to the left of the imaginary axis of the complex plane.

Proof. By subtracting the proposed observer (21) from the augmented system state equation (19), the following estimation error dynamics is obtained:

$$\dot{\widetilde{\mathbf{e}}}_{\mathbf{x}}(t) = (\mathbf{A} - \boldsymbol{\alpha}\mathbf{C})\,\widetilde{\mathbf{e}}_{\mathbf{x}}(t) + \mathbf{B}_{\mathbf{a}}\tau_a^{(p)}(t) = \mathbf{A}_{\mathbf{a}}\widetilde{\mathbf{e}}_{\mathbf{x}}(t) + \mathbf{B}_{\mathbf{a}}\tau_a^{(p)}(t), \tag{23}$$

where the eigenvalues of $\mathbf{A}_{\mathbf{a}} = (\mathbf{A} - \boldsymbol{\alpha}\mathbf{C})$ can be placed as desired by selecting the gain vector $\boldsymbol{\alpha}$.

In order to obtain an ultimate bound for $\widetilde{\mathbf{e}}_{\mathbf{x}}(t)$, let $\mathbf{Q} \in \mathbb{R}^{(p+3)\times(p+3)}$ be a constant, positive definite symmetric matrix. The proper stable character of the matrix $\mathbf{A}_{\mathbf{a}}$ implies the existence of a positive definite matrix $\mathbf{P} \in \mathbb{R}^{(p+3)\times(p+3)}$ such that $\mathbf{A}_{\mathbf{a}}^{\mathbf{T}}\mathbf{P} + \mathbf{P}\mathbf{A}_{\mathbf{a}} = -\mathbf{Q}$. Consider the Lyapunov function candidate $V(\widetilde{\mathbf{e}}_{\mathbf{x}}) = (1/2)\widetilde{\mathbf{e}}_{\mathbf{x}}^{\mathbf{T}}(t)\mathbf{P}\widetilde{\mathbf{e}}_{\mathbf{x}}(t)$. The time derivative of V satisfies

$$\dot{V}(\widetilde{\mathbf{e}}_{\mathbf{x}}, t) = \frac{1}{2}\left[\widetilde{\mathbf{e}}_{\mathbf{x}}^{\mathbf{T}}(-\mathbf{Q})\,\widetilde{\mathbf{e}}_{\mathbf{x}}\right] + \mathbf{B}_{\mathbf{a}}^{\mathbf{T}}\mathbf{P}\widetilde{\mathbf{e}}_{\mathbf{x}}\tau_a^{(p)}(t). \tag{24}$$

For $Q = I$, that is, an identity matrix, $\dot{V}(\widetilde{\mathbf{e}}_{\mathbf{x}}, t)$ satisfies

$$\begin{aligned}\dot{V}(\widetilde{\mathbf{e}}_{\mathbf{x}}, t) &= \frac{1}{2}\left[\widetilde{\mathbf{e}}_{\mathbf{x}}^{\mathbf{T}}(-\mathbf{Q})\,\widetilde{\mathbf{e}}_{\mathbf{x}}\right] + \mathbf{B}_{\mathbf{a}}^{\mathbf{T}}\mathbf{P}\widetilde{\mathbf{e}}_{\mathbf{x}}\tau_a^{(p)}(t) \\ &\le -\frac{1}{2}\left\|\widetilde{\mathbf{e}}_{\mathbf{x}}\right\|_2^2 + \left\|\mathbf{B}_{\mathbf{a}}^{\mathbf{T}}\right\|_2\|\mathbf{P}\|_2\left\|\widetilde{\mathbf{e}}_{\mathbf{x}}\right\|_2 K_{\tau_a} < 0.\end{aligned} \tag{25}$$

Given that $\|\mathbf{B}_{\mathbf{a}}^{\mathbf{T}}\|_2 = 1$ and according to (25), $\dot{V}(\widetilde{\mathbf{e}}_{\mathbf{x}}, t)$ is strictly negative if

$$\left\|\widetilde{\mathbf{e}}_{\mathbf{x}}\right\|_2 > 2K_{\tau_a}\|\mathbf{P}\|_2. \tag{26}$$

Therefore, $\dot{V}(\widetilde{\mathbf{e}}_{\mathbf{x}}, t)$ is strictly negative outside the following disc:

$$D_x = \left\{\widetilde{\mathbf{e}}_{\mathbf{x}}(t) \in \mathbb{R}^{p+3}, \left\|\widetilde{\mathbf{e}}_{\mathbf{x}}\right\|_2 \le 2K_{\tau_a}\|\mathbf{P}\|_2\right\}. \tag{27}$$

Consequently, a uniform ultimate bounded (UUB) result was obtained regarding the estimation error phase variables $\widetilde{\mathbf{e}}_{\mathbf{x}}(t)$. □

Remark 8. GPI observers are bandwidth limited by the roots location of the estimation error characteristic polynomial. Generally, the larger the observer bandwidth is, the more accurate the estimation will be. However, a large observer bandwidth will increase noise sensitivity. Then, the selection of the roots of the estimation error characteristic polynomial affects the bandwidth of the GPI observer and also the influence of measurement noises on the estimations. Therefore, GPI observers are usually tuned in a compromise between disturbance estimation performance (set by the internal model approximation degree) and noise sensitivity.

3.3. Robust GPI Observer-Based Control Design for Energy Capture Maximization. Based on (6), the generator angular speed $\omega_g(t)$ satisfies the following dynamics:

$$\begin{aligned}\frac{d\omega_g(t)}{dt} &= \frac{B_{dt}\eta_{dt}}{J_g N_g}\omega_r(t) - \frac{B_g + \left(B_{dt}\eta_{dt}/N_g^2\right)}{J_g}\omega_g(t) \\ &\quad + \frac{K_{dt}\eta_{dt}}{J_g N_g}\theta_\Delta(t) - \frac{1}{J_g}\tau_g(t).\end{aligned} \tag{28}$$

Then, by reorganizing and lumping together some terms of (28), the following simplified system (typical of the ADR philosophy) can be obtained:

$$\dot{\omega}_g(t) = \kappa\tau_g(t) + \Delta(t) + \varphi(t) \tag{29}$$

with

$$\begin{aligned}\kappa &= -\frac{1}{J_g}, \\ \varphi(t) &= \frac{B_{dt}\eta_{dt}}{J_g N_g}\omega_r(t) - \frac{B_g + \left(B_{dt}\eta_{dt}/N_g^2\right)}{J_g}\omega_g(t) \\ &\quad + \frac{K_{dt}\eta_{dt}}{J_g N_g}\theta_\Delta(t),\end{aligned} \tag{30}$$

where κ is a known constant, $\varphi(t)$ is a state dependent input perturbation, and $\Delta(t)$ is an input perturbation function that lumps together all the uncertainty associated to the system. The perturbation $\Delta(t)$ contains the rest of the system dynamics (actuator), including some unmodeled dynamics, disturbances of additive nature, actuator faults, parameter variations, and nonlinear effects of the WECS.

In relation to the simplified system (29), the following assumption is stated.

Assumption 9. For a sufficiently large positive integer m, the disturbance input $\Delta(t)$ exhibits a uniformly absolute bounded time derivative of order m. This condition assures the existence of an unknown but finite constant, K_Δ, such that $\sup_{t\ge 0}|\Delta^{(m)}(t)| \le K_\Delta$.

Assumption 10. The unknown input perturbation $\Delta(t)$ can be modeled by the approximation of its internal model given by

$$\frac{d^m\Delta(t)}{dt^m} \approx 0. \tag{31}$$

Consider the following disturbance states, related to (31),

$$\mathbf{x}_{\Delta}(t) = \left[\Delta(t) \;\; \dot{\Delta}(t) \;\; \cdots \;\; \Delta^{(m-2)}(t) \;\; \Delta^{(m-1)}(t)\right]^{T}, \tag{32}$$

where their corresponding dynamics is given by:

$$\frac{d}{dt}\mathbf{x}_{\Delta}(t) = \mathbf{A}_{\Delta}\mathbf{x}_{\Delta}(t) + \mathbf{B}_{\Delta}\Delta^{(m)}(t), \qquad \Delta(t) = \mathbf{C}_{\Delta}\mathbf{x}_{\Delta}(t) \tag{33}$$

with

$$\mathbf{A}_{\Delta} = \begin{bmatrix} 0 & 1 & 0 & \cdots & 0 \\ 0 & 0 & 1 & \cdots & 0 \\ \vdots & \vdots & \vdots & \ddots & \vdots \\ 0 & 0 & 0 & \cdots & 1 \\ 0 & 0 & 0 & \cdots & 0 \end{bmatrix}, \qquad \mathbf{B}_{\Delta} = \begin{bmatrix} 0 \\ 0 \\ \vdots \\ 0 \\ 1 \end{bmatrix}, \qquad \mathbf{C}_{\Delta} = \begin{bmatrix} 1 & 0 & 0 & \cdots & 0 \end{bmatrix}, \tag{34}$$

where $\mathbf{x}_{\Delta}(t) \in \mathbb{R}^{m\times 1}$, $\mathbf{A}_{\Delta} \in \mathbb{R}^{m\times m}$, $\mathbf{B}_{\Delta} \in \mathbb{R}^{m\times 1}$, and $\mathbf{C}_{\Delta} \in \mathbb{R}^{1\times m}$.

Then, it is possible to augment the simplified system in (29) with the unknown input perturbation state vector $\mathbf{x}_{\Delta}(t)$; thus,

$$\frac{d}{dt}\mathbf{x}_{c}(t) = \mathbf{A}_{c}\mathbf{x}_{c}(t) + \mathbf{B}_{c1}\tau_{g}(t) + \mathbf{B}_{c2}\varphi(t) + \mathbf{B}_{c3}\Delta^{(m)}(t), \qquad y(t) = \mathbf{C}_{c}\mathbf{x}_{c}(t) \tag{35}$$

with

$$\mathbf{x}_{c}(t) = \begin{bmatrix} \omega_{g}(t) \\ \mathbf{x}_{\Delta}(t) \end{bmatrix}, \qquad \mathbf{A}_{c} = \begin{bmatrix} 0 & \mathbf{C}_{\Delta} \\ 0 & \mathbf{A}_{\Delta} \end{bmatrix}, \qquad \mathbf{B}_{c1} = \begin{bmatrix} \kappa \\ \mathbf{0} \end{bmatrix}, \qquad \mathbf{B}_{c2} = \begin{bmatrix} 1 \\ \mathbf{0} \end{bmatrix}, \qquad \mathbf{B}_{c3} = \begin{bmatrix} 0 \\ \mathbf{B}_{\Delta} \end{bmatrix}, \qquad \mathbf{C}_{c} = \begin{bmatrix} 1 & \mathbf{0} \end{bmatrix}, \tag{36}$$

where $\mathbf{x}_{c}(t) \in \mathbb{R}^{(m+1)\times 1}$, $\mathbf{A}_{c} \in \mathbb{R}^{(m+1)\times(m+1)}$, $\mathbf{B}_{c1}, \mathbf{B}_{c2}, \mathbf{B}_{c3} \in \mathbb{R}^{(m+1)\times 1}$, and $\mathbf{C}_{c} \in \mathbb{R}^{1\times(m+1)}$.

It is desired that the generator angular speed $\omega_{g}(t)$ accurately tracks the optimal reference trajectory $\omega_{g_{\text{opt}}}(t)$, with tracking error defined by $e_{\omega}(t) = \omega_{g}(t) - \omega_{g_{\text{opt}}}(t)$ absolutely bounded by a small quantity ε; that is, $\sup_{t\geq 0}|e_{\omega}(t)| \leq \varepsilon$. Then, based on (29), (31), and (35), the following GPI observer-based control is proposed.

Theorem 11. *Given Assumptions 9 and 10, the estimation of the perturbation function $\Delta(t)$, denoted as $\widehat{\Delta}(t)$, is given by the following GPI observer:*

$$\frac{d}{dt}\widehat{\mathbf{x}}_{c}(t) = \mathbf{A}_{c}\widehat{\mathbf{x}}_{c}(t) + \mathbf{B}_{c1}\tau_{g}(t) + \mathbf{B}_{c2}\widehat{\varphi}(t) + \boldsymbol{\sigma}\left(y(t) - \mathbf{C}_{c}\widehat{\mathbf{x}}_{c}(t)\right), \tag{37}$$

$$\widehat{\Delta}(t) = \begin{bmatrix} 0 & \mathbf{C}_{\Delta} \end{bmatrix}\widehat{\mathbf{x}}_{c}(t) \tag{38}$$

with,

$$\widehat{\varphi}(t) = \frac{B_{dt}\eta_{dt}}{J_{g}N_{g}}\widehat{\omega}_{r}(t) - \frac{B_{g} + \left(B_{dt}\eta_{dt}/N_{g}^{2}\right)}{J_{g}}\widehat{\omega}_{g}(t) + \frac{K_{dt}\eta_{dt}}{J_{g}N_{g}}\widehat{\theta}_{\Delta}(t), \tag{39}$$

where $\widehat{\mathbf{x}}_{c}(t) = \left[\widehat{\omega}_{g}(t) \;\; \widehat{\Delta}(t) \;\; \dot{\widehat{\Delta}}(t) \;\; \cdots \;\; \widehat{\Delta}^{(m-2)}(t) \;\; \widehat{\Delta}^{(m-1)}(t)\right]^{\mathbf{T}}$ is the estimated system state vector, $\boldsymbol{\sigma} = \left[\sigma_{m+1} \;\; \sigma_{m} \;\; \cdots \;\; \sigma_{2} \;\; \sigma_{1}\right]^{T}$ is the observer gains, and $\widehat{\varphi}(t)$ is the estimation of $\varphi(t)$ reconstructed by using the states of the aerodynamic torque observer given in (21) that asymptotically and exponentially reconstructs the perturbation input $\Delta(t)$, forcing the state estimation error $\widetilde{\mathbf{e}}_{\mathbf{x}_{c}}(t) = \mathbf{x}_{c}(t) - \widehat{\mathbf{x}}_{c}(t)$ to converge towards the interior of a disk centered in the origin of the corresponding estimation error phase space, provided the set of coefficients: $\{\sigma_{m+1}, \ldots, \sigma_{2}, \sigma_{1}\}$, which are chosen in such a way that the polynomial $P_{\Delta}(s)$, in the complex variable s, defined by

$$P_{\Delta}(s) = s^{m+1} + \sigma_{m+1}s^{m} + \cdots + \sigma_{2}s + \sigma_{1} \tag{40}$$

is a Hurwitz polynomial, with roots located to the left of the imaginary axis of the complex plane.

Proof. By subtracting the proposed GPI observer (37) from the augmented system state equation (35), the following estimation error dynamics is obtained:

$$\dot{\widetilde{\mathbf{e}}}_{\mathbf{x}_{c}}(t) = \left(\mathbf{A}_{\mathbf{c}} - \boldsymbol{\sigma}\mathbf{C}_{\mathbf{c}}\right)\widetilde{\mathbf{e}}_{\mathbf{x}_{c}}(t) + \mathbf{B}_{\mathbf{c3}}\Delta^{(m)}(t) = \mathbf{A}_{\mathbf{ac}}\widetilde{\mathbf{e}}_{\mathbf{x}_{c}}(t) + \mathbf{B}_{\mathbf{c3}}\Delta^{(m)}(t), \tag{41}$$

where the roots of $\det(s\mathbf{I} - \mathbf{A}_{\mathbf{ac}}) = s^{m+1} + \sigma_{m+1}s^{m} + \cdots + \sigma_{2}s + \sigma_{1}$ can be placed as desired by selecting the gain vector $\boldsymbol{\sigma}$.

Following the same idea of the proof of Theorem 7, let $\mathbf{Q}_{\mathbf{c}} = \mathbf{I} \in \mathbb{R}^{(m+1)\times(m+1)}$ be a constant, positive definite symmetric matrix; then, a positive definite matrix $\mathbf{P}_{\mathbf{c}} \in \mathbb{R}^{(m+1)\times(m+1)}$ exists such that $\mathbf{A}_{\mathbf{ac}}^{\mathbf{T}}\mathbf{P}_{\mathbf{c}} + \mathbf{P}_{\mathbf{c}}\mathbf{A}_{\mathbf{ac}} = -\mathbf{Q}_{\mathbf{c}}$. Consider the Lyapunov function candidate $V(\widetilde{\mathbf{e}}_{\mathbf{x}_{c}}) = (1/2)\widetilde{\mathbf{e}}_{\mathbf{x}_{c}}^{\mathbf{T}}(t)\mathbf{P}_{\mathbf{c}}\widetilde{\mathbf{e}}_{\mathbf{x}_{c}}(t)$. The time derivative of V, that is, $\dot{V}(\widetilde{\mathbf{e}}_{\mathbf{x}_{c}}, t)$, is strictly negative outside the disc:

$$D_{xc} = \left\{\widetilde{\mathbf{e}}_{\mathbf{x}_{c}}(t) \in \mathbb{R}^{m+1}, \left\|\widetilde{\mathbf{e}}_{\mathbf{x}_{c}}\right\|_{2} \leq 2K_{\Delta}\left\|\mathbf{P}_{\mathbf{c}}\right\|_{2}\right\}. \tag{42}$$

Consequently, a uniform ultimate bounded (UUB) result was obtained regarding the estimation error phase variables $\widetilde{\mathbf{e}}_{\mathbf{x}_{c}}(t)$. □

Theorem 12. *Assume that there is an accurate estimation of $\varphi(t)$, $\Delta(t)$, $\tau_{a}(t)$, and $\dot{\tau}_{a}(t)$; then, for the simplified system (29), the following control law is proposed:*

$$\tau_{g}(t) = \frac{1}{\kappa}\left[\dot{\widehat{\omega}}_{g_{\text{opt}}}(t) - k_{c}\left(\omega_{g}(t) - \widehat{\omega}_{g_{\text{opt}}}(t)\right) - \widehat{\varphi}(t) - \widehat{\Delta}(t)\right] \tag{43}$$

with

$$\dot{\widehat{\omega}}_{g_{\text{opt}}}(t) = \frac{N_g \lambda_{\text{opt}}}{2R}\sqrt{\frac{2\lambda_{\text{opt}}}{\rho\pi R^3 C_{p_{\text{opt}}}}}\frac{1}{\sqrt{\widehat{\tau}_a(t)}}\dot{\widehat{\tau}}_a(t), \tag{44}$$

where $\widehat{\tau}_a(t)$ *and* $\dot{\widehat{\tau}}_a(t)$ *are provided by the aerodynamic torque observer given in* (21), $\widehat{\varphi}(t)$ *is reconstructed by the estimated states of the aerodynamic torque observer given in* (21), *and* $\widehat{\Delta}(t)$ *is provided by the GPI disturbance observer given in* (37) *and* (38).

Such law asymptotically and exponentially forces the closed loop system tracking error $e_\omega(t)$ *to converge towards the interior of a disk of radius as small as desired centered in zero, provided that the coefficient is* $k_c > 0$.

Proof. By replacing (43) in (29), the following dynamics is obtained:

$$\begin{aligned}\dot{\omega}_g(t) - \dot{\widehat{\omega}}_{g_{\text{opt}}}(t) + k_c\left(\omega_g(t) - \widehat{\omega}_{g_{\text{opt}}}(t)\right)\\ = -\widehat{\varphi}(t) - \widehat{\Delta}(t) + \Delta(t) + \varphi(t).\end{aligned} \tag{45}$$

Then, by defining some estimation errors: $\widetilde{e}_{\omega_{\text{opt}}} = \omega_{g_{\text{opt}}}(t) - \widehat{\omega}_{g_{\text{opt}}}(t)$, $\widetilde{e}_\Delta(t) = \Delta(t) - \widehat{\Delta}(t)$, and $\widetilde{e}_\varphi(t) = \varphi(t) - \widehat{\varphi}(t)$ and by replacing them in (45), the following control system tracking error dynamics is obtained:

$$\begin{aligned}\left(\dot{\omega}_g(t) - \dot{\omega}_{g_{\text{opt}}}(t)\right) + k_c\left(\omega_g(t) - \omega_{g_{\text{opt}}}(t)\right)\\ = -\dot{\widetilde{e}}_{\omega_{\text{opt}}}(t) - k_c\widetilde{e}_{\omega_{\text{opt}}}(t) + \widetilde{e}_\Delta(t) + \widetilde{e}_\varphi(t),\end{aligned}$$

$$\dot{e}_\omega(t) + k_c e_\omega(t) = -\dot{\widetilde{e}}_{\omega_{\text{opt}}}(t) - k_c\widetilde{e}_{\omega_{\text{opt}}}(t) + \widetilde{e}_\Delta(t) + \widetilde{e}_\varphi(t). \tag{46}$$

Therefore, as long as $k_c > 0$ and the estimation errors $\widetilde{e}_{\omega_{\text{opt}}}(t)$, $\widetilde{e}_\Delta(t)$, and $\widetilde{e}_\varphi(t)$ are ultimately bounded by the GPI observers (21) and (37), the tracking error dynamics $e_\omega(t)$ will remain stable and bounded since the right side of (46) is also bounded. □

Since the relative order of the WECS is one and system order is three, zero dynamics come into play and in consequence are analyzed. Considering the third-order system dynamics defined in (7), the zero dynamics is given by $\omega_r(t)$ and $\theta_\Delta(t)$ with $\omega_g(t)$ set to zero:

$$\begin{bmatrix}\dot{\omega}_r(t)\\ \dot{\theta}_\Delta(t)\end{bmatrix} = \underbrace{\begin{bmatrix}-\dfrac{B_{dt}+B_r}{J_r} & -\dfrac{K_{dt}}{J_r}\\ 1 & 0\end{bmatrix}}_{A_{\text{zero}}}\begin{bmatrix}\omega_r(t)\\ \theta_\Delta(t)\end{bmatrix} + \begin{bmatrix}\dfrac{1}{J_r}\\ 0\end{bmatrix}\tau_a(t). \tag{47}$$

Then, the internal dynamics is now given by the eigenvalues of A_{zero} (48). In this work, the eigenvalues are stable since the parameters of the WECS B_{dt}, B_r, K_{dt}, and J_r are positive:

$$\left|sI - A_{\text{zero}}\right| = \begin{vmatrix}s + \dfrac{B_{dt}+B_r}{J_r} & \dfrac{K_{dt}}{J_r}\\ -1 & s\end{vmatrix} = s^2 + \frac{B_{dt}+B_r}{J_r}s + \frac{K_{dt}}{J_r}. \tag{48}$$

Some troubles may arise in the control system when the internal dynamics is poorly damped; however, in the studied case, such internal dynamics does not lead to any problem. In cases where the internal dynamics became problematic, some methods are used [31].

Remark 13. Note that for the GPI observer-based control strategy defined in (43) and (37), the energy capture maximization depends on the accurate reconstruction of the optimal reference trajectory $\omega_{g_{\text{opt}}}(t)$.

4. Benchmark Model

The simulations are carried out using a benchmark model for wind turbine control implemented in MATLAB/Simulink. This benchmark model was published by Odgaard et al. in [25] and can be used to evaluate both fault tolerant and classic control schemes in any region of operation of a wind turbine. The test bench model is based on a realistic nonlinear generic three-bladed horizontal-axis variable-speed wind turbine, containing sensors, actuators, system faults, tower shadow and wind shear effects, full converter coupling, and rated power at 4.8 MW.

For wind speeds between 0 and 12.5 m/s, the turbine is controlled to operate in region 2. The wind profile used has an average hub-height wind speed of 8.68 m/s and a turbulence intensity of 12%. The test bench defines a standard torque control strategy for the operation in region 2 with the following control law: $\tau_{g,\text{ref}}(t) = k_{\text{opt}}\omega_g^2(t)$ with $k_{\text{opt}} = 1.2171$, $C_{p_{\text{opt}}} = 0.4554$, and $\lambda_{\text{opt}} = 8.0$. The converter model has the following constraints: max torque gradient = 1.25×10^4 N·m/s, min torque gradient = -1.25×10^4 N·m/s, max torque = 3.6×10^4 N·m, and min torque = 0 N·m.

5. Results and Discussion

The proposed aerodynamic torque GPI observer (21) and the GPI observer-based control (37)–(43) were implemented and tested on the nonlinear wind turbine benchmark model described previously. Figure 2 shows the system scheme of the proposed control strategy used for simulations. The parameters of the GPI observers and the control strategy were selected as follows:

GPI observer for aerodynamic torque estimation: $m = 3$, $\sigma_1 = 1000$, and $\sigma_2 = 1028.22$, $\sigma_3 = 1028.62$, $\sigma_4 = 0.39$, $\sigma_5 = 234.81$, $\sigma_6 = 28.46$.

GPI observer-based control: $p = 3$, $k_c = 1$, $\alpha_1 = 39.38$, $\alpha_2 = 61.69$, $\alpha_3 = 35.30$, and $\alpha_4 = 8.66$.

5.1. Aerodynamic Torque Estimation. The estimate of the aerodynamic torque obtained by the GPI observer in (21) is shown in Figure 3(a). The aerodynamic torque estimation error is shown in Figure 3(c). The estimation of the generator speed optimal reference trajectory $\widehat{\omega}_{g_{\text{opt}}}(t)$ is shown in Figure 3(b), and its estimation error $\widetilde{e}_{\omega_{\text{opt}}} = \omega_{g_{\text{opt}}}(t) - \widehat{\omega}_{g_{\text{opt}}}(t)$ can be detailed in Figure 3(d). Note that this estimation error

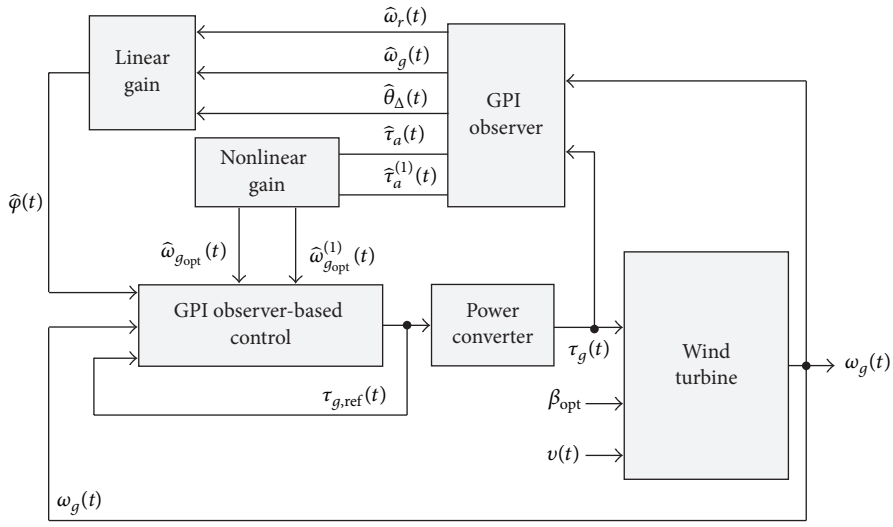

Figure 2: Closed loop system schema of the proposed control strategy.

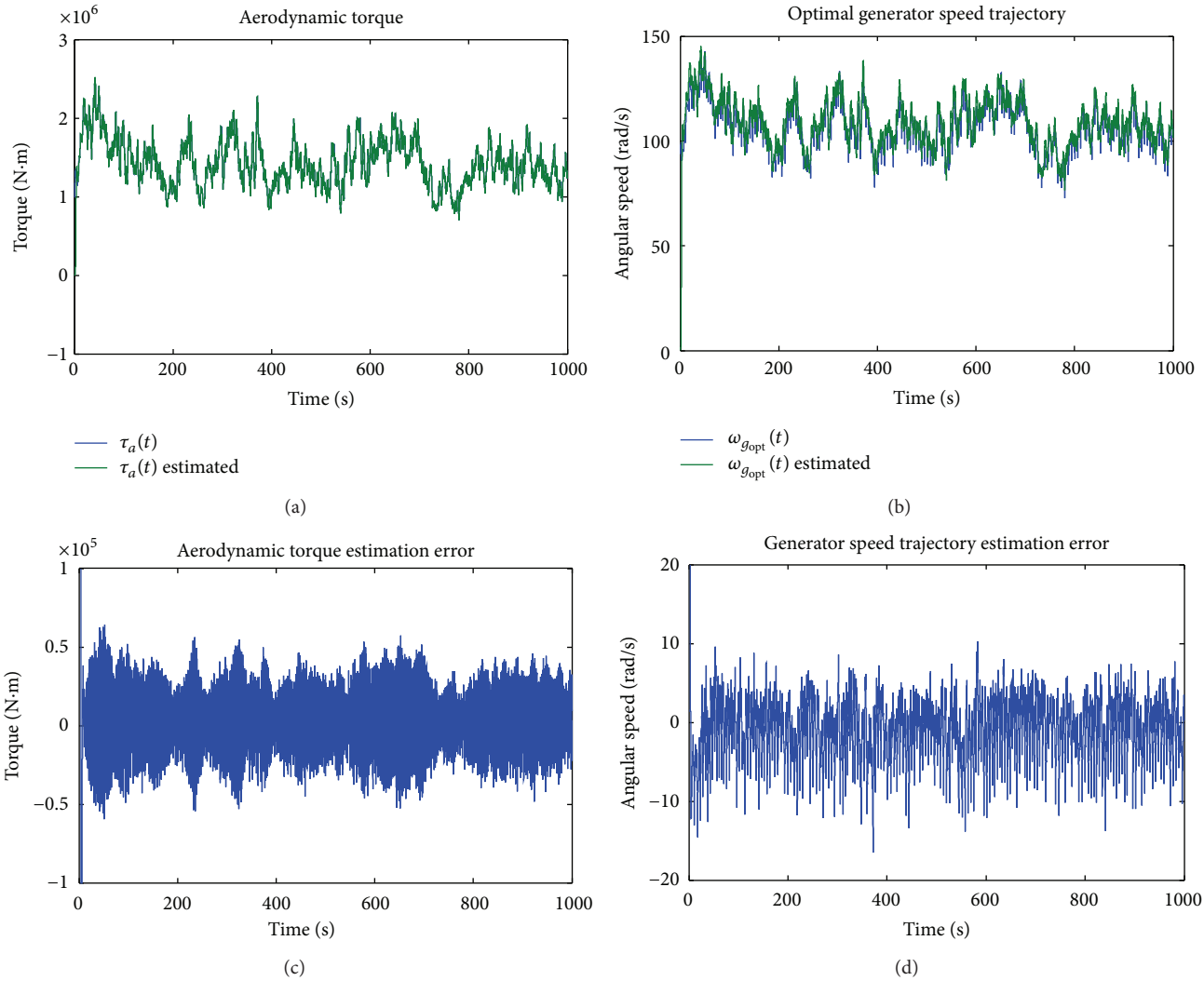

Figure 3: Aerodynamic torque estimation results: (a) aerodynamic torque, (b) generator speed optimal trajectory, (c) aerodynamic torque estimation error, and (d) generator speed trajectory estimation error.

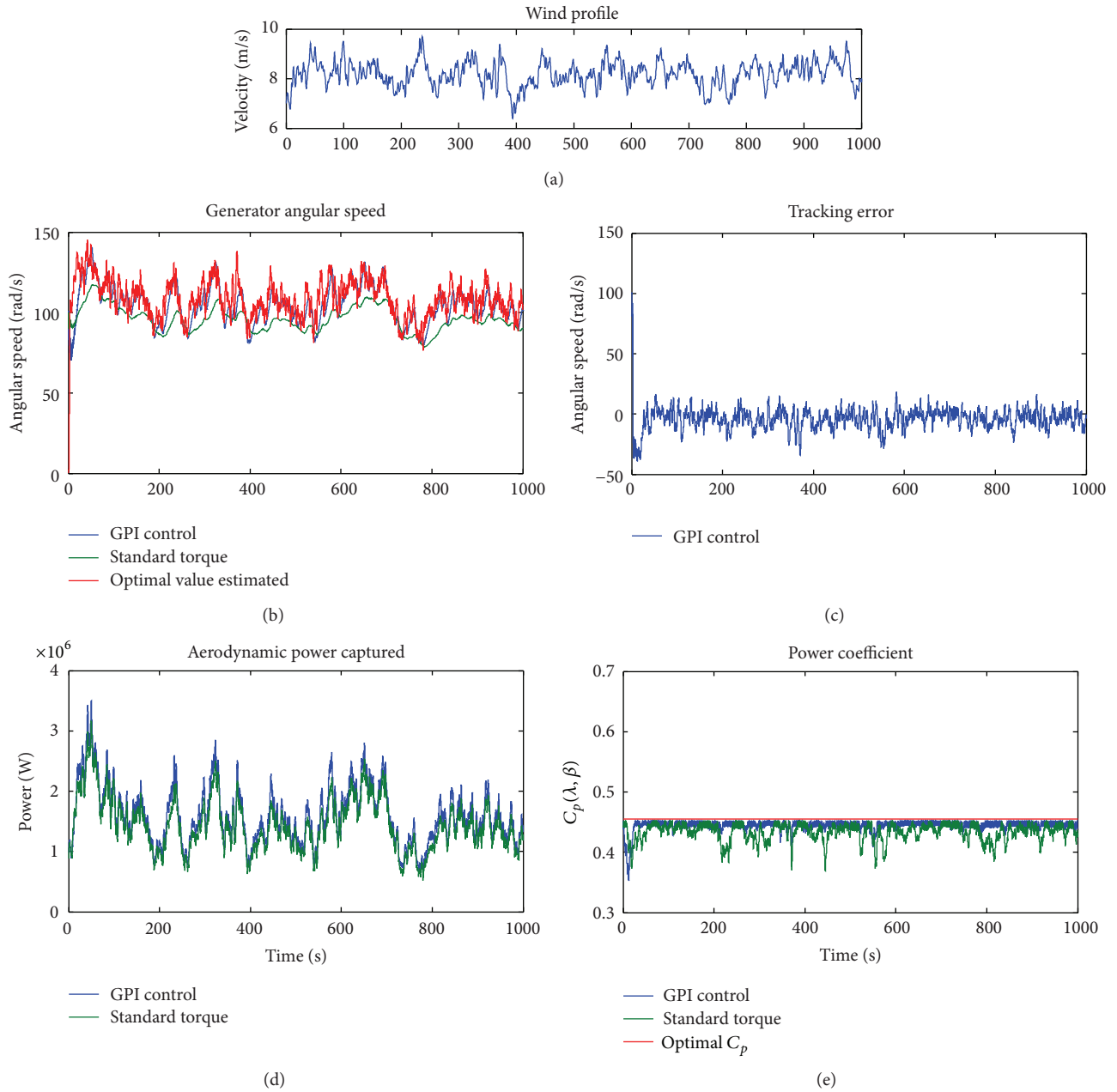

FIGURE 4: Simulation results of the proposed GPI observer-based control: (a) wind profile, (b) generator angular speed, (c) tracking error, (d) aerodynamic power captured, and (e) power coefficient.

has a small offset of −1.0811 rad/s, which in turn will cause a slight offset in the aerodynamic power coefficient control.

5.2. Energy Capture Maximization. The simulation results of the proposed control strategy are shown in Figure 4. Under nominal conditions, the control system tracks the optimal reference trajectory to force the WECS power coefficient C_p close to its optimal value (see Figures 4(b) and 4(e)). Despite the external disturbances and nonlinearities of the benchmark model, the tracking error of the control system is near to zero as shown in Figure 4(c). In order to achieve a compromise between energy capture and dynamic loads on the low speed shaft, a medium performance on the control gain k_c was selected. Most of the fast fluctuations of the aerodynamic torque transferred to the generator speed optimal trajectory are not tracked (see Figure 4(b)).

Figures 4(d) and 4(e) detail the aerodynamic power captured by the GPI observer-based control and the evolution in time of the WECS power coefficient, respectively. It is observed that the captured aerodynamic power with the proposed control is greater than the power captured by the standard torque control defined in the benchmark. In addition, it is noted that the proposed control strategy forces the power coefficient to stay close to its optimal value $C_{p_{\text{opt}}} = 0.4554$, which allows better power capture.

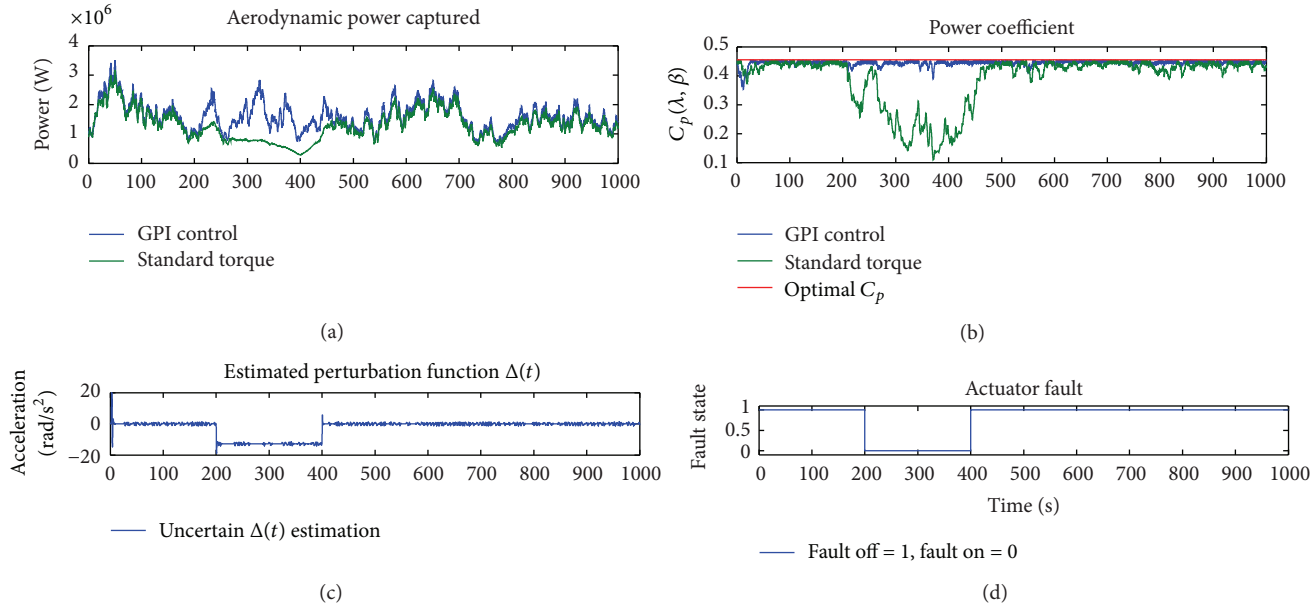

FIGURE 5: Simulation results on power converter fault.

The performance of each control system is compared using an aerodynamic efficiency index η_{aero} [24]. It is defined as follows:

$$\eta_{\text{aero}}(\%) = \frac{\int_{t_i}^{t_f} P_a(t)\,dt}{\int_{t_i}^{t_f} P_{a_{\text{opt}}}(t)\,dt}, \qquad P_{a_{\text{opt}}}(t) = \frac{1}{2}\rho\pi R^2 C_{p_{\text{opt}}} v(t)^3. \tag{49}$$

The evaluation of the criteria defined in (49) stated that the aerodynamic efficiency obtained by the proposed control technique is 98.8%, while the efficiency of the classical controller (benchmark) is 95.6%.

5.3. Active Disturbance Rejection Evaluation. The benchmark model [25] contains faults which require the control system to be reconfigured to continue power generation, as well as very severe faults which require a safe and fast shutdown of the wind turbine. In this work, in order to evaluate the active disturbance rejection capability of the proposed GPI observer-based control strategy, a typical malfunction in the internal power converter control loops is used. As a consequence, this nonsevere fault must be accommodated in some way, and the wind turbine must continue its operation.

The fault considered is an offset, denoted as $\Delta\tau_g$, on the generator torque, which can be caused by an error in the initialization of the converter controller [32]. The converter offset is configured to $\Delta\tau_g = 5000\,\text{N·m}$.

Figure 5 shows the closed loop performance of both the standard torque control and the proposed GPI observer-based control approach under the actuator fault. The fault occurs from 200 s to 400 s as seen in Figure 5(d). As the fault is active, the GPI observer (37), via the observer state $\widehat{\Delta}(t)$, estimates the perturbation function on line (see Figure 5(c)) and actively rejects the internal perturbation applying the GPI observer-based control law (43).

It is observed in Figure 5(a) that the perturbation is rejected by the proposed control and any captured aerodynamic power lost is appreciated. Figure 5(b) shows that the power coefficient of the WECS is still close to its optimal value. On the other hand, the standard torque control of the benchmark cannot handle the actuator fault, and much of the aerodynamic power is lost. The evaluation of the criteria defined in (49) stated that the aerodynamic efficiency obtained by the proposed control is 98.65%, while the efficiency of the classical controller (benchmark) is 85.88%.

6. Conclusions

In this paper, a linear active disturbance rejection control strategy based on two GPI observers for maximum wind energy capture of variable-speed wind turbines operating at partial load has been proposed. In order to create the generator speed optimal trajectory towards an optimum point at which the WECS power coefficient is maximum, an ADR philosophy-based GPI observer was developed to estimate the aerodynamic torque and its first derivative. Then, an ADR philosophy-based GPI observer-based controller was designed, and it was able to absolutely and arbitrarily bound the generator speed tracking error.

The proposed design strategy solved the control problem based on linear active estimation of possible nonlinearities and perturbations of the WECS, and these accurate estimations were used by a simplified linear control law, in which the captured wind energy was maximized.

It was shown through simulation tests on a fully nonlinear benchmark model that the proposed dual GPI observer control strategy maximized the captured wind energy even when an actuator fault was applied. This is a demonstration of some robustness added by the GPI observer-based control.

Since performance of wind turbines is significantly affected by the used control strategy, considering new alternative linear control strategies that can improve the performance of the WECS is a motivation to use, adapt, and evaluate linear GPI observer-based controllers to operate wind turbines at partial load.

It is worth noting that the proposed control strategy is related to exact feedback linearization, but there are some important differences between both strategies which give advantages to GPI observer-based control, such as the following: (a) GPI observer-based control does not require system state measurements, (b) any mismatch between the system model and the real system is lumped together in a perturbation function that is estimated and rejected on line, (c) GPI observers are capable of estimating a certain number of perturbation function derivatives (useful to determine $\dot{\omega}_{g_{\text{opt}}}$), and (d) ADR philosophy plays a very important role in GPI observer-based control since the internal model of the perturbation functions is taken into account in the design process.

References

[1] I. Munteanu, A. I. Bratcu, N.-A. Cutululis, and E. Ceanga, *Optimal Control of Wind Energy Systems*, Springer, London, UK, 2008.

[2] F. D. Bianchi, R. S. Sánchez-Peña, and M. Guadayol, "Gain scheduled control based on high fidelity local wind turbine models," *Renewable Energy*, vol. 37, no. 1, pp. 233–240, 2012.

[3] G. A. Parker and C. D. Johnson, "Improved speed regulation and mitigation of drive-train torsion fatigue in flexible wind turbines, using disturbance utilization control: part one," in *Proceedings of the 41st Southeastern Symposium on System Theory (SSST '09)*, pp. 171–176, March 2009.

[4] L. Y. Pao and K. E. Johnson, "Control of wind turbines: approaches, challenges, and recent developments," *IEEE Control Systems Magazine*, vol. 31, no. 2, pp. 44–62, 2011.

[5] E. Iyasere, M. Salah, D. Dawson, J. Wagner, and E. Tatlicioglu, "Optimum seeking-based non-linear controller to maximise energy capture in a variable speed wind turbine," *IET Control Theory & Applications*, vol. 6, no. 4, pp. 526–532, 2012.

[6] K. Pierce, "Control Method for Improved Energy Capture below Rated Power," National Renewable Energy Laboratory NREL/CP-500-26322, 1999.

[7] K. A. Stol, "Disturbance tracking control and blade load mitigation for variable-speed wind turbines," *Journal of Solar Energy Engineering, Transactions of the ASME*, vol. 125, no. 4, pp. 396–401, 2003.

[8] W. E. Leithead and B. Connor, "Control of variable speed wind turbines: design task," *International Journal of Control*, vol. 73, no. 13, pp. 1189–1212, 2000.

[9] H. Vihriälä, R. Perälä, P. Mäkilä, and L. Söderlund, "A gearless wind power drive: part 2: performance of control system," in *Proceedings of the European Wind Energy Conference,*, pp. 1090–1093, 2001.

[10] C. Evangelista, P. Puleston, F. Valenciaga, and A. Dávila, "Variable gains super-twisting control for wind energy conversion optimization," in *Proceedings of the 11th International Workshop on Variable Structure Systems (VSS '10)*, pp. 50–55, June 2010.

[11] B. Beltran, M. E. H. Benbouzid, and T. Ahmed-Ali, "Second-order sliding mode control of a doubly fed induction generator driven wind turbine," *IEEE Transactions on Energy Conversion*, vol. 27, pp. 261–269, 2012.

[12] C. Evangelista, P. Puleston, F. Valenciaga, and L. M. Fridman, "Lyapunov-designed super-twisting sliding mode control for wind energy conversion optimization," *IEEE Transactions on Industrial Electronics*, vol. 60, pp. 538–545, 2013.

[13] M. Fliess, R. Marquez, E. Delaleau, and H. Sira-Ramírez, "Correcteurs proportionnels-intégraux généralisés," *ESAIM. Control, Optimisation and Calculus of Variations*, vol. 7, pp. 23–41, 2002.

[14] A. Luviano-Juárez, J. Cortés-Romero, and H. Sira-Ramírez, "Synchronization of chaotic oscillators by means of generalized proportional integral observers," *International Journal of Bifurcation and Chaos in Applied Sciences and Engineering*, vol. 20, no. 5, pp. 1509–1517, 2010.

[15] H. Sira-Ramírez and V. F. Batlle, "Robust Σ-Δ modulation-based sliding mode observers for linear systems subject to time polynomial inputs," *International Journal of Systems Science*, vol. 42, no. 4, pp. 621–631, 2011.

[16] M. Fliess, R. Marquez, and E. Delaleau, "State feedbacks without asymptotic observers and generalized PID regulators," in *Nonlinear Control in the Year 2000*, A. Isidori, F. Lamnabhi-Lagarrigue, and W. Respondek, Eds., vol. 258, pp. 367–384, Springer, Berlin, Germany, 2001.

[17] H. Sira-Ramírez, F. González-Montañez, J. Cortés-Romero, and A. Luviano-Juarez, "A disturbance rejection approach for the induction motor through observer based Generalized PI control," in *Proceedings of the American Control Conference*, Fairmont Queen Elizabeth, Montréal, Canada, 2012.

[18] H. Sira-Ramírez, A. Luviano-Juárez, and J. Cortés-Romero, "Flatness-based linear output feedback control for disturbance rejection and tracking tasks on a Chua's circuit," *International Journal of Control*, vol. 85, no. 5, pp. 594–602, 2012.

[19] H. Sira-Ramírez, A. Luviano-Juárez, and J. Cortés-Romero, "Robust input-output sliding mode control of the buck converter," *Control Engineering Practice*, vol. 21, pp. 671–678, 2013.

[20] C. D. Johnson, "Accommodation of external disturbances in linear regulator and servomechanism problems," *IEEE Transactions on Automatic Control*, vol. 16, no. 6, pp. 635–644, 1971.

[21] J. Han, "From PID to active disturbance rejection control," *IEEE Transactions on Industrial Electronics*, vol. 56, no. 3, pp. 900–906, 2009.

[22] G. Tian and Z. Gao, "From poncelet's invariance principle to active disturbance rejection," in *Proceedings of the American Control Conference (ACC '09)*, pp. 2451–2457, June 2009.

[23] Z. Gao, Y. Huang, and J. Han, "An alternative paradigm for control system design," in *Proceedings of the 40th IEEE Conference on Decision and Control (CDC '01)*, pp. 4578–4585, December 2001.

[24] B. Boukhezzar and H. Siguerdidjane, "Nonlinear control of a variable-speed wind turbine using a two-mass model," *IEEE Transactions on Energy Conversion*, vol. 26, no. 1, pp. 149–162, 2011.

[25] P. F. Odgaard, J. Stoustrup, and M. Kinnaert, "Fault tolerant control of wind turbines—a benchmark model," in *Proceedings of the 7th IFAC Symposium on Fault Detection, Supervision and Safety of Technical Processes*, pp. 155–160, Barcelona, Spain, July 2009.

[26] G. A. Parker and C. D. Johnson, "Improved speed regulation and mitigation of drive-train torsion fatigue in flexible wind turbines, using disturbance utilization control: part two," in

Proceedings of the 41st Southeastern Symposium on System Theory (SSST '09), pp. 177–183, March 2009.

[27] L. B. Freidovich and H. K. Khalil, "Performance recovery of feedback-linearization-based designs," *IEEE Transactions on Automatic Control*, vol. 53, no. 10, pp. 2324–2334, 2008.

[28] S. Zhao and Z. Gao, "An active disturbance rejection based approach to vibration suppression in two-inertia systems," in *Proceedings of the American Control Conference (ACC '10)*, pp. 1520–1525, July 2010.

[29] S. Zhao, Q. Zheng, and Z. Gao, "On model-free accommodation of actuator nonlinearities," in *Proceedings of the 10th World Congress on Intelligent Control and Automation*, Beijing, China, 2012.

[30] Q. Zheng, Z. Chen, and Z. Gao, "A practical approach to disturbance decoupling control," *Control Engineering Practice*, vol. 17, no. 9, pp. 1016–1025, 2009.

[31] C. Sloth, T. Esbensen, and J. Stoustrup, "Robust and fault-tolerant linear parameter-varying control of wind turbines," *Mechatronics*, vol. 21, no. 4, pp. 645–659, 2011.

[32] P. F. Odgaard and K. E. Johnson, "Wind turbine fault detection and fault tolerant control-a second challenge," in *Proceedings of the 8th IFAC Symposium on Fault Detection, Supervision and Safety of Technical Processes*, 2012.

Hindawi Publishing Corporation
Mathematical Problems in Engineering
Volume 2013, Article ID 481364, 5 pages
http://dx.doi.org/10.1155/2013/481364

Research Article

Improved Formulation for the Optimization of Wind Turbine Placement in a Wind Farm

Zong Woo Geem and Junhee Hong

Department of Energy IT, Gachon University, Seongnam 461-701, Republic of Korea

Correspondence should be addressed to Zong Woo Geem; geem@gachon.ac.kr

Received 19 February 2013; Revised 14 June 2013; Accepted 16 June 2013

Academic Editor: Ming-Hung Hsu

As an alternative to fossil fuels, wind can be considered because it is a renewable and greenhouse gas-free natural resource. When wind power is generated by wind turbines in a wind farm, the optimal placement of turbines is critical because different layouts produce different efficiencies. The objective of the wind turbine placement problem is to maximize the generated power while minimizing the cost in installing the turbines. This study proposes an efficient optimization formulation for the optimal layout of wind turbine placements under the resources (e.g., number of turbines) or budget limit by introducing corresponding constraints. The proposed formulation gave users more conveniences in considering resources and budget bounds. After performing the optimization, results were compared using two different methods (branch and bound method and genetic algorithm) and two different objective functions.

1. Introduction

Wind has a power which can be converted into energy (electricity) generated by wind turbines and mechanical power generated by wind mills. Because wind energy is abundant, renewable, and clean without producing greenhouse gas, it can be an alternative to fossil fuels.

In order to cost-efficiently obtain the wind energy, researchers have considered optimization techniques for the layout of wind turbines in wind farms [1–5]. Mosetti et al. [1] first applied genetic algorithm (GA) to this wind turbine position optimization. However, they did not provide detailed numerical information to replicate, while Grady et al. [2] provided full numerical dataset to replicate and compare the results from various algorithms. Emami and Noghreh [3] explained in more detail the physical wake function from continuity equation of mass conservation law. Rasuo and Bengin [4] expanded the application from flat surface into arbitrary configured terrain. Samorani [5] provided a more realistic power function from subdivided wind velocities.

The optimization formulations in the above-mentioned literature have majorly two types of objective functions (cost per unit power and one over power). However, they do not have any budgetary or technical constraint that can efficiently control budget limitation or turbine number. Thus, this study proposes a more realistic optimization formulation for placing wind turbines in a wind farm by considering the available number of turbines and the available budget. Also, the computational results are to be compared with those from the previous literature.

2. Physical Wake Model

The previous literature [1–3] has used the following wake decay model for two consecutive turbines (e.g., turbine 0 and turbine 1):

$$u_1 = u_0 \left[1 - \frac{2a}{\left(1 + \alpha x / r_r\right)^2} \right], \tag{1}$$

where u_1 is wind speed after the turbine 0, u_0 is wind speed before the turbine 0, a is axial induction factor, α is entrainment constant, x is distance between two turbines; and r_r is rotor radius of turbines (=40 m in this study).

The axial induction factor a can be obtained using the following relationship:

$$C_T = 4a(1-a), \tag{2}$$

where C_T is turbine thrust coefficient (=0.88 in this study).

The entrainment constant α can be obtained using the following empirical function [1–3]:

$$\alpha = \frac{0.5}{\ln(z/z_0)}, \tag{3}$$

where z is hub height of the turbine (=60 m in this study) and z_0 is surface roughness (=0.3 m in this study).

More fundamentally, the wake decay model in (1) can be derived from a continuity equation for mass conservation [3]. If the wind speed immediately after the turbine is assumed to be 1/3 of the original speed, the following continuity equation can be formulated:

$$\rho\frac{u_0}{3}A_r + \rho u_0(A_1 - A_r) = \rho u A_1. \tag{4}$$

Here, ρ is wind density which is represented as mass divided by volume. Under the mass conservation law, the total mass directly passing a wind turbine rotor ($\rho(u_0/3)A_r$) and nearly passing the rotor ($\rho u_0(A_1 - A_r)$) should be equal to the total mass ($\rho u A_1$) at the distance of x. Because $A_r = \pi r_r^2$, $A_1 = \pi r_1^2$, and $r_1 = \alpha x + r_r$, (4) can be substituted with (1). Here, r_1 is downstream rotor radius and a (axial induction factor) is assumed to be 1/3. For (1), this study uses r_1 instead of r_r in order to fairly compare this study with previous ones [1–3] although it is not exact.

3. Cost and Power Functions

The total cost of all turbines in a wind farm can be calculated with the following function [1–3]:

$$C_t = N\left(\frac{2}{3} + \frac{1}{3}e^{-0.00174N^2}\right), \tag{5}$$

where N is the total number of turbines in a wind farm.

The total power (kW-year) generated from all turbines can be calculated with the following function [2, 3]:

$$P_t = \sum_{i}^{N} 0.3u_i^3, \tag{6}$$

where u_i is the wind speed at each turbine.

4. New Optimization Formulation

For the objective function of this optimal wind turbine placement problem, researchers have proposed two different types:

$$\text{Minimize } z_1 = w_1\frac{C_t}{P_t} + w_2\frac{1}{P_t}, \tag{7}$$

$$\text{Minimize } z_2 = \frac{C_t}{P_t}. \tag{8}$$

Equation (7), proposed by Mosetti et al. [1] and Emami and Noghreh [3], combines two objective functions (cost per unit power and one over power). The objective function of cost per unit power is designed to find the most cost-effective (or minimal cost per unit power) solution while the objective function of one over power is designed to find the most power-effective (or maximal power) solution. Meanwhile, (8), proposed by Grady et al. [2], uses only one objective function.

Although Emami and Noghreh claimed that (7) is better than (8), the former has the following limitations: (1) because the weights (w_1, w_2) are arbitrarily assigned by users, the proper setting of the weight values requires tedious trial-and-error process for users; (2) nonetheless, it cannot specifically control budget limit or turbine number; (3) more importantly, it does not significantly improve the performance of (8) (this point will be discussed later). In this sense, (8) is actually better than (7) because the former is simple and easy to use and does not require tedious extra process.

Here, for both equations, the following modifications can be considered to avoid any divided-by-zero error, which happens if searching methods start with $P_t = 0$:

$$\text{Minimize } z_1 = w_1\frac{C_t}{P_t + \Delta} + w_2\frac{1}{P_t + \Delta}, \tag{9}$$

$$\text{Minimize } z_2 = \frac{C_t}{P_t + \Delta}, \tag{10}$$

where Δ is tiny amount (e.g., $\Delta = 0.0001$).

In order to consider exact turbine number or budget limit, the following additional constraints can be also introduced:

$$N = N_a, \tag{11}$$

$$C_t \le C_a. \tag{12}$$

Equation (11) denotes that the total number of turbines in a wind farm should be equal to the available number of turbines, N_a. Equation (12) denotes that the total cost of turbines installed in a wind farm should be less than or equal to the available budget, C_a.

5. Numerical Example

The above-mentioned optimization formulation was applied to a popular wind turbine placement problem [1–3] as shown in Figure 1. The wind farm, where wind flows from the top into the bottom with a uniform speed of 12 meter per second, has 100 candidate turbine locations and each location has an area of 200 m × 200 m. For the optimization, each location has a binary value. If the binary variable has a value of 1, it means a turbine is installed at the location. Otherwise, it means a turbine is not installed. Actually, this is a huge combinatorial problem because total searching space is $2^{100} \approx 1.3 \times 10^{30}$.

For this large-scale problem, a metaheuristic approach, GA, has been actively applied [1–3]. This is because traditional branch and bound (B&B) method does not give good results. When this study applied B&B method (commercial code named Solver) to the problem, the objective function

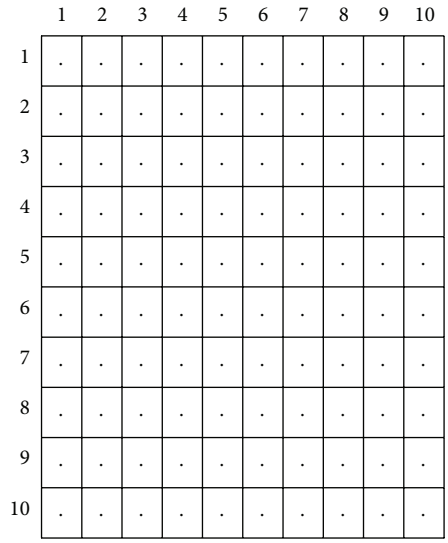

Figure 1: Schematic of wind farm.

Table 1: Comparison of results from two objective functions.

Function type	No. of function evaluations	Time taken (mm:ss)	w_1	w_2
Equation (10)	130,883	18:07	NA	NA
Equation (9)	136,360	19:07	0.5	0.5
	126,765	15:01	0.3	0.7
	347,547	40:41	0.7	0.3

value of 2.2824 (unit: unit cost $\times 10^{-3}$) was obtained with the cost of 34.18 and the power of 14977.44 (kW/year) as shown in Figure 2(a) ($N = 51$). Meanwhile, GA approach (commercial code named Evolver) found the objective function value of 1.5579 with the cost of 22.09 and the power of 14178.82 as shown in Figure 2(b) ($N = 30$). The result of GA is much better than that of B&B because the former's generation efficiency is 641.8 (unit: kW/year/unit cost) while the latter's generation efficiency is 438.2.

The above GA approach utilized (10) as an objective function. However, (9) was also tested with different weight values ($w_1 = 0.5$, $w_2 = 0.5$; $w_1 = 0.3$, $w_2 = 0.7$; and $w_1 = 0.7$, $w_2 = 0.3$) as shown in Table 1. When (10) was compared with (9), the former outperformed the latter in two cases ($w_1 = 0.5$, $w_2 = 0.5$ and $w_1 = 0.7$, $w_2 = 0.3$) in terms of number of function evaluations while all four approaches found the identical global optimum ($C_t = 22.09$) as shown in Figure 2(b). It should be noted that because C_t/P_t in (9) (or in (7)) is greater than $1/P_t$ by C_t times, the approach with bigger w_2 performed better which considers more balance between C_t/P_t and $1/P_t$.

As stated previously, in order to more efficiently consider turbine number or budget limit, corresponding constraints should be introduced to the optimization formulation. Table 2 shows the results of GA approaches with different available numbers of turbines, also shown in Figure 2(b) ($N = 30$), Figure 3(a) ($N = 10$), Figure 3(b) ($N = 20$), and Figure 3(c) ($N = 40$). The objective function becomes minimal (1.5579) when N is 30, while the second best solution was obtained with $N = 20$; the third best solution was obtained with $N = 40$; and the fourth best solution was obtained with $N = 10$.

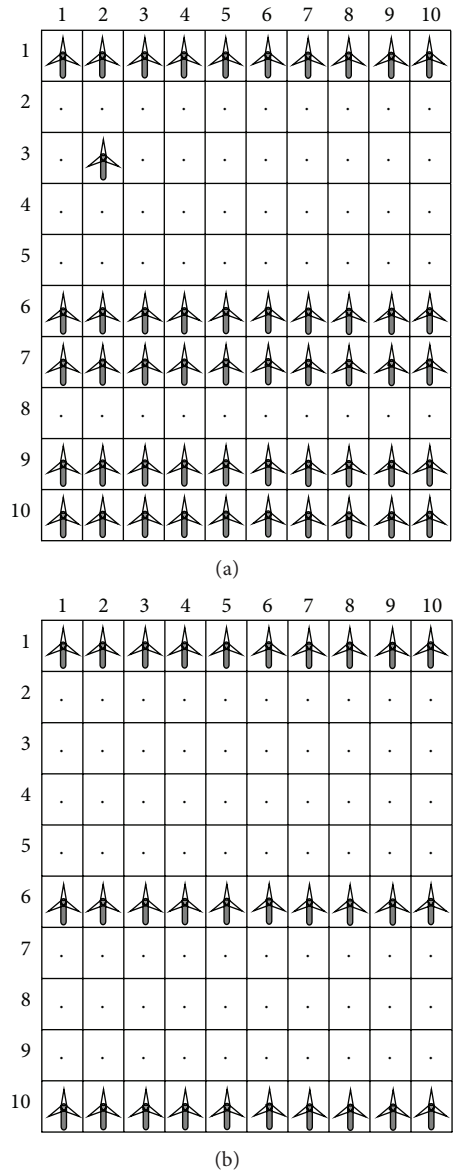

Figure 2: Best results from branch and bound method and genetic algorithm.

Table 2: Comparison of results from different turbine numbers.

N	C_t/P_t (10^{-3})	C_t	P_t
10	1.8286	9.47	5,177.64
20	1.6332	16.66	10,198.82
30	1.5579	22.09	14,178.82
40	1.6745	27.49	16,417.49

By considering the budget limit in (12), the optimal function value of 1.5978 was obtained with the cost of 19.48

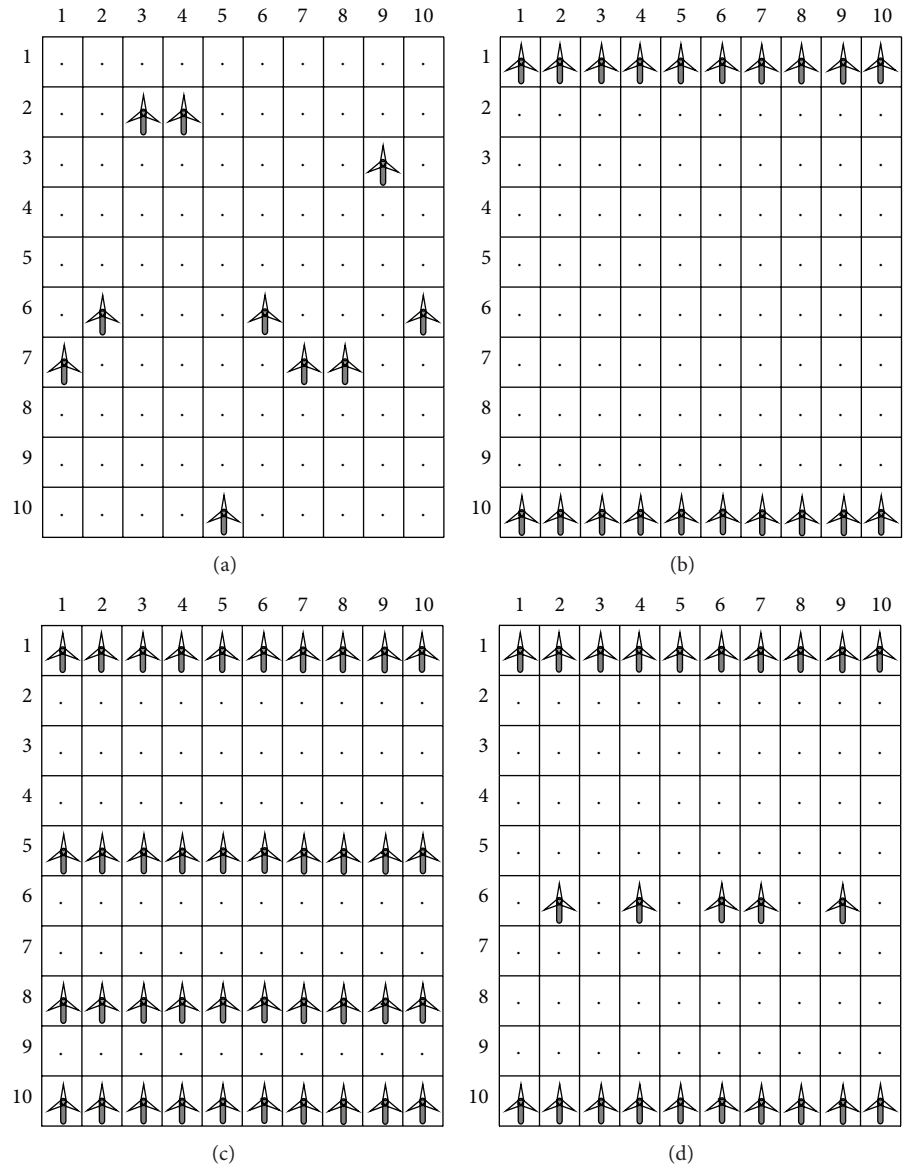

Figure 3: Results of genetic algorithm with different constraints.

and the power of 12,188.82 if available budget C_a is 20. Figure 3(d) shows the corresponding result ($N = 25$).

Previous researches [1–3] did not consider the above turbine number and budget limit constraints. However, these constraints can be efficiently utilized under the limited resources or expenditures.

When the best solution in this study ($C_t/P_t = 1.5579 \times 10^{-3}$ when $N = 30$) was compared with other solutions, it outperformed the result by Mosetti et al. [1] according to the comparison by Grady et al. [2]. Also, the best solution here is identical to those by Grady et al. [2] and Emami and Noghreh [3]. However, in terms of the number of objective function evaluations, this study outperformed that by Grady et al. [2] because this study found the best solution after 126,765 evaluations while that by Grady et al. found the identical one after 721,800 evaluations (600 individuals and 1203 generations). Although Emami and Noghreh [3] found the identical best solution, a fair comparison cannot be made because they did not provide the number of total evaluations.

6. Conclusions

This study improved the existing optimization formulation for wind turbine placement in a wind farm by introducing (1) nonzero denominator, (2) budget constraint, and (3) resource constraint (number of available turbines). Also, two existing objective functions were compared. In addition, the reason why GA, rather than traditional B&B method, has vigorously tackled the problem was demonstrated. That is because GA obtained much better result than B&B for this huge enumeration problem (1.3×10^{30}).

When the results were compared, the best solution in this study outperformed those from previous studies (Mosetti et al. [1] and Grady et al. [2]). Although all approaches, including this study, utilized GA techniques, the variant here appeared better than other variants.

Hopefully, future research will include more complicated and practical issues such as minimum power requirement, territory topography, wind direction, wind velocity variability, and power generation by factory-made turbine. Also, other metaheuristic algorithms such as ant colony optimization (ACO) [6] or harmony search (HS) [7] are expected to tackle the problem.

Acknowledgment

This work was supported by the Gachon University research fund of 2013 (GCU-2013-R166).

References

[1] G. Mosetti, C. Poloni, and B. Diviacco, "Optimization of wind turbine positioning in large windfarms by means of a genetic algorithm," *Journal of Wind Engineering and Industrial Aerodynamics*, vol. 51, no. 1, pp. 105–116, 1994.

[2] S. A. Grady, M. Y. Hussaini, and M. M. Abdullah, "Placement of wind turbines using genetic algorithms," *Renewable Energy*, vol. 30, no. 2, pp. 259–270, 2005.

[3] A. Emami and P. Noghreh, "New approach on optimization in placement of wind turbines within wind farm by genetic algorithms," *Renewable Energy*, vol. 35, no. 7, pp. 1559–1564, 2010.

[4] B. Rasuo and A. C. Bengin, "Optimization of wind farm layout," *FME Transactions*, vol. 38, pp. 107–114, 2010.

[5] M. Samorani, "The wind farm layout optimization problem," Tech. Rep., Leeds School of Business, University of Colorado at Boulder, Boulder, Colo, USA, 2010.

[6] M. Dorigo, V. Maniezzo, and A. Colorni, "Ant system: optimization by a colony of cooperating agents," *IEEE Transactions on Systems, Man, and Cybernetics, Part B*, vol. 26, no. 1, pp. 29–41, 1996.

[7] Z. W. Geem, J. H. Kim, and G. V. Loganathan, "A new heuristic optimization algorithm: harmony search," *Simulation*, vol. 76, no. 2, pp. 60–68, 2001.